UNIVERSITY OF OKLAHOMA

GRADUATE COLLEGE

NUMERICAL MODELING AND DIAGNOSTICS OF INTER- AND INTRA-WELL INTERFERENCE IN TIGHT OIL RESERVOIRS: TOWARDS OPTIMAL WELL SPACING DECISIONS

A DISSERTATION

SUBMITTED TO THE GRADUATE FACULTY

in partial fulfillment of the requirements for the

Degree of

DOCTOR OF PHILOSOPHY

By

MOUIN M. ALMASOODI
Norman, Oklahoma
2019

NUMERICAL MODELING AND DIAGNOSTICS OF INTER- AND INTRA-WELL INTERFERENCE IN TIGHT OIL RESERVOIRS: TOWARDS OPTIMAL WELL SPACING DECISIONS

A THESIS APPROVED FOR THE
MEWBOURNE SCHOOL OF PETROLEUM AND GEOLOGICAL ENGINEERING

BY THE COMMITTEE CONSISTING OF

Dr. Zulfiquar Reza, Chair

Dr. Younane Abousleiman

Dr. Deepak Devegowda

Dr. Chandra Rai

Dr. Matthew Pranter

Dedicated to Reham, Dana, and Lara without whom this dissertation would have been completed two years earlier!

Acknowledgments

Dr. Reza's nonpareil patience and encouragement of independent thinking have played a remarkable role in the success of this work. I would like to sincerely thank him for giving me the opportunity to join his research group, the freedom to explore different research ideas, and the guidance along with the support through my research.

I am thankful for the generous fund that Devon Energy has provided to cover the expenses of the doctoral degree. Also, I am thankful to Devon's commitment to fund this research despite the epic roller-coaster of oil prices.

Furthermore, I want to extend my gratitude to my committee members for influencing the development of my scientific character. Namely, I am thankful to Dr. Younane Abousleiman. His catalytic impact on shaping my personality will last forever. Sound arguments, clarity of thoughts, and tenacity are few attributes that I learned from him. Additionally, Dr. Chandra Rai, Dr. Deepak Devegowda, and Dr. Matthew Pranter are greatly acknowledged for their humbleness and acceptance to serve on my PhD committee. I am thankful to all the teachers and mentors who instilled in me that while having a laser focus on maximizing economics, I shall not compromise safety, integrity, and uphold the utmost devotion to the engineers' code of conduct.

Finally, this work would not have been possible without the unconditional love and ceaseless support of my wife, and parents.

Abstract

The main objective of this dissertation is to provide sound understanding and mitigation solutions to the perplexing problem of well interference and its implications on completions design, well-spacing decisions, and ultimately the economics of unconventional reservoirs. Optimal fracture spacing has eluded reservoir and completions engineers since the inception of multi-stage hydraulic fracturing. Very small cluster spacing results in fracture-to-fracture interference and higher completions cost, whereas very large cluster spacing leads to inefficient oil recovery which is detrimental to the economics of the well. Furthermore, when US onshore oil producers transitioned from appraisal to development, they were surprised not only by oil price volatility, but also by the magnitude of infill degradation due to well interference. In simple words, lucrative results from appraisal efforts were not representative of infill operations.

Hence, several numerical models were constructed to better understand inter- and intra-well interference based on finite-difference, and finite-volume methods. The physical principals utilized in these models are conservation of mass, Darcy's law, thermodynamic equilibrium of fluid components between phases, and the definitions of phase saturation and mole fraction to complete the system. Numerical models presented in this work are three-phase, transient, and consider compressible fluid flow. Fluid thermodynamics were addressed via equation of state.

Since the numerical solutions are non-unique, actual production data were utilized from different basins to calibrate the numerical models via history-matching process. Additionally, available geologic data were integrated to construct fit-for-purpose geologic models that were used as flow domains.

Findings from intra-well interference simulation suggest that drawdown strategy is more impactful to short-term oil productivity than hydraulic fracture spacing. Drawdown strategy is even more impactful on short-term oil recovery than 20% error in porosity, or water saturation. Results suggest that the profile of producing gas-oil ratio depends on fracture spacing and has been interpreted within the context of linear-flow theory. Also, results clearly show that drawdown strategy and magnitude of intra-well interference can be optimized based on the desired economic metric (NPV, or IRR). For instance, if the objective is to maximize rate of return, then tighter fracture spacing may be accepted

Simulation results from inter-well interference show that the unpropped fracture geometry could be higher than matrix permeability by a factor of 10 to 20. History-match results confirm that hydraulic fracture half-length could exceed 2,000 ft depending on the completions design. Results also show that a certain level of inter-well interference improves oil recovery. Based on observations from sector modeling, the acceptable level of inter-well interference is dependent on the business commercial objectives, oil pricing, and well cost structure. These analyses provide a diagnostic technique to evaluate inter-well interference and its impact on development decisions.

Table of Contents

List of Tables

List of Figures

Chapter 1: Introduction

1.1 Overview

The intent of this chapter is to provide relevant studies, and key concepts needed for succeeding analyses. First, an overview of the most recent production outlook will be discussed, then the definitions of inter- and intra-well interference will be provided. A critical component in understanding well interference is interference monitoring and diagnostics. Hence, the advantages and disadvantages of various diagnostics techniques will be highlighted. Thermodynamic properties such gas-oil ratio and its relevance to well interference will be explained as well. For instance, the stages of gas-oil ratio will be described and related to pressure drawdown. Furthermore, recent advancements in computational geosciences and pore-scale imaging have made it possible to extract three-dimensional pore geometries from tight rock samples. Hence, it will be discussed how these pore geometries can be utilized via computational fluid dynamics to compute transport properties relevant to well interference. The chapter ends with few remarks on dual-permeability and dual-porosity paradigms to simulate well interface.

1.2 Tight Oil Reservoirs: Production Outlook and Challenges

Although tight oil reservoirs have gained prominence in recent years, well performance variability is not fully understood. The advent of horizontal drilling in conjunction with the ability to complete with multiple transverse fracture stages has made

economical production from these unconventional reservoirs possible. The following discussion is based on the most recent update from the US Energy Information Administration ("Annual Energy Outlook 2018 with Projections to 2050" 2018) which provides a fresh look at some of the interesting dynamics that are related to hydrocarbon supply and demand relationship, commodity price influence on energy mix, and the recent trends in population and energy consumption.

Large shares of global capital investments to be focused on tight oil reservoirs in the United States due to high operator efficiency and lower service cost. It is worth mentioning that although, the EIA base forecast assumes current laws and regulations remain unchanged throughout the projection period, the base case includes trend improvement in known technologies. One interesting takeaway from the report is the relationship between population and energy consumption. Although there is considerable increase in population and economics standard per capita, energy and carbon intensities are projected to decline as shown in Figure 1-1.

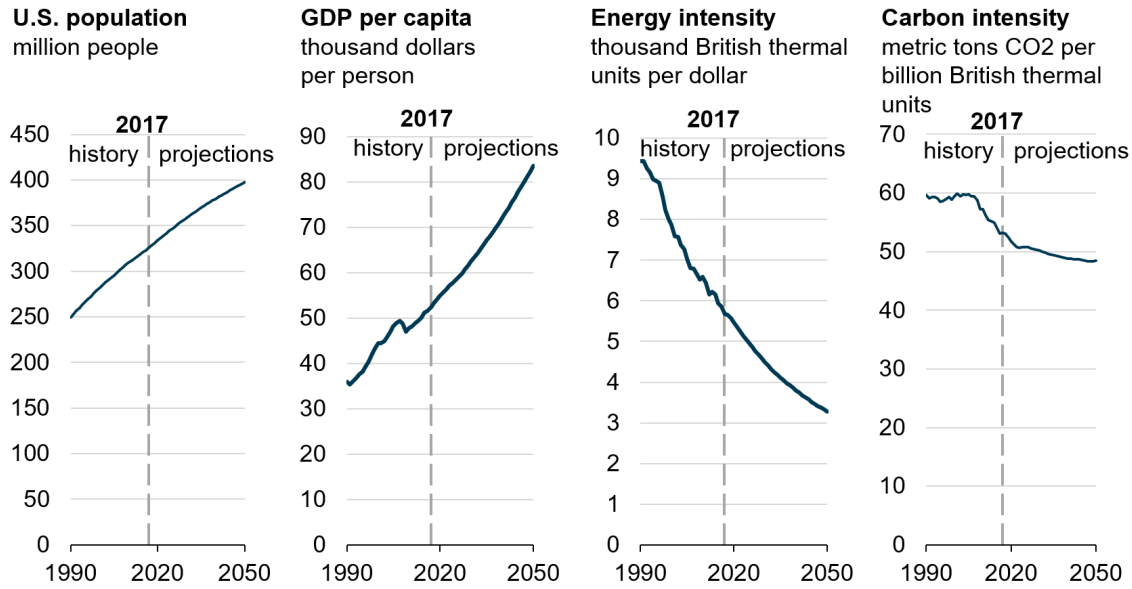

Figure 1-1- Energy and carbon intensities relative to economics and population growth.

The amount of energy consumed per one unit of economic growth is defined as energy intensity whereas the amount of CO2 emissions produced as a result of energy consumption is defined as carbon intensity. Both intensities have been declining steadily for many years. Those trends are projected to persist due to number of factors such as structural shifts in the economy, and improvement in technologies related to fuel economy (powertrain downsizing and weight reduction). Carbon intensity has been declining as well due to several political initiatives (regional, national, and international) that influenced the energy mix to use less carbon fuels. In fact, according to EIA, energy intensity and carbon intensity are projected to be 42% and 9% lower than 2017 by 2050. Production from tight oil reservoirs remains the leading source of energy in the United States from 2017 to 2050. Most of the US tight oil production comes from onshore the

lower 48. Tight oil production is projected to account for about 65% of the cumulative domestic production by year 2050 as shown in Figure 1-2.

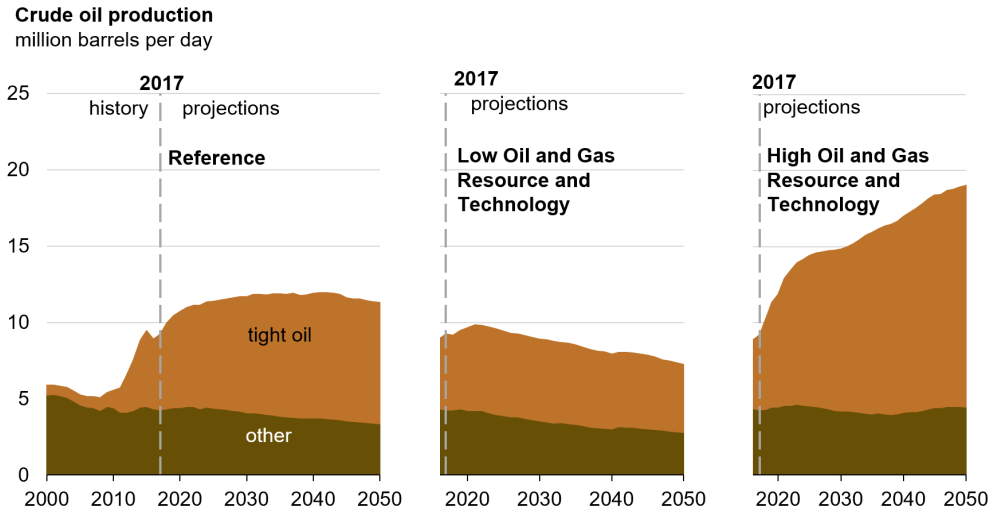

Figure 1-2- Tight oil reservoirs are the leading source of US crude oil production.

Recent announcement regarding deep water discoveries in the Gulf of Mexico will lead to increase in production through 2021. Offshore production then declines and flatten through 2050 as production from new discoveries balances the decline from legacy fields. As expected, the Southwestern region will lead the growth in US crude oil production. Figure 1-3 shows the projected oil production for each region within the US. The Permian basin dominates the growth of the Southwestern region because it includes the most prolific plays on onshore the United States such as Wolfcamp, Bone Spring, and Spraberry. On the other hand, Bakken and Niobrara tight oil reservoirs will be leading growth in Rocky Mountains and Dakotas. As drilling and production in the Eagle Ford shale become less productive, production in the Gulf Coast region is projected to flatten through 2025.

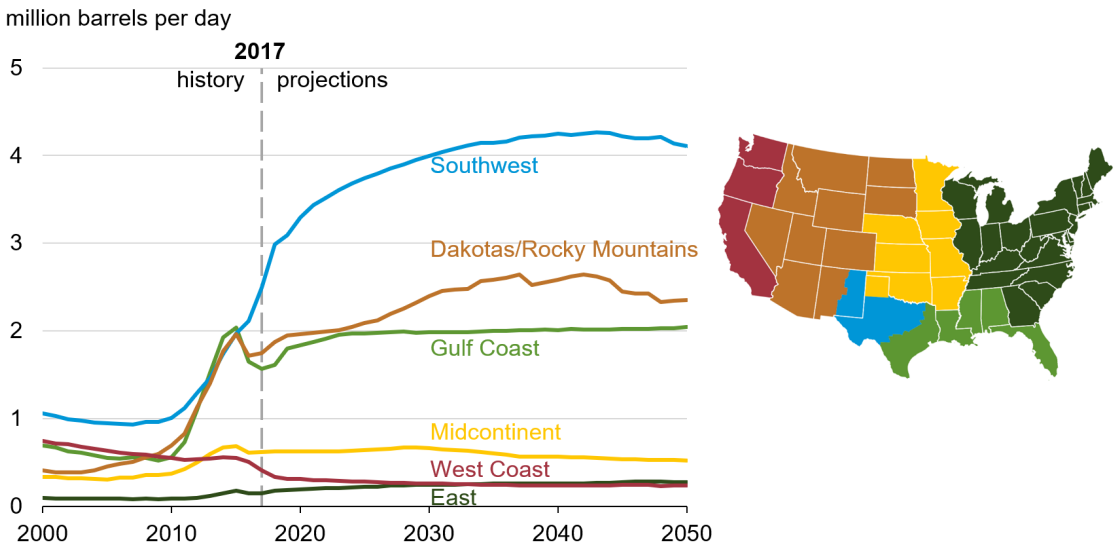

Figure 1-3- Lower 48 onshore crude oil production by region.

The necessity to develop less productive areas as well as productivity decline of existing wells are considered major challenges that impend the longevity of tight oil reservoirs in the United States. In fact, despite rising oil prices, EIA projections show that U.S. crude oil production levels off between 11 million and 12 million barrels per day. Furthermore, most tight oil reservoirs have little production history which make the task of production forecast difficult adding uncertainty to resource estimate and future projections. Additionally, extraction techniques (drilling and completions) continue to evolve rapidly due to better understanding of the subsurface challenges and technology improvements. The objective of this study is to address one of those challenges which is well interference. In simple words, it has been challenging to optimally produce tight reservoirs due to difficulties in identifying the optimal number of wells that is needed to drain the oil and gas efficiently. The difficulties are mainly attributed to substantial

uncertainty in the subsurface petrophysical, and geomechanical properties. Shale hydraulic tortuosity and intrinsic permeability are two examples of those properties that are highly uncertain, expensive, and difficult to measure in the laboratory. To improve and optimize the well performance, there is a need for collaborative effort from all disciplines such as land, geology, geophysics, completions, productions, and reservoir engineering. This collaboration is critical especially in a challenged pricing environment.

1.3 Literature Review

1.3.1 Definitions of Inter- and Intra-Well Interference

Understanding the relative contribution of the rock and fluid characteristics versus drilling and completions practices and their inter-connected nature on production performance of unconventional wells is key for successful decision making. Well interference in unconventional reservoirs developed with multi-stage hydraulic fractures can be classified into two categories which are intra-well (fracture-to-fracture) interference, and inter-well (well-to-well) interference. Inter-well interference occurs when a horizontal well "child" is hydraulically fractured next to a producing well "parent", the new well's fracture geometry tends to be asymmetric because the fractures of the child well preferentially grow in the direction of the parent well. Hence, the new infill well will be underperforming because it is producing from a zone that has been already depleted. On the other hand, intra-well interference is primarily associated with fracture spacing along the lateral of the horizontal well. Very small fracture spacing (i.e. densely spaced fracturing) results in higher completions cost, whereas very large fracture

spacing leads to inefficient oil recovery which is detrimental to the economics of the well. The following discussion will summarize recent efforts to tackle the problem of interference. I will give the main takeaways from each effort and provide perspective on areas that can benefit from modification, or enhancement.

1.3.2 Well Interference Relevant Studies

Simulation studies have been of limited utility to identify optimal well completions and spacing in unconventional reservoirs. Most studies are either single well simulation with structured grids, or un-coupled with the rock mechanics. Those limitation made it impossible to capture inter-well interference effects in unconventional reservoirs. The problem becomes more challenging in multi-bench developments such as operations in the Permian and Anadarko basins. (Siddiqui and Kumar 2016) attempted to simulate a three-well configuration by constructing conceptual liquid-rich reservoirs with unstructured grids to investigate the impact on production rates and the efficiency of different multiwall designs. As the wells are spaced closely, the onset of well interference represents the transition from adding reserves by infill drilling to accelerating production, thus it is critical to specify the economic metrics to be optimized. Given the current low commodity prices, operators are concentrating the efforts to reduce capital expenditure in which well drilling, and completions costs have the highest weight. (Siddiqui and Kumar 2016) modeled a reservoir with 9 layers based on typical properties from Eagle Ford shale. Each layer has a thickness of 30 ft. The study assumed isotropic porosity and permeability distribution. The model covers an area of 690 acres with dimensions of 5000

ft X 6000 ft X 270 ft. Total number of unstructured grids was 380,214; the authors didn't provide information regarding their simulation run time. The reservoir fluid was liquid rich with CGR of 150 MMscf/STB and initial reservoir pressure of 10900 psia at 300ºF. The reservoir simulation was run under compositional mode in which reservoir fluid was described with seven pseudo-components. Identical relative permeability tables were used for both matrix and hydraulic fractures. The authors observed that the well-to-well interference is related to fracture geometry and separation distance between wells. The interference effect became more pronounced with higher matrix permeability. The study didn't capitalize on the use of unstructured cells to investigate the impact of natural fractures.

If natural fractures are present in the reservoir, they will enhance the interference signature and perhaps result in asymmetric depletion pattern depending on their spatial distribution. However, the study succeeded in illustrating the impact well-spacing distance on production interference through forward modeling without relying on actual production data. Such techniques provide helpful insight into the complex reservoir dynamics at minimum cost. This work will be extended to cover a fluid from the Meramec formation, and by considering the presence of natural fractures and their impact on the growth of hydraulic fracture height and length.

Furthermore, (Lalehrokh and Bouma 2014) attempted to address the interplay between optimal well-spacing and production interference analytically. The predicament is that wells need to be spaced far from each other to minimize hydraulic fractures overlap

and thus over capitalization. Yet, wells need to be spaced close to each other to drain the entire unit and maximize recovery in timely manner. The study was conducted on the Eagle Ford shale which is a major resource play in North America. The effects of varying fracture half-length and permeability have been evaluated. Authors chose discounted profitability index along with net present value as economic metrics for well-spacing evaluation. The corporate economics threshold has not been disclosed in the study. Three scenarios (3000 ft, 1500 ft, and 1000 ft) were evaluated analytically. Figure 1-4 presents schematic of the spacing scenarios. Element of symmetry has been used in which the reservoir width is reduced to mimic different spacing scenarios.

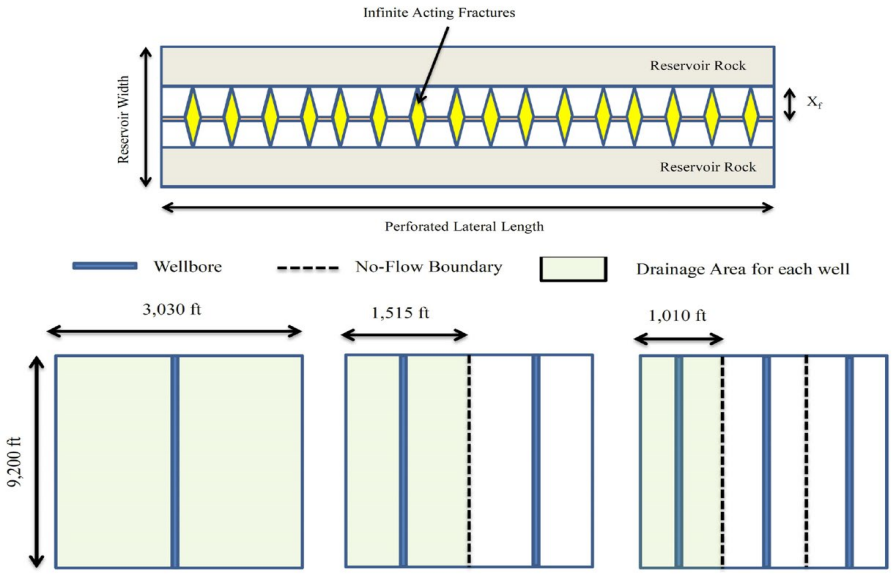

Figure 1-4- Well-spacing scenarios based on element of symmetry and by using analytical approach.

The reservoir was modeled as a homogenous porous media with two fluid types which are black oil with GOR of 1000 scf/bbl and condensate system with condensate to gas ratio of 150 bbl/MMscf. Reservoir pressure was set to 8200 psi with porosity of 9%, 29% water saturation and thickness of 130 ft. The well was completed with 19 hydraulically fractured stages at 4 clusters per stage. The lateral length was set to 6200 ft. Three permeabilities were modeled which are (20, 50, and 100 nD). Based 50 nD permeability, and 150 ft hydraulic fracture half length, 330 ft maximizes net present value in black oil Eagle Ford shale whereas 400 ft maximizes net present value in retrograde gas condensate. Gas condensate reservoirs can be drained with less wells due to higher fluid mobility. The study also illustrates the effect of fracture half-length, and oil price variation.

Operators in the continental United States have moved from delineating their plays and lease retention to full field development. Wine rack development, or Stack staggered configuration is a well-spacing technique to maximize recovery in multi-zone formations such as the Meramec formation in Oklahoma. The new well-spacing paradigm poses several challenges to reservoir simulators that are regarded as the primary vehicle to recommend optimal number of wells per unit. Despite the availability of several workarounds to model complex reservoirs, most simulators stand helpless in front advanced physics such as pore confinement, and dynamic optimization of stack staggered scenarios.

Traditional simulators model hydraulic fractures as planer features that are perpendicular to the wellbore due to gridding limitation. However, (Siddiqui, Walser, and Dusterhoft 2016) utilized a reservoir simulator with unstructured gridding capability that allows mapping hydraulic and natural fracture networks with complicated geometries. The study has considered the impact of the presence of conductive natural fractures. The simulation study deploys compositional fluid model with seven pseudo-components that were developed using commercial PVT software package. Three horizontal wells with multi-stage hydraulic fractures were considered. The primary objective of the numerical simulation was to understand the impact of vertical and lateral spacing in stacked-staggered development. The second objective was to understand the impact of timing to complete additional well after two existing wells were already online for few years. Seven major effects were explored which are matrix permeability, CGR, fracture length, wells staggering, time of well placement, presence of natural fractures, and conductivity degradation. Three multi-stage hydraulically fractured horizontal wells were numerically simulated for a maximum runtime of five years with 20 compositional runs.

The reservoir model covers an area of 1102 acres with dimensions of 8000ft long, 6000 ft wide, and 400 ft thick. It has five distinctive layers with varying petrophysical properties. Permeability was assumed to be 0.44 micro Darcy in X, Y, and Z directions. A common practice is model permeability in the Z direction to be less than X, and Y. The average reservoir porosity is 5.2%. Water saturation was set to be a constant of 35%. The most interesting aspect of the model is that the hydraulic fractures were not perpendicular

to the wellbore. Instead, they were modeled with an azimuth of N75W. The three wells were staggered in elevation. The middle well was at a lower elevation relative to the exterior wells. The exterior wells were placed at the same elevation. Initial reservoir pressure was set to 4800 psi at 170°F. The saturation pressure was set to 4765 psi. Reservoir fluid was modeled as retrograde condensate with seven components. The ratio of condensate to gas was set to 250 MMscf/STB. The study has investigated several effects which are well staggering, completions delay, natural fractures, loss of conductivity, and matrix conductivity. The study did not consider the impact of drawdown strategy, effect of critical gas saturation, and well spacing. The study concluded that completions delay of one year is inconsequential for 5-year productivity. Though, the delay could be impactful if the newly completed well has smaller fracture half length. The study also showed that higher productivity can be obtained by increasing conductive fracture height. More commonly, wells are being completed with slickwater fluid. Thus, they can suffer from severe loss of conductivity. Thus, the study sheds light on the importance of fluid selection to well performance.

The study argued that despite commercial success, understanding reservoir response to different completions practices and hydraulic fracturing techniques in shale rocks is poorly understood. The paper provides a multitude of completions parameters that can be investigated via numerical simulation. Based on the limited simulation runs, authors concluded the stack-staggering has no effect on well productivity. Additionally,

authors acknowledged that interference of wells need to be addressed explicitly to better predict well performance.

1.3.3 Comparing Interference in Unconventional to Conventional Reservoirs

Differences in well interference signature between conventional and unconventional reservoirs are mainly attributed to the well development pattern, and rock properties. While conventional reservoirs are developed via vertical drilling, unconventional reservoirs are developed using multi-stage hydraulic fractures in either a wine-rack configuration, or single bench development. Also, from well testing perspective, techniques such as multi-well interference test are not practical in tight oil reservoirs due to low matrix permeability, and the need to shut-in the well. Early life of unconventional wells is very important to the overall value of the project, and thus operators try to avoid shut-in wells as much as possible. In the next section, alternative diagnostics for well interference in tight oil reservoirs will be discussed.

1.3.4 Advantages and Limitations of Interference Diagnostics

A critical component in understanding well interference is interference monitoring via diagnostics such as pressure gauges, micro-seismic, chemical tracers, and fiber optics. Due to large number of wells being completed in tight oil reservoirs, it has become a major concern for operators when producing wells are being disturbed by offset hydraulic fracture operations. This form of inter-well interference is known in the industry as “frac hits”. Producing wells could lose more 50% of their reserves due to hydraulic fracture

hits. Therefore, interference tests can be used during the fracturing job to evaluate when and what stages are in communication. Besides, interference tests allow better placement of hydraulic fractures and wells within the reservoir. Recently, (Scott, Chu, and Flumerfelt 2015) applied real-time bottom-hole pressure gauges to improve field development strategies for the Wolfcamp shale in the Midland basin. Authors have outlined two challenges. First, the Wolfcamp thickness lend itself for multi-bench stacked development which poses significant challenges in terms of optimal well-spacing (interference). Second, multi-phase flow complicates reservoir engineering analyses to predict bottom-hole pressure from surface pressures and flow rates.

Additionally, since most of unconventional wells need to be on artificial lift early in their life, the efficiency of the artificial lift technique needs to be accounted for in the well performance analysis. 100 pressure gauges were run to evaluate depletion between horizontal wells, develop flowback strategies, optimize artificial lift, and characterize the fracture system within the reservoirs. For instance, two wells with different drawdown strategies were compared and skin damage was identified. Well 1 was flowed aggressively whereas Well 2 was flowed conservatively. Pressure analysis revealed that Well 2 had higher rate and productivity. It is worth mentioning that two wells were drilled in comparable geology and completed similarly. Skin damage was detected through the separation between pressure derivative curves of Well 1 and Well 2. Figure 1-5 presents a comparison of the two wells which was modified from (Scott, Chu, and Flumerfelt 2015).

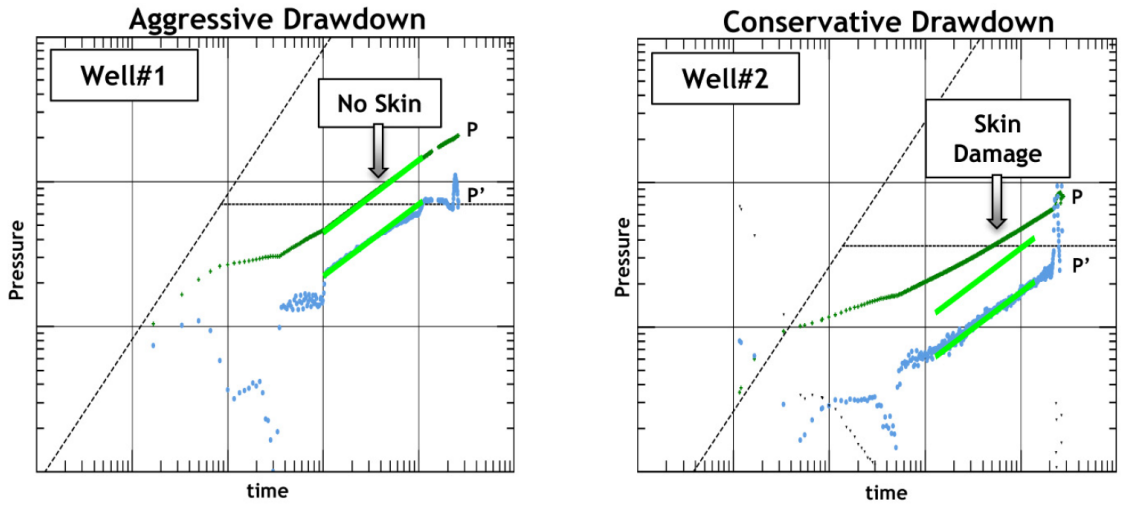

Figure 1-5- Example of using BHP gauges to identify skin damage via pressure diagnostics.

Furthermore, bottom-hole pressure gauges can be of great utility to identify the magnitude and direction of well to well interference and optimize well-spacing configuration. The example shown in Figure 1-6 illustrates how bottom-hole pressure gauges can be used to detect connectivity between wells in the Wolfcamp formation. The development contains five horizontal wells. Two wells were placed in the upper Wolfcamp and three wells in the lower Wolfcamp. Well 5 was equipped with BHP gauge and surrounded by four wells. As soon as Well 1 was opened, pressure decline was observed in Well 5. Further decline was observed when Well 2 was opened. These observations indicate interference between Well 5, 1, and 2. Also, it appears that there is higher connectivity vertically than laterally. Utilizing BHP gauges can drastically improve the understanding of well to well interference with respect to time, distance, and

magnitude. Finally, the value of pressure gauges to development decisions far exceeds the cost of deployment.

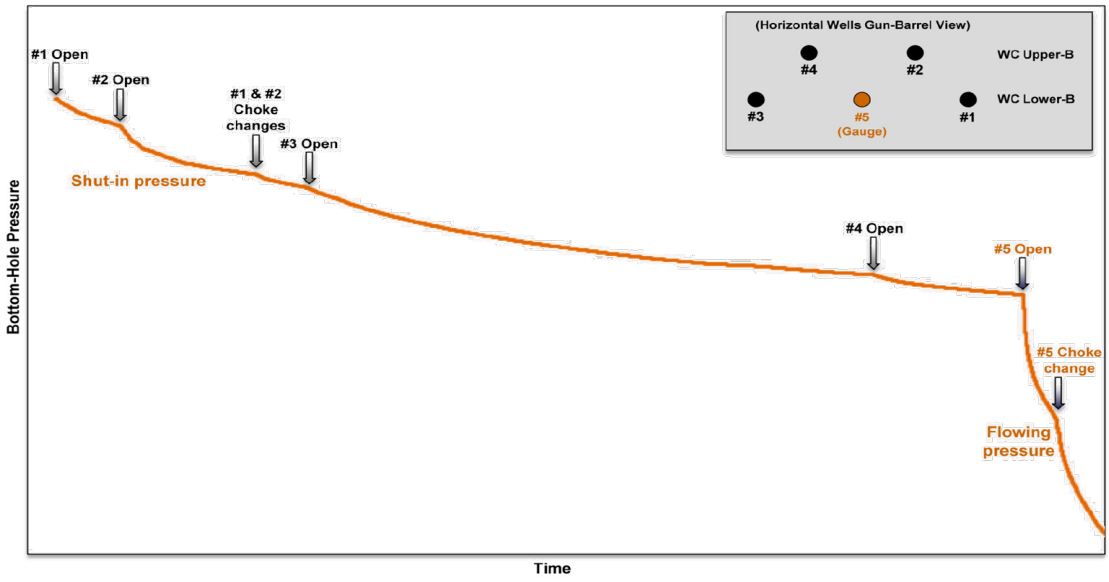

Figure 1-6- Interference test in a stack-staggered configuration from the Wolfcamp formation.

Microseismic monitoring is another experimental technique to image hydraulic fracture geometry to understand inter-well connections. Depending of the scope of the measurement, microseismic can be either recorded via downhole array, or from surface sensors. It is a passive technique which means acoustic source is not used in the experiment. Microseismic monitoring during stimulation has the ability to:

- Differentiate planer from complex fracture networks.
- Provide an estimate of the maximum fracture height and length.
- Estimate the stimulated rock volume

A major limitation of microseismic is that the stimulated rock volume measured by quantifying the microseismic cloud is not representative of the drainage volume. Drainage volume is influenced by the degree of fracture conductivity which is related to proppant placement. In other words, microseismic events measured while stimulating the rock are not necessarily propped pathways for fluid flow.

Moreover, there is a growing literature on fiber optics technology (DTS & DAS) as being another effective way of measuring cluster efficiency and thus it helps to predict well interference apriori. (Haustveit et al. 2017) used Distributed Temperature Sensing (DTS) and Distributed Acoustic Sensing (DAS) to monitor temperature changes during hydraulic stimulation before the well is produced. Results suggest strong heel-bias[1] in most of the stages. Fiber optics cables are installed either permanently (behind casing), or temporarily. (Huckabee 2009) has demonstrated that fiber optics technology enables quantitative inflow distribution measurement in commingled multiple intervals completions. Author shows that fiber optics is more superior to PLT (Production Logging Tool) in dry gas systems. Author also suggests that further evaluations are needed in reservoirs with higher liquid to gas ratio. Despite advantages, fiber optics cables are subject to deterioration when exposed to extreme temperature and pressure, and thus measurements might not be reliable in such environments.

[1] Heel-bias refers to the unequal distribution of fracturing fluid within a stage. Fracture clusters closer to the heel of the horizontal well take most of the fluid leaving other cluster under-stimulated.

Several studies have been conducted to understand inter- and intra-well interference. It is unnecessary to summarize all of them. Instead, pertinent studies will categorized in bullet points as shown below:

- **Well-Spacing Optimization in Stacked Reservoirs (Inter-Well Interference)**: (Lalehrokh and Bouma 2014; Shin and Popovich 2017; Yu and Sepehrnoori 2014; Iino et al. 2018; Liang, Du, and Yanez 2019).
- **Optimization of Fracture Spacing in Horizonal Wells (Intra-Well Interference:** (Bazan et al. 2010; Min et al. 2018; Sen et al. 2018; Cheng 2012).
- **Fracture Hits Due to Offset Operations:** (Liang, Khan, and Tang 2017; Sun et al. 2017; Swanson et al. 2018; Pankaj 2018).
- **Interference Diagnostics and Modeling:** (Siddiqui and Kumar 2016; Wu et al. 2012; Ajisafe et al. 2017; Fu et al. 2017; Hwang, Szabian, and Sharma 2017; Yu et al. 2016; Kumar et al. 2018; Blasingame et al. 1989).
- **Modeling and Mitigation of Child-Parent Interference:** (Gala, Manchanda, and Sharma 2018; Manchanda et al. 2018, 2017; Nieto et al. 2018; Agrawal and Sharma 2018).

1.4 Geomechanics Role in Well Interference

1.4.1 Parent and Infill Wells Interference

A pivotal concept to understanding the effect of geomechanics on well interference is the concept of effective stresses. Although, there are different ways to define effective

stresses acting on a rock, the effective stress can be simply defined as the total stress acting on a rock due to gravitational pull (overburden), or tectonic actions (side-burden) minus the effect of pore pressure. As illustrated in Chapter 1, reservoir simulation studies are routinely performed to obtain optimal number of horizontal wells that are needed to drain hydrocarbon resources efficiently with minimum interference. However, reservoir simulators often treat porosity and permeability as constants during the simulation period and neglect the impact of rock deformation on those properties. In contrast, coupled reservoir-geomechanics models permit porosity and permeability to vary in response to stress changes due to hydraulic fracturing operations and subsequent reservoir production. Inaccurate calculation of effective stresses may lead to poor well-spacing decision that results in well-to-well production interference. It is worth mentioning that Geomechanics plays even much bigger role when it comes to development near depleted areas.

For instance, when a new horizontal well is drilled next to a depleted zone, the new well's fracture geometry tends to be asymmetric. Hydraulic fractures of the new well grow in the direction of the depleted zone because it is the path of least resistance. Hence, the new well will be producing from a zone that has been depleted already. The new well often called "child" well whereas the initial development is called "parent" well.

In recent years, oil and gas operators have seen considerable amount of interference between existing production wells and infill wells. In most cases, the interference impacts the production rates negatively and thus plummeting the economics of the development

project. (Manchanda et al. 2018) built 3D single fracture model to investigate the nature of interference between an existing well (parent) and an infill well (child). The numerical simulator that was used in this study, implements geomechanical formulation to calculate effective stresses due to pressure depletion. The model accounts for vertical variability, but it does not consider horizontal heterogeneity that could be of a great effect when high permeability streaks are present. The study propounds the view that infill wells drilled near depleted zone have asymmetric hydraulic fractures. In other words, child well hydraulic fractures tend to grow toward the depleted zone of the parent well. This behavior results in less effective stimulation job and thus reducing the economics of the child wells. The paper provides possible mitigation strategies to address child well under-performance such as re-fracturing of the parent well to pressurize the depleted zone and thus reducing effective stresses.

Furthermore, Parent-Child interference could be either positive in which enhance parent production may occur, or negative in which reduction in parent well production may occur. In other words, interference could be constructive, or destructive to the parent well. (Miller et al. 2016) have examined more than 3000 well interference instance from 5 major basins within the United States which are Woodford, Bakken, Eagle Ford, Niobrara, and Haynesville as shown in Figure 1-7.

	Bakken	Eagle Ford	Haynesville	Woodford	Niobrara
Positive Hit - Long Term	17%	9%	20%	2%	0%
Positive Hit - Short Term	33%	14%	38%	2%	6%
Positive Hit Total	**50%**	**24%**	**58%**	**4%**	**6%**
No Change	**35%**	**36%**	**24%**	**32%**	**38%**
Negative Hit Total	**15%**	**41%**	**19%**	**64%**	**56%**
Negative Hit - Short Term	7%	13%	5%	20%	19%
Negative Hit - Long Term	6%	17%	5%	41%	31%
Shut-in Post Offset Hit	2%	10%	9%	3%	6%
Instances Included	**649**	**1,210**	**366**	**259**	**32**
Original No. of Instances	827	1,561	449	283	49
Instances with Invalid Data	178	351	83	24	17

Figure 1-7- Classification of positive and negative interference events from major tight reservoirs in the US.

Findings show mixed interference behavior (positive and negative) could exists within the same basin. Despite the Meramec formation was not included in this study, public data indicates negative interference between parent and child wells.

1.4.2 Understanding the Effect of "Stress Shadowing"

Hydraulic fractures branches in various directions depending on the mechanical properties of the rock matrix and the orientation along with the mechanical properties of the natural fractures. Each open hydraulic fracture applies additional stress on the adjacent rock which will consequently impact the growth of the next hydraulic fracture due to induced stresses. "Stress shadowing" is a colloquial term that describes stress changes induced by the rock deformation. While the effect of "stress shadowing" is nascent to the petroleum industry, this effect has been studied extensively in Civil

Engineering. For instance, the induced stresses caused by a point load on a mass of soil - known as Boussinesq effect for stress distribution- are analogous to the induced stresses when hydraulic fractures are treated during plug and perf operations.

"Stress shadowing" is a major contributor to two practical issues which are the restriction of the hydraulic fracture width and the alteration of hydraulic fracture path. Fracture width restriction leads to screen-outs[2] and thus negatively impacts the cost of well completions whereas the alteration of hydraulic fracture path leads to inefficient fractures that have poor communication with formations. Additionally, induced stresses increase the potential of having dominant fractures which lead to well interference. The dynamics of well to well interference through hydraulic fractures is discussed in Chapter 3.

The following discussion draws on the research conducted by (Wu et al. 2012) in which the authors discuss the propagation and interaction of hydraulic fractures in naturally fractured formation. The study explored the interaction between hydraulic and natural fractures via three numerical case studies which are parallel fractures in a horizontal well, complex fractures computed from microseismic, and multi-stage example that illustrates how stress shadowing from previous stage can alter the growth pattern of fractures in upcoming treatments. In the first case, five parallel fractures were considered; each fracture have a constant height of 100 ft. The fractures were spaced at

[2] Rapid rise in pump pressure due to proppant bridging across the perforation orifice.

65 ft. Other essential properties such as Young's modulus, Poisson's ratio, rate, viscosity, height, leakoff coefficient, stress anisotropy, number of perforations per fracture were provided. The objective of this case was to compare the fracture half-length generated by the UFM model to the modified PKN model. The PKN model was modified to include the stress shadowing calculation. However, it is worth mentioning that the modified PKN does not capture the change in hydraulic fracture path due to stress shadowing while the UFM formulation allows point by point stress shadow calculation along the path of fracture which permits the simulation of fracture turning. Results present the length of the five fractures during injection for both models for a period of 35 minutes. Also, results suggest that interior fractures have smaller width when compared to exterior fractures. The fractures with smaller width result in higher resistance to flow and thus shorter half length. The first case is extended by investigating key parameters that influence the magnitude of stress shadowing such as fracture spacing, stress anisotropy, and perforation friction.

Based on the results, there seems to be a compelling reason to believe that when the perforation friction is too high, it delivers a large diversion force that equally distributes the flow rate into all perforation clusters. Therefore, the stress shadowing effect can be dissipated and hydraulic fractures with equal dimensions can be developed. Larger fracture spacing has also diminished the effect of stress shadowing which results in fractures with similar dimensions. The second case study builds on the work conducted by (Cipolla et al. 2012). UFM model was implemented to simulated four stages in

horizontal well from the Barnett shale. Since the analyses were performed in 2011, the UFM model didn't have the full stress shadow calculation. Hence, the second case study used the same dataset from the previous study to re-run the simulation based on the most recent UFM model. Sonic logs indicated that there is high stress anisotropy toward the toe of the well which led to less fracture branching into the formation, especially in stage one and two. In the last case study, the issue under security is the influence of discrete fracture network coupled with the effect of stress shadowing on the growth and distribution of hydraulic fracture network in a formation with isotropic stress state. The case comprises four stages in a horizontal well that is cased and cemented. The first and second stages were pumped through three clusters whereas the third and fourth stages were pumped through four perforated clusters. The study presents two solutions for the hydraulic fracture network (HFN). The fist solution does not consider the influence of stress shadowing on the upcoming stage whereas the second solution considers the induced stresses due to the injection of prior stage. The challenge of validating the numerical results still has not been addressed. On the other hand, the results indirectly stress the need for accurate geomechanical description of the formation. Additionally, geomechaical properties such as Young's modulus and Poisson's ratio need to be calibrated to laboratory measurements prior to utilization in the hydraulic fracture simulator.

1.5 Transport Properties Influence on Well Interference

Matrix permeability represents a major unknown in unconventional tight reservoirs. Unconventional reservoirs that have permeabilities (0.1 – 1 micro Darcy) are often drilled with higher number of horizontal wells to drain them efficiently. Therefore, it is imperative to have an accurate estimate of the reservoir permeability to identify optimal number of horizontal wells, minimize interference, and mitigate economical risks due to over capitalization. Recent advancements in computational geosciences and pore-scale imaging have made it possible to extract realistic three-dimensional pore geometries from tight rock samples. Those pore geometries can be utilized to determine transport properties such as permeability and tortuosity of tight reservoirs using techniques from Computational Fluid Dynamics (CFD). In chapter 4, some of the key gaps in recent literature will be addressed:

- Develop a method to compute rock hydraulic tortuosity from FIB-SEM images.
- Evaluate permeability dependence on mesh density and verify that high-quality meshing metrics can be achieved at the nano-scale (such as aspect ratio close to 1, non-orthogonality, and reduced skewness).
- More importantly, investigate whether FIB-SEM images provide enough resolution and scale to compute transport properties such as permeability.

Understanding the architecture of tight reservoirs pore geometry is a daunting task that has inspired researchers to investigate pore-scale physics and advance modeling

methods. The following discussion provides essential definitions and sheds light on relevant studies.

1.5.1 Definitions and Relevant Studies

Pore structures of tight reservoirs are characterized by geometrical complexity that cannot be well explained by traditional descriptors such as packing of spheres, or bundle of tubes. Hence, in order to predict the movement of fluids within tight reservoirs, it is necessary to develop knowledge about their morphology. Tortuosity is a morphological property that measures the resistance of porous media to flow. (Carman 1937) was first to allude to the concept of tortuosity; his work was an upgrade and a generalization to (Kozeny 1927) permeability formulation through which he realized that Kozeny's assumption of straight and parallel tubes is not accurately capturing the transport behavior. Therefore, he introduced a dimensionless parameter called hydraulic tortuosity which is defined as the ratio of the average length of the fluid paths to the geometrical length of the sample. However, the average length of the fluid paths cannot be measured experimentally. Hence, several numerical studies were conducted to compute tortuosity. The most recent work was done by (Saomoto and Katagiri 2015) in which 2-D theoretical porous media was constructed to compare electric tortuosity to hydraulic tortuosity using finite element analysis. Authors found that, on average, hydraulic tortuosity is 15% greater than the electric one. Similarly, the concept of tortuosity has gained prominence in the lithium-ion battery industry as battery manufactures are primarily interested in

reducing the electric tortuosity of porous electrodes to improve battery efficiency and reduce waste heat (Delattre et al. 2018; Ebner et al. 2014).

Rapid progress in pore-scale imaging, processing, and parallel computing have made it possible to simulate fluid flow through realistic pore geometries and investigate pore-scale physics such as multiphase behavior (Zuo et al. 2017), relative permeability (Zhang 2017), and capillary action (Ruspini, Farokhpoor, and Oren 2017). Computational rock physics, known as digital rock physics, utilizes numerical techniques of various physical phenomena to extract transport properties (e.g., electrical conductivity and permeability), and to gain insights into flow dynamics within the reservoir. These computational techniques are directly applied to the pore geometry of the rock which eliminate the need for using theoretical pore networks to represent the pore geometry. Conversely, traditional rock physics involves either empirical relationships based on experimental data, or theoretical models based on idealized microstructures (Andrä et al. 2013). Despite the valuable insights that conventional rock physics provides, it is challenged to capture the inherent complexity of the pore morphology needed to accurately characterize tight reservoirs. Several studies have demonstrated the utility of coupling the imaging technology with the well-established physics of fluid dynamics (Berg et al. 2016; Madonna et al. 2013; Mohammadmoradi and Kantzas 2016; Piri and Blunt 2005; Raeini, Blunt, and Bijeljic 2014). However, despite the extensive research, there is a research gap in modeling 3D porous network extracted from tight reservoirs. Likewise, the impact of mesh refinement on transport properties such as permeability has

not been fully analyzed until now. This is mainly due to the large mesh sizes that could easily exceed 30 million cells for a sample of 1 cubic micron.

Besides the oil and gas industry, there are many other industries interested in computational pore-scale modeling. For instance, (Aslannejad and Hassanizadeh 2017) illustrated that papers used in the printing industry usually contain thin porous coating covering a thicker fibrous base layer. The morphology of the pore structure within the coating layer has a significant impact on the flow pattern and properties of the ink inside the paper medium. The authors illustrate that upon arrival of an ink droplet, fluid starts invading the pore space and thus displacing the air that was initially filling the pore space. Essentially, this process is similar to imbibition in oil and gas reservoirs. Full understanding of imbibition requires the characterization of the pore morphology, wettability, and effect of capillarity. Furthermore, (Silin et al. 2011) used 3D images generated using Synchrotron based X-ray microtomography of pore space as input for the Maximal Inscribed Spheres (MIS) method to predict two-phase fluid distribution in capillary equilibrium. The study showed agreement between the computed fluid distribution in the pores and experimental data. Even though the MIS method is incapable of capturing the morphological detail of the pore geometry, the study suggests that micro-computed tomography (micro-CT) along with MIS is a viable approach to study the pore-scale mechanisms of CO_2 injection into an aquifer. Furthermore, (Blunt et al. 2013) described in detail the imaging of the rock pore space from the nanometer scale and upwards. They provided three examples to illustrate the range of scientific problem that

can be addressed. The first example was the dispersion of highly heterogeneous carbonate rocks. Second, imaging of super critical CO_2 to illustrate the possibility of capillary trapping in geological carbon storage. The third example focused on the computation of relative permeability for mixed-wet carbonates and discussed implications for oilfield waterflood recovery. The authors have concluded that pore-scale modeling has the potential to transform the understanding of multiphase flow processes, improve contaminants removal, and safe carbon storage. More Recently, (Zapata and Sakhaee-Pour 2016) have attempted to characterize the pore space of shale formation by using data from mercury intrusion and nitrogen adsorption experiments. Authors were able to distinguish pore bodies, from pore throats. In order to account for the restrictions within the connected path of the pore space, authors needed to implement acyclic pore model. Alternatively, the rock sample could have been imaged to extract the pore geometry which then can be directly used in the flow simulation of the mercury injection experiment.

1.6 Interpretation of Well Interference through Rate Transient Analysis

Even though Decline Curve Analysis (DCA) is the most common technique for forecasting production data and it is accepted by federal agencies for reserves estimation, decline curve analysis has many limitations that could be detrimental to the accuracy of the production forecast such as inability to acc. ount for changes in flow regimes and

operational procedures. Besides, DCA is oblivious transitions from single to multiphase flow.

Unlike decline curve analysis, modern approaches, such as Rate Transient Analysis (RTA), utilize pressure data in addition to the production rates (oil, gas, and water). If a downhole pressure gauge is unavailable, most wells have casing and tubing pressure gauges that can be used to compute bottom-hole flowing pressure via nodal analysis. Unconventional tight oil reservoirs are characterized by low permeability. Thus, wells drilled in those reservoirs requires very large surface area to be exposed to the formation to achieve efficient drainage. (Blasingame et al., 2008) attempted to document the progression of technology and characterization in tight oil reservoirs.

RTA method capitalizes on the pronounced linear flow in tight reservoirs to help us identify well interference and estimate key parameters related to completions efficiency. RTA assumes that drainage beyond the simulated region is negligible. In other words, the effective drainage boundary in an unconventional well coincides with the hydraulic fracture length. RTA solutions were developed for a single fracture centered in a rectangular reservoir through which the hydraulic fracture length extends to the reservoir boundary as illustrated in Figure 1-8.

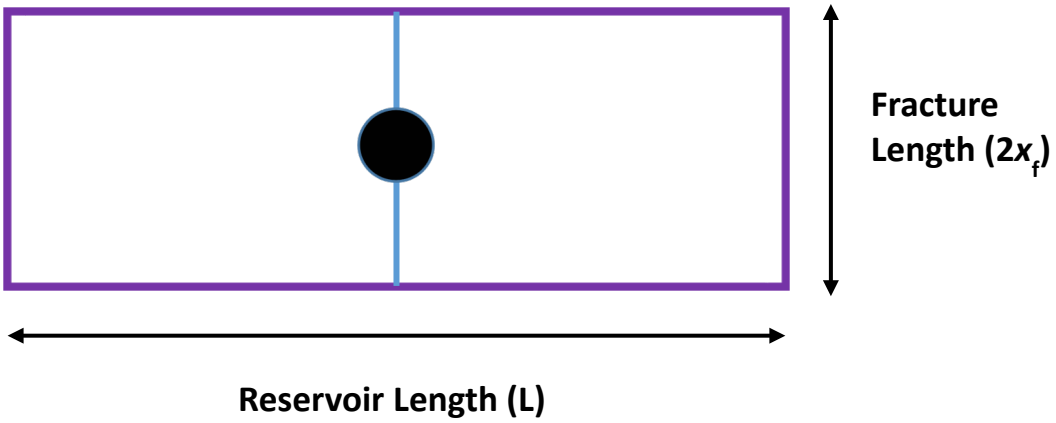

Figure 1-8- Plan view shows reservoir geometry for rate transient analysis.

The following discussion provides the necessary background to analyze production data using (rate vs. square root time) plot. In such analysis, linear flow manifests itself as straight line with an intercept that represents near wellbore effects. Diffusivity equation for flow of a slightly compressible single liquid phase in porous media with respect to time and distance can be written as follow:

$$\nabla^2 p = \frac{\varphi \mu c_t}{k} \frac{\partial p}{\partial t} \qquad (1)$$

Where:

p: Pressure

φ: Porosity

k: Permeability

μ: Viscosity

t: Time

∇^2: Laplace operator

Equation (1) was developed by applying mass balance over a control volume, transport equation (Darcy's law), and the equation of isothermal compressibility.

To obtain a solution to the diffusivity equation, two boundary conditions and one initial condition need to be imposed. The two boundary conditions are the well is producing at a constant production rate, and the reservoir behaves as infinite in size. The initial condition states that reservoir is at a uniform pressure at initial time. By considering the geometry illustrated in Figure 1-8, the constant terminal pressure solution in field units is shown below:

$$\frac{1}{q} = J\sqrt{t} + S \qquad (2)$$

Where:

q: Flow rate (STB/day)

S: Near wellbore effects such as finite conductivity, non-Darcy flow, and wellbore damage

$$J = \frac{31.3\ B}{h\ x_f\ \sqrt{k}} * \sqrt{\frac{\mu}{\varphi c_t}} * \frac{1}{p_i - p_{wf}} \qquad (3)$$

Hence, production data can be plotted as shown in Figure 1-9 to identify linear flow and to estimate time to end linear flow. Wells drilled with tight fracture spacing in relatively high permeability reservoirs will show much faster deviation from the linear

trend indicting *Intra-well interference*. Such technique can be applied to optimize fracture spacing and reduce completions cost in tight reservoirs such as the Meramec formation.

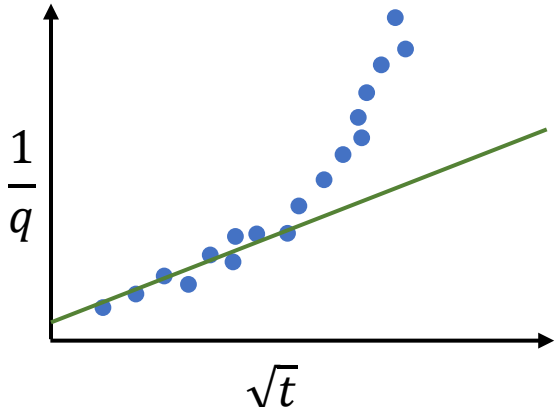

Figure 1-9- Illustration of the square root diagnostic plot used to identify linear flow regime in tight reservoirs.

By rearranging Equation (2) and taking the log of both sides, another diagnostic plot for linear flow identification can be obtained as shown below:

$$\log(q) = -\log(J) - \frac{1}{2}\log(t) \qquad (4)$$

Equation (4) demonstrates that linear flow in unconventional well can be recognized as straight line with slope of –1/2 on a log-log plot. It is worth mentioning that the existence of near wellbore effects (pseudo skin) might mask linear flow on a log-log diagnostic plot. Thus, it is recommended to divide the reciprocal of rate by drawdown and then plot the result versus square root time.

1.7 Gas-Oil Ratio as an Indicator of Interference

The profile of producing gas-oil ratio in tight oil reservoirs, such as the Meramec formation, has attracted the attention of reservoir engineers and much work has been done in an effort to understand its influencing factors. Solution gas-oil ratio is the amount of dissolved gas in the oil phase. Depending on the composition of reservoir fluid, the solution gas-oil ratio could vary from 0 for a dead oil to 3200 scf/bbl for a volatile light oil. In contrast, producing gas-oil ratio is the ratio of produced gas to oil from the wellhead.

Based on several numerical studies, (Jones, 2017) conducted the most comprehensive analysis to explain the producing gas-oil ratio trend observed from field data in the Meramec formation. The author has identified 4 stages of gas-oil ratio, and they are summarized below:

- **Stage 1:** GOR=Rsi, while FBHP is above the bubble point.
- **Stage 2:** GOR rises as FBHP declines below the bubble point.
- **Stage 3:** transient GOR plateau. When FBHP reaches a minimum and becomes constant, GOR stabilizes at a level well above Rsi, and remains there throughout transient linear flow.
- **Stage 4:** GOR rise during boundary-dominated flow, due to depletion between fractures.

Stage 4 presents an evidence that producing gas-oil ratio is sensitive to hydraulic fracture spacing such that closely spaced fractures result in steeper rise of gas-oil ratio. This behavior was modeled in detail in section 2.4. Furthermore, (Khoshghadam et al. 2017) illustrated via numerical simulation that the behavior of producing gas-oil ratio in unconventional reservoirs is related to the loss of hydraulic fracture conductivity. The product of fracture permeability and fracture width is often considered finite which means that there is no pressure drop along the hydraulic fractures, and thus pressure changes in the wellbore transfer quickly to the fractures. However, in reality, hydraulic fractures are finite conductivity conduits which means that the rise of producing gas-oil ratio could be delayed depending on the degree of conductivity.

On the other hand, (Pathak et al. 2017; Khoshghadam, Khanal, and Lee 2015) propounds the view that changes in producing gas-oil ratio of liquid rich shale plays occur because of the effect of confinement of oil phase in nano-pores. For instance, (Pathak et al. 2017) argues that the kerogen divides the oil phase into two phases which are preferred absorbed phase and less preferred free oil phase. Authors substantiate their claim by experimental analysis conducted on light sweet crude from Wyoming. The study shows a change in oil bubble point due to the presence of nano porous kerogen. Similarly, (Khoshghadam, Khanal, and Lee 2015) argue that transient GOR plateau, Stage 3 from (Jones, 2017), is caused by delayed development of multi-phase flow as a results of reduction in the bubble point pressure in nano-pores. Authors propose a correlation for

PVT properties in nano-pores based on modeling deviation in critical properties due to pore proximity effect.

Moreover, enhancement of critical gas saturation due to pore proximity influences the profile of producing gas-oil ratio observed in the field. (Chu et al. 2015) illustrated that critical gas saturation is smaller in high permeability formations due to larger pores, and thus the fraction of pores needed to be occupied by gas molecules is much smaller. Conversely, lower permeability reservoirs with smaller pore throats, need higher critical gas saturation to establish a continuous flow path. The effect of critical gas saturation on producing gas-oil ratio was modeled in section 2.8.

1.8 Dual-Permeability and Dual-Porosity Paradigms

Dual-permeability and dual-porosity approaches represent two distinct modeling paradigms to model naturally fractured reservoirs. Dual-porosity approach assumes natural fractures have significantly higher permeability and lower porosity than the matrix. During well production, hydrocarbon flows within the permeable natural fractures to the wellbore. Once the natural fractures are drained, petroleum fluid starts to flow from matrix to nearby natural fractures. All the fluid is transported to the wellbore via natural fractures. In contrast, dual-permeability approach allows the possibility of hydrocarbon flow through the matrix. Thus, dual-permeability approach allows fluid flow to the wellbore directly from the matrix without the need for natural fractures. Interference simulations presented in this dissertation have utilized both single and dual permeability-porosity approaches.

1.9 Dissertation Layout

Supported by field data, Chapter 2 presents a compelling case regarding the impact of intra-well interference from operations, and financial perspectives. Chapter 3 presents a multi-well simulation that explains child-parent interactions and develops numerical technique to diagnose inter-well interference. Chapter 4 sheds light on the importance of transport properties to well interference and presents a novel method to compute tortuosity from SEM images via finite-volume method. Finally, Chapter 5 presents key takeaways from this research and provides recommendations that will benefit practicing reservoir and completions engineers who are interested in optimizing well-spacing and completions designs to maximize the value of tight oil reservoirs.

Chapter 2: Modeling of Intra-Well Interference

Intra-well interference is primarily associated with fracture spacing and treatment efficiency along the lateral of the well. As discussed in Chapter 1, very small fracture spacing results in higher completions cost, whereas very large fracture spacing leads to inefficient oil recovery which is detrimental to the economics of the well. Additionally, completions cost is directly proportional to the number of stages. Thus, reducing the number of stages leads to significant cost savings. However, it much more challenging to efficiently treat longer stages and hence the effect of dominant fractures is often amplified. The following analyses will utilize production data from a Meramec well to identify its optimal cluster spacing. In addition, the effect of drawdown on well performance will be investigated. One of the limitations of these analyses that they assume uniform fracture height and length along the lateral. This limitation is addressed in Chapter 3.

2.1 Well Overview

A Meramec well was drilled in Kingfisher county in Oklahoma and the lateral was fully landed in the Meramec formation. It was kicked off at 9600 ft true vertical depth with 4700 ft effective lateral length. The entire lateral was completed successfully using plug and per method. The well came online in summer 2016 with initial oil rates above

1000 stb/day and initial gas oil ratio of 3000 scf/bbl (volatile oil system). The well has a unique production profile because it is unbounded by other wells and it has more than two years of continuous production without being disturbed by offset operations. Due to extensive appraisal and development efforts in the area, production rates and pressures of most wells are affected by offset activities which makes it difficult to analyze the signature of intra-well interference. Therefore, this well represents an excellent opportunity extract useful insights on optimal fracture spacing and drawdown strategies in the Meramec formation.

Regarding pressure data, casing and tubing pressures were recorded via surface gauges. Hagedorn and Brown correlation was used for pressure loss calculations. True vertical depth was used to calculate pressure drop due to hydrostatic head whereas the entire pipe length was used to compute friction losses. Figures 2-1 to 2-6 present normalized daily rates (normalized due to data confidentiality), calculated bottom-hole pressure, gas-oil ratio, and water-oil ratio. Normalized monthly averages are shown as well.

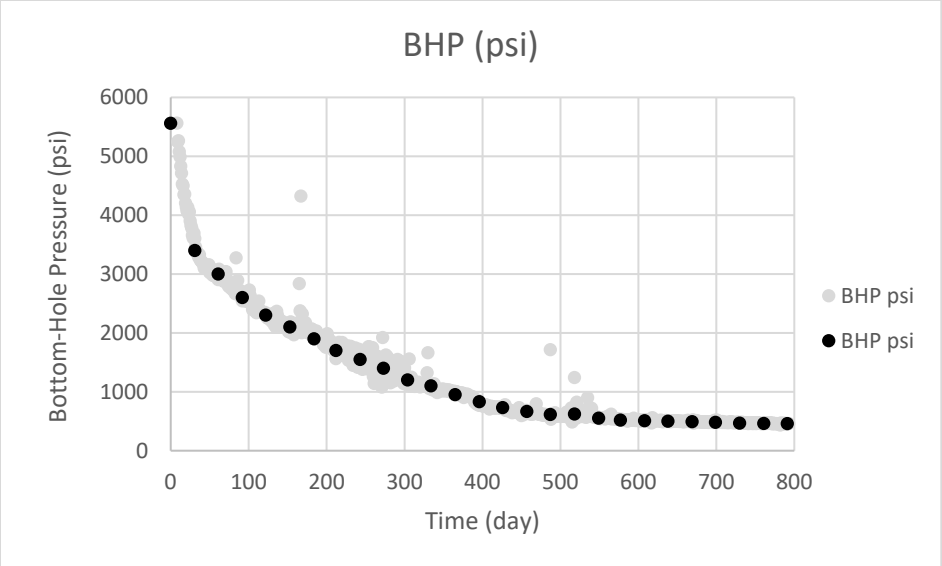

Figure 2-1- Calculated flowing bottom-hole pressure.

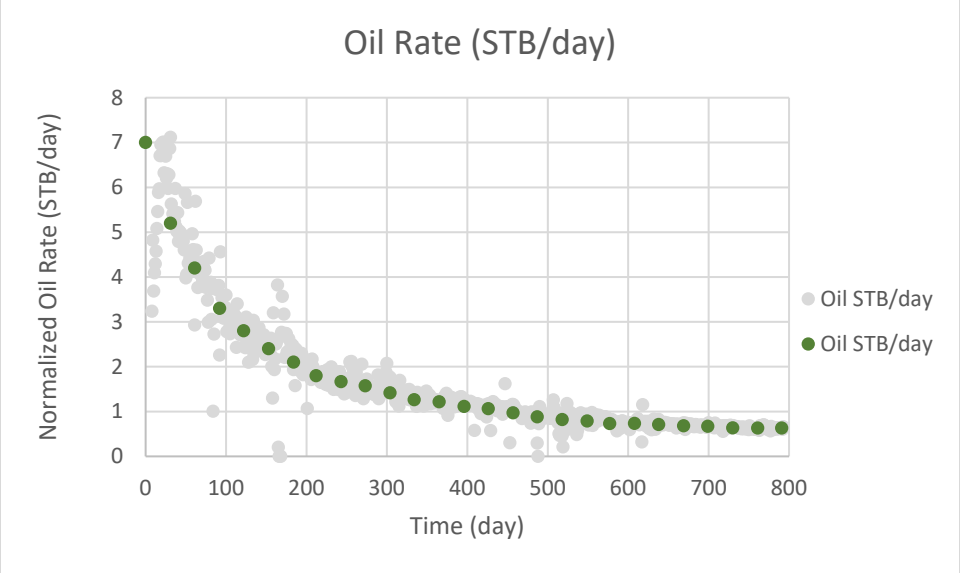

Figure 2-2- Normalized daily and monthly oil rate production.

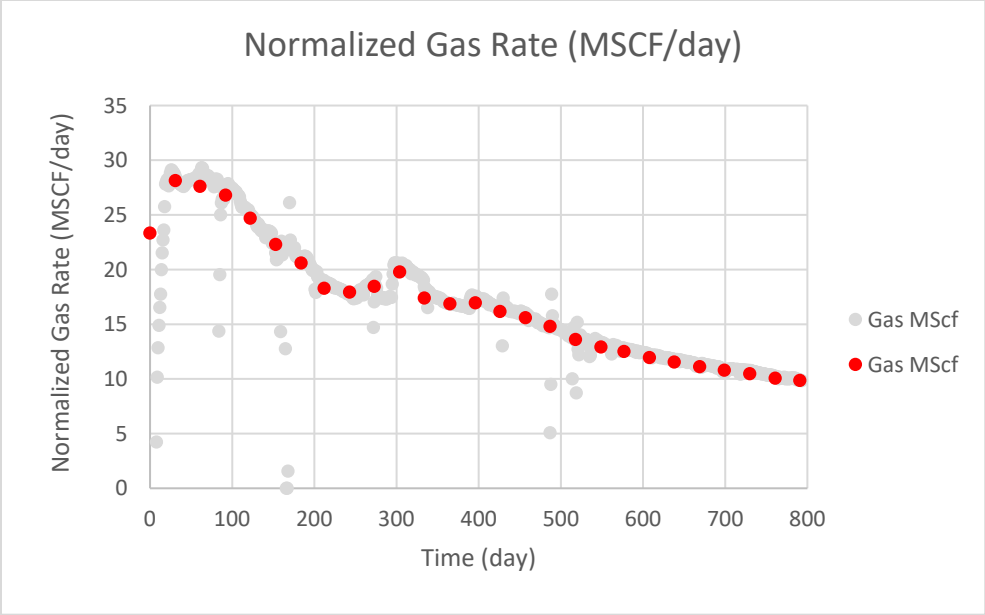

Figure 2-3- Normalized gas rate production.

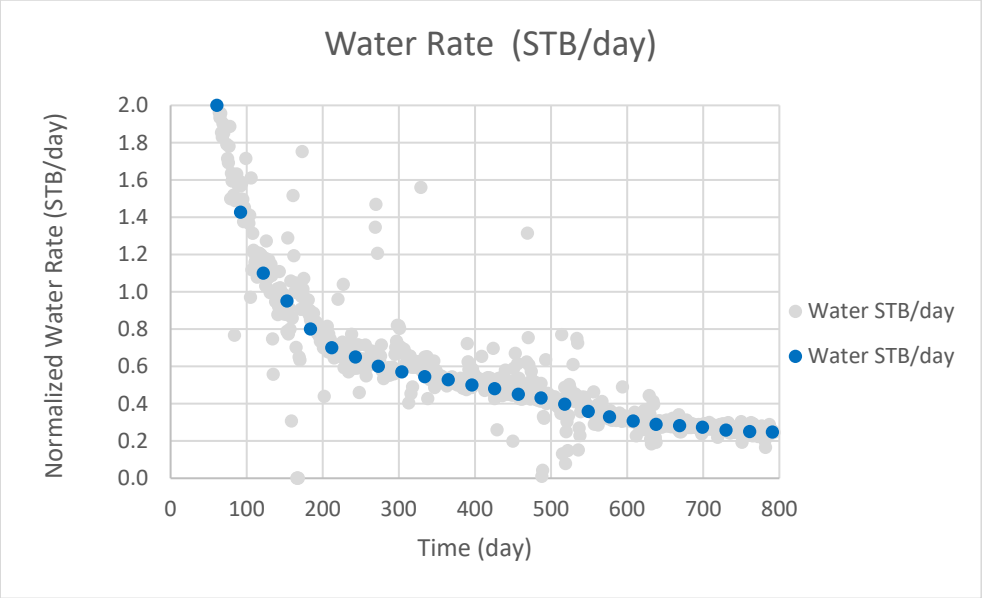

Figure 2-4- Normalized water rate production.

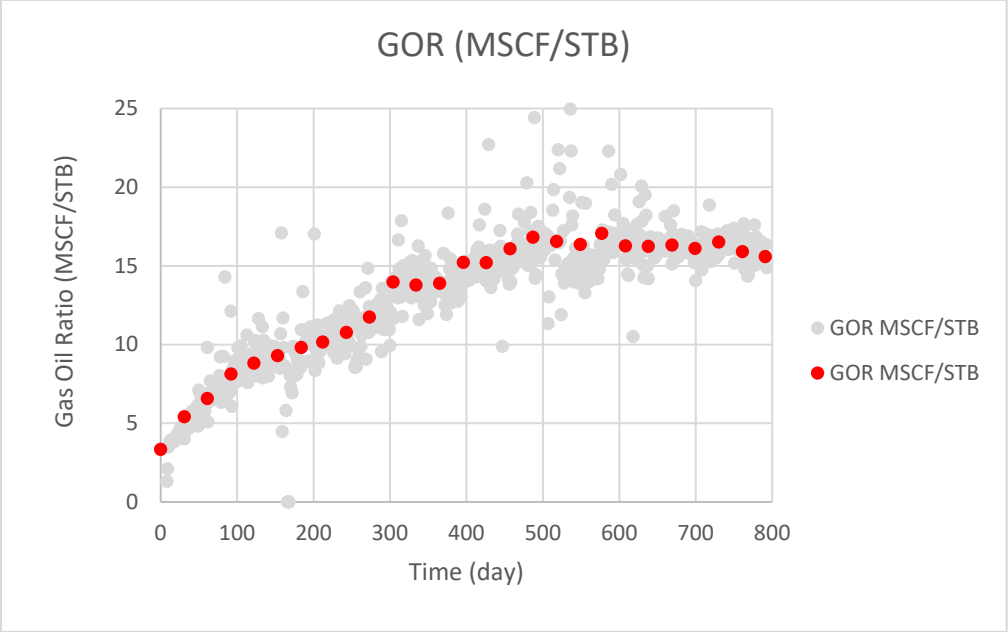

Figure 2-5- Producing gas-oil ratio.

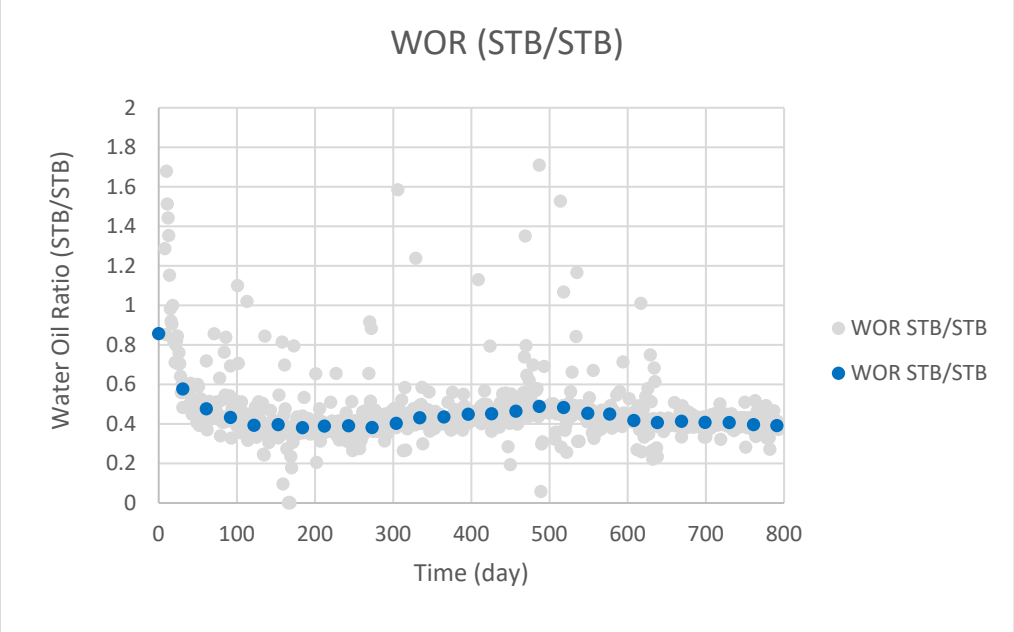

Figure 2-6- Water-oil ratio.

2.2 Fluid Characterization

Field data were not available to analyze the phase behavior of the petroleum fluid in the Meramec. Hence, (Velarde et al., 1997) correlation was used to predict fluid properties as function of pressure. Chapter 3 provides detailed fluid characterization based on a fluid sample collected from the field. Furthermore, (Beggs and Robinson, 1975) correlation was used to predict crude viscosity due to pressure change. Figure 2-7, Figure 2-8, and Figure 2-9 present solution gas-oil ratio, oil formation volume factor, density, and viscosity.

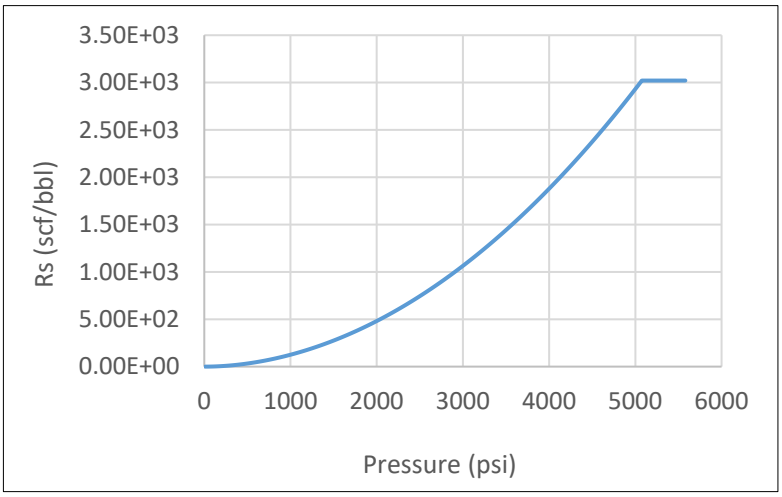

Figure 2-7- Solution gas oil ratio.

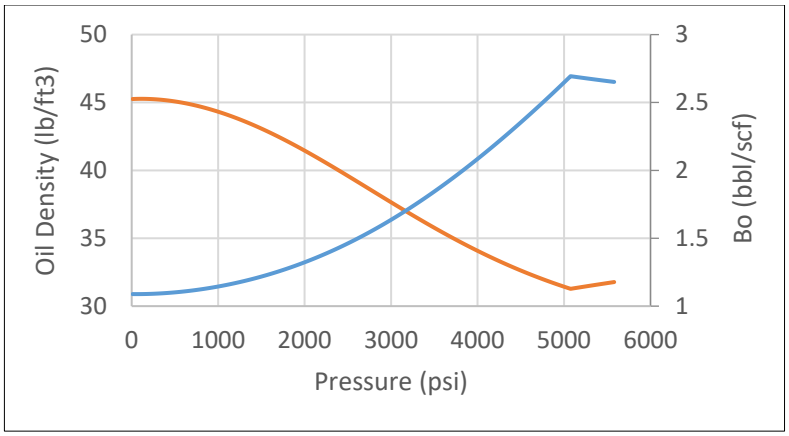

Figure 2-8- Oil formation volume factor and density.

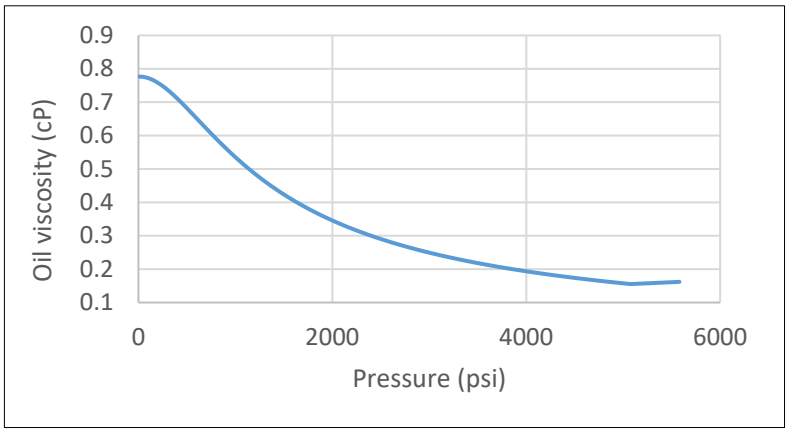

Figure 2-9- Oil viscosity.

2.3 Model Setup

Available geologic data were integrated to construct a geologic model. The static model covers an area of 640 acres that encompasses a multi-stage hydraulically fractured horizontal well. Single fracture was modeled as element of symmetry as shown in Figure 2-10. The no flow boundary was adjusted based on completions efficiency while the reservoir width was chosen to be one mile. The reservoir encompasses four major geologic units which are Woodford, Osage, Meramec and Chester. The well was landed

in the Meramec formation, as shown in Figure 2-11, and it was placed along the J direction and perpendicular to the I direction. The static model consists of a global grid and a local grid that represents the hydraulic fracture. The average cell size of the global grid in the K direction is 19 ft and 10 ft for the I and J directions.

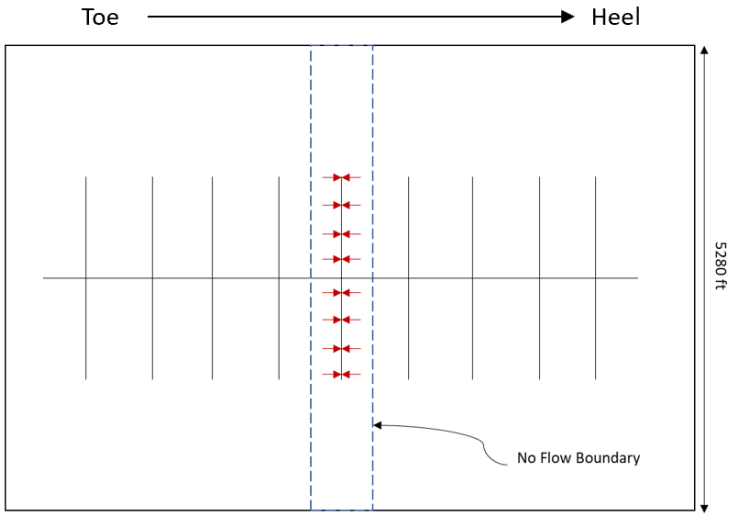

Figure 2-10- Plan view of a schematic that shows the horizontal well along with hydraulic fractures. Red arrows illustrate fluid flow normal to the fracture face.

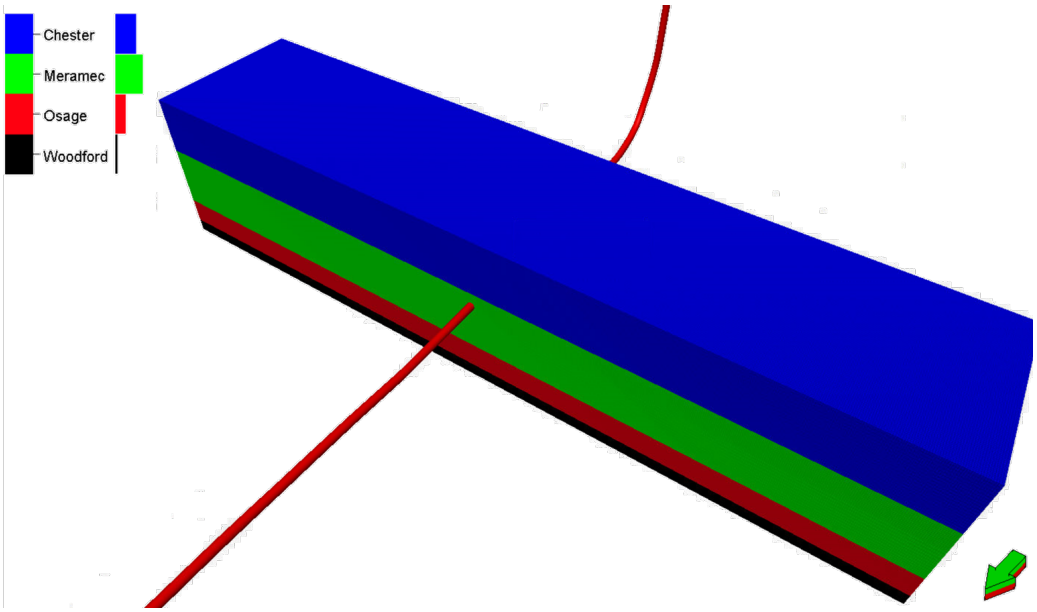

Figure 2-11- 3D view shows geologic units within the model along with the horizontal wellbore.

The local grid was logarithmically refined along the J direction. The host cell was refined into three cells in the I direction, 3.3 ft each. Refinement was not applied for the K direction. The fracture width was set to 0.5 ft. Figure 2-12 illustrates the three regions that constitute the reservoir model. Those regions were used to assign different permeability values within the reservoir. Region 1 represents the hydraulic fracture, Region 2 represents enhanced permeability zone due to fracturing, and Region 3 represents the matrix prior to hydraulic fracturing. It is worth mentioning that it is difficult to validate the existence and the thickness of the enhanced region. The enhanced region might be necessary in certain unconventional wells to obtain a history match. However, in this case, history-match was achieved without invoking enhanced permeability region. In other words, regions 2, and 3 have a similar permeability value.

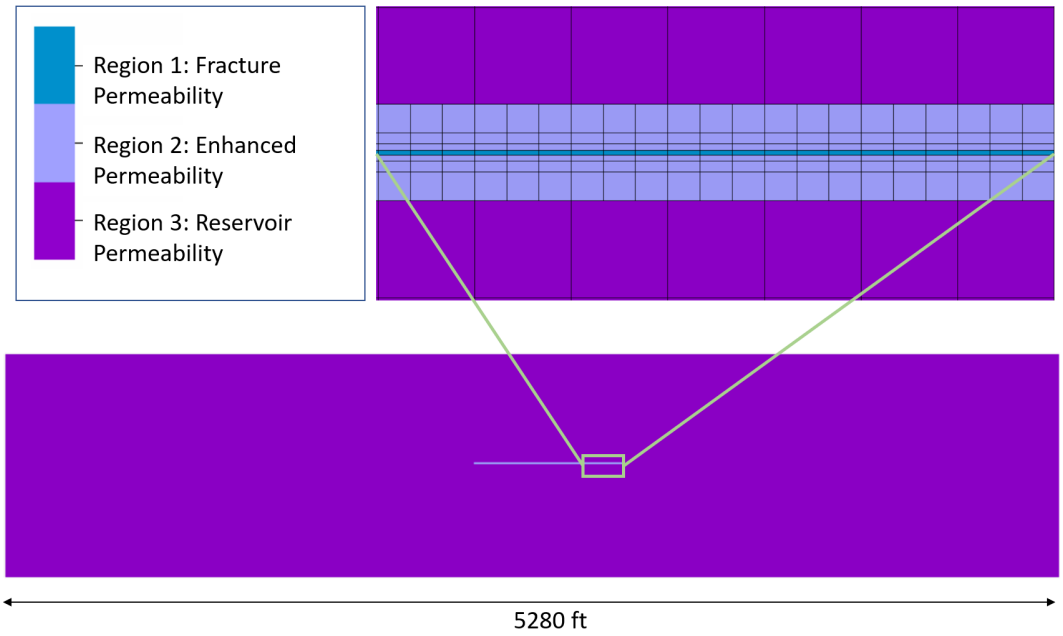

Figure 2-12- Plan view shows reservoir and fracture cells with a zoomed view to show the different regions within the reservoir model and logarithmic refinement along the J direction

Regarding reservoir pressure, the reservoir fluid is undersaturated with initial pore pressure gradient, estimated from DIFT data, of 0.66 psi/ft. Relative permeability is a critical property to predict well performance. However, it is difficult to measure in tight oil reservoirs. Relative permeability ends points and exponents were obtained from history matching the production data as it will be illustrated in the next section.

2.4 History Matching Results

History match was obtained to three-phase production and flowing bottom-hole pressure as shown in Figure 2-13. The simulator was constrained to produce total

reservoir fluid. Obviously, the history match parameters are non-unique and there could be other scenarios that equally fit the observed field data. However, this realization aligns well with other simulation studies conducted within the same area of interest.

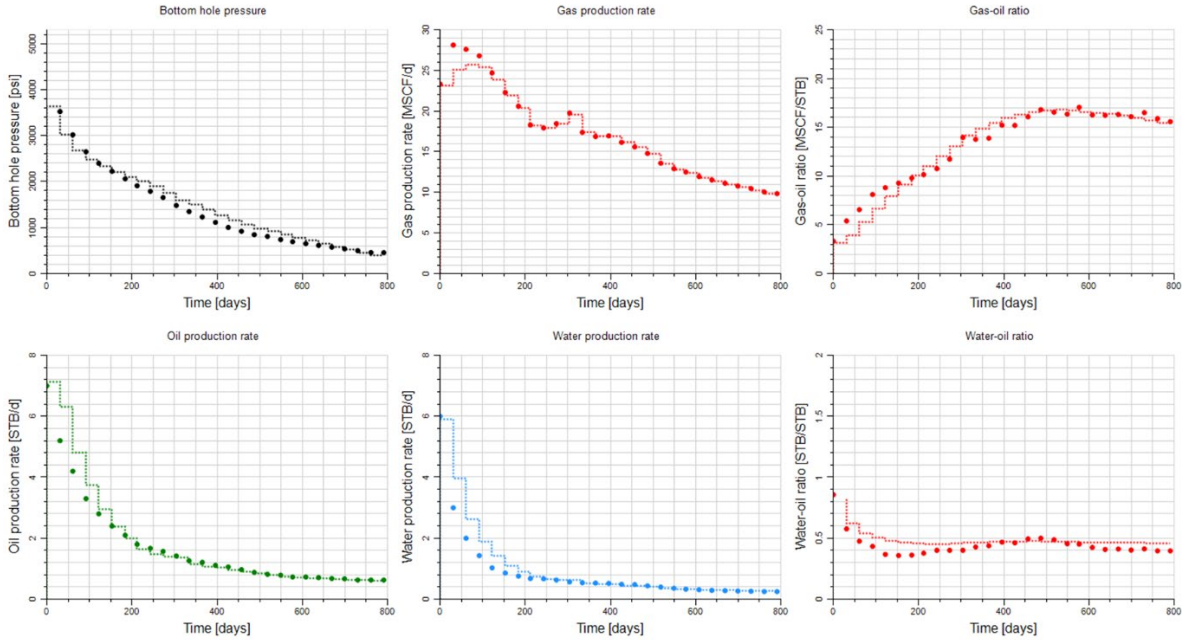

Figure 2-13- Simulated versus observed values. Line represents simulation results whereas dots represent observed field data.

Table 1 presents three phase relative permeability parameters used to achieve the history match, whereas Table 2 and 3 present reservoir and hydraulic fracture parameters. Permeabilities in the I and J directions were set to be equal. Permeability in the K direction was set to be one sixth of permeability in the I direction.

Table 1- History match relative permeability parameters.

Critical Gas Saturation	0.07	**Sorw**	0.175	**Swmin**	0.25
Corey gas	3.8	**Sorg**	0.175	**Swcr**	0.25

Krg@Swmin	1	**Corey O/W**	2	**Corey water**	2.6
Krg@Sorg	1	**Corey O/G**	2	**Krw@Sorw**	0.8
		Kro@Somax	1	**Kr@S=1**	0.8

Table 2- Petrophysical properties.

Geologic Units	Perm I (mD)	Phi (fraction)	Sw (fraction)
Chester	0.0005	0.01	0.8
Meramec	0.001	0.04	0.35
Osage	0.0005	0.024	0.35
Woodford	0.0005	0.045	0.1

Table 3- Reservoir and hydraulic fracture properties.

Initial Reservoir Pressure (psia)	5580
Bubble Point Pressure (psia)	5000
Contacted Height (ft)	170
Fracture Half Length (ft)	365

Reduction in hydraulic fracture conductivity was modeled by reducing the hydraulic fracture flow capacity (K_f*W_f) based on the exponential function shown in Figure 2-14. Detailed discussion on modeling loss of hydraulic fracture conductivity is presented in section 2.8.1.

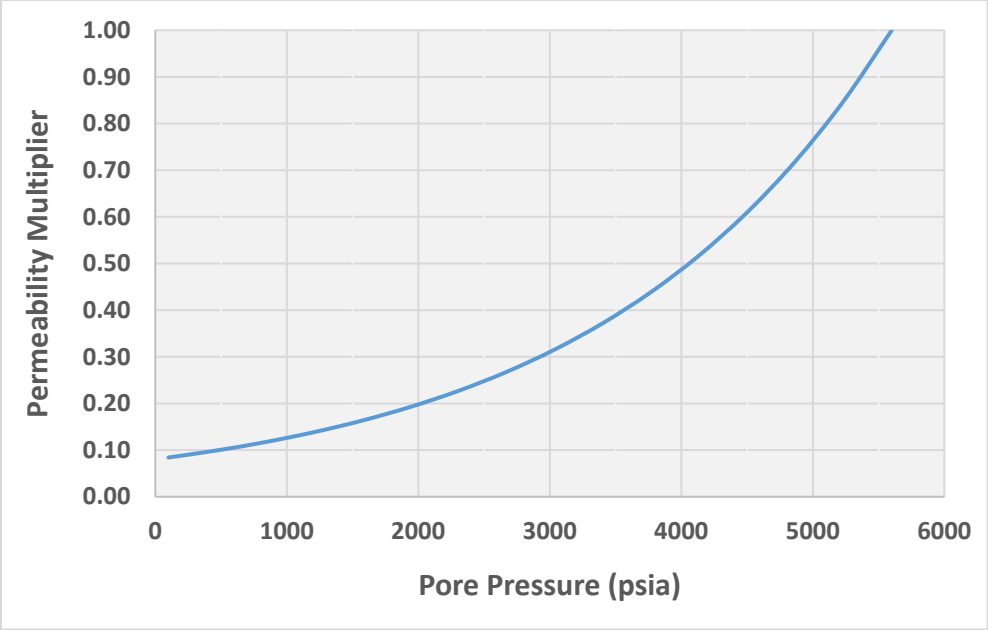

Figure 2-14- Pressure dependent permeability in the hydraulic fracture.

Now that the reservoir model has been calibrated to honor production data, completions, and petrophysical properties, the following will be investigated to understand intra-well interference:

- The performance of the well under varying cluster spacing (fracture spacing)
- The relationship (if any) between producing gas-oil ratio and cluster spacing
- The relative contribution of reservoir characteristics and completions parameters on short and long term well performance. In other words, an attempt will be made to answer the question of *where does the importance of fracture spacing rank relative to other variables?*

2.5 Cluster Spacing Impact on Well Performance

One of the primary objectives in the development of unconventional assets is to identify optimal perforation cluster spacing needed to complete an unconventional well. The most straight-forward and decisive technique to optimize cluster spacing involves fields trials in which statistically significant number of wells are needed to be drilled, completed, and production is monitored for at least 6 months to determine which cluster spacing is the most effective. Clearly, this approach is time and capital intensive. In this section, numerical approach will be used instead. Numerical models were constructed with varying cluster spacing, then directed sensitives were run to evaluate long and short term well performance. Figure 2-15 presents three models with 30 ft, 50 ft, and 90 ft cluster spacing. The models were produced under similar BHP schedule for 30 years without considering artificial-lift mechanisms during the life of the well.

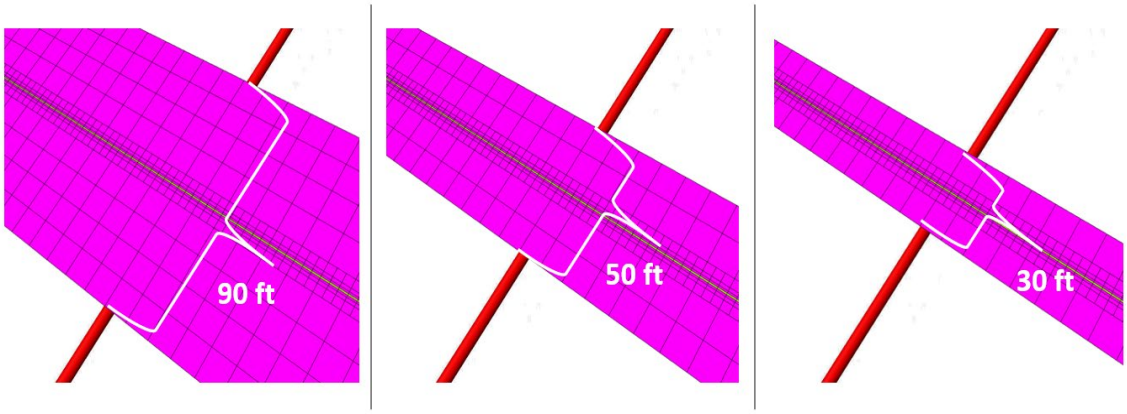

Figure 2-15- 3D models with varying hydraulic fracture spacing.

Figures 2-13, 2-14, and 2-15 presents profiles of oil rate, cumulative oil production, and gas-oil ratio respectively.

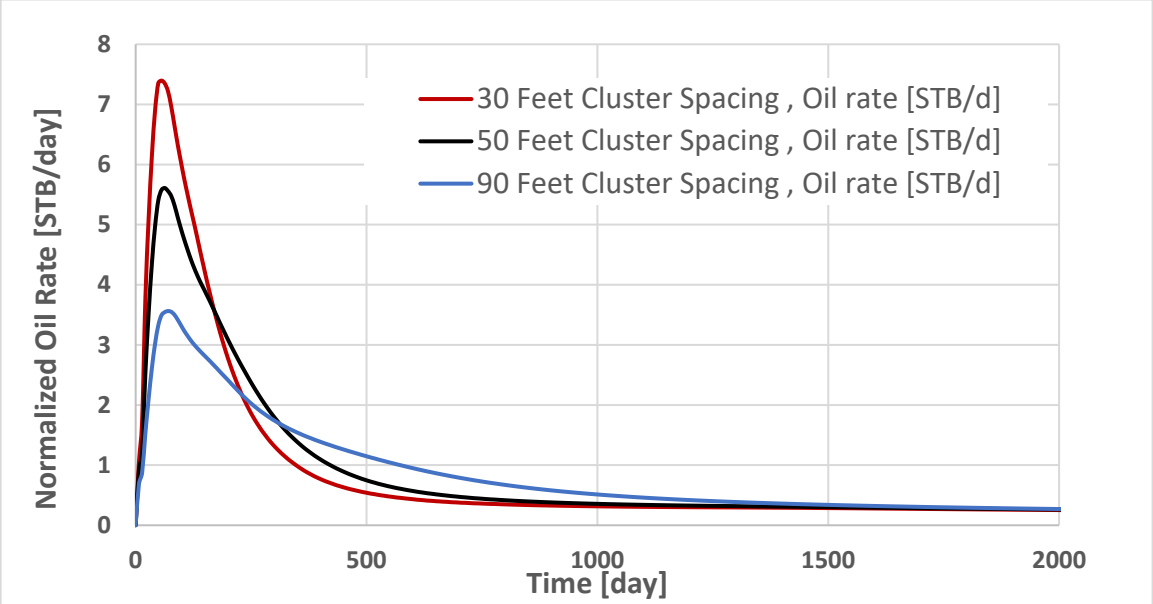

Figure 2-16- Oil rate profiles for different cluster spacing.

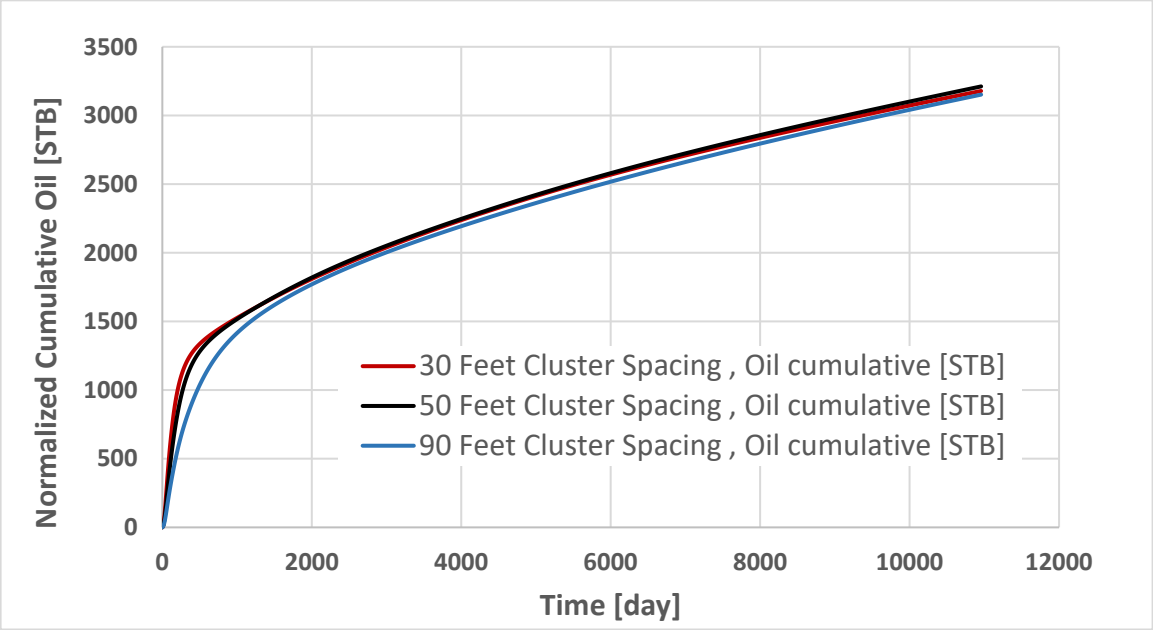

Figure 2-17- Oil cumulative production for different cluster spacing.

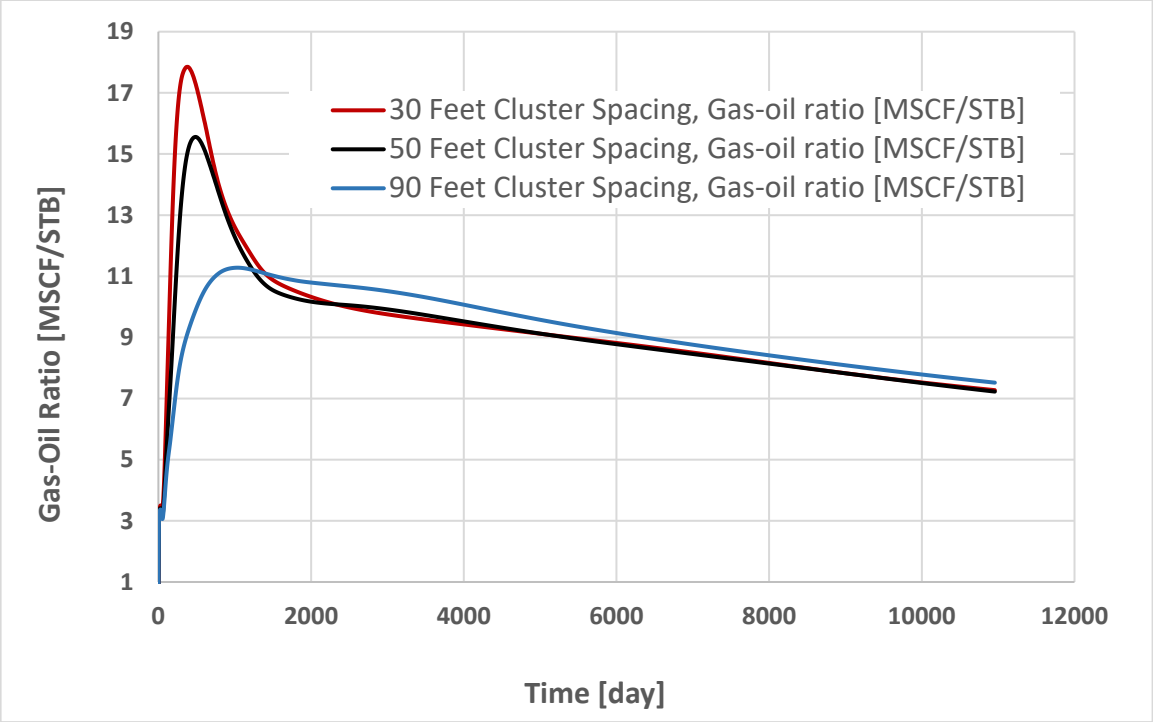

Figure 2-18- Producing gas-oil ratio for different cluster spacing.

Normalized oil rate graph clearly illustrates that tighter cluster spacing results in higher initial oil production rates. Higher number of fractures (tighter cluster spacing) means larger surface area and thus the higher initial productivity due higher number of fractures per lateral length. However, the expected ultimate oil recovery is very comparable between the three scenarios as illustrated in Figure 2-17. Looking at the gas-oil ratio, closely spaced fractures have steeper gas-oil ratio rise. Once the pressure wave reaches the boundary (boundary dominated flow), the pressure begins to decline at a constant rate, and the average gas saturation increases which causes producing gas-oil ratio to increase. Gas-oil ratio results are well aligned with observations from (Jones, 2017).

2.6 Investigation of the Effect of Drawdown Strategy on Well Performance

Most of the efforts in the unconventional space have been focused on identifying sweet spots and optimizing completions designs. However, understanding how to operate the well is equally important to develop unconventional resources economically. “Choke management” and “drawdown strategy” are often used interchangeably to describe the practice of regulating fluid flow. A choke is a mechanical device that is integrated in the wellhead equipment. It is designed to regulate fluid flow by changing the flow area. Choke management is often implemented during the initial life of the well, which is known as the flowback period. Researchers are in alignment that aggressive drawdown strategies can be detrimental to well performance. Aggressive drawdown strategies lead to excessive effective stress on the fracture face due to rapid pore pressure depletion. Higher effective stresses lead to several geomechanical issues as discussed by (Rojas and Lerza 2018; Almasoodi, Abousleiman, and Hoang 2014). Despite the loss of hydraulic fracture conductivity and the potential to drop below the saturation pressure much faster than desired, some operators choose to adopt aggressive choke management approach to chase business goals such as quarterly volumes, higher rate of return, or both.

In order to methodically investigate the implications of aggressive and conservative drawdown strategies on well performance, three drawdown schedules were constructed (aggressive, managed, and conservative). The history-matched model was used to

investigate oil and gas production profiles and the economics associated with them. Figure 2-19 present number of days to deplete 50% of initial reservoir pressure such that 80, 160, and 320 days correspond to conservative, managed, and conservative drawdown managements respectively. Figure 2-20 presents functions of exponential decay that were used to model bottom-hole pressure schedules to mimic different drawdown strategies.

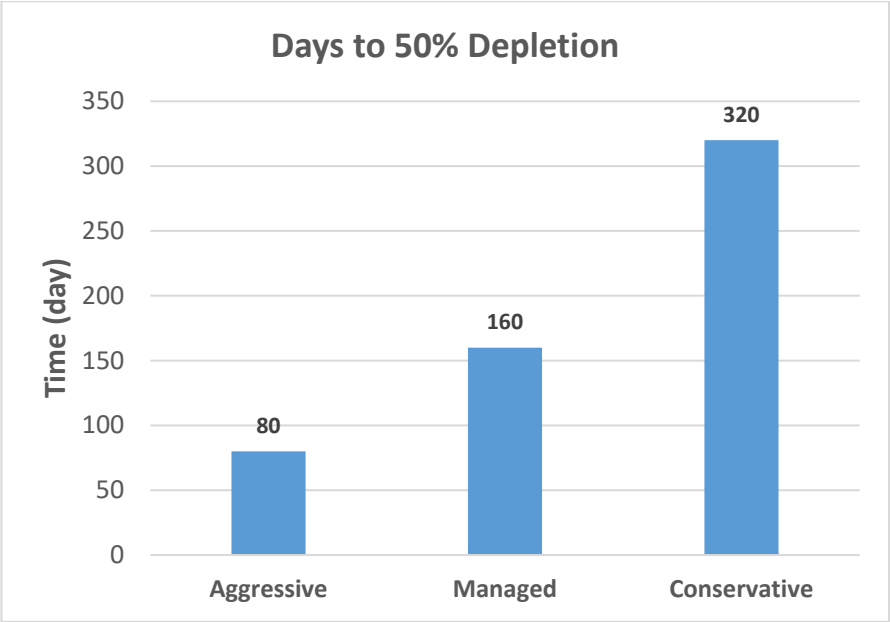

Figure 2-19- Time to reduce the initial reservoir pressure by 50%.

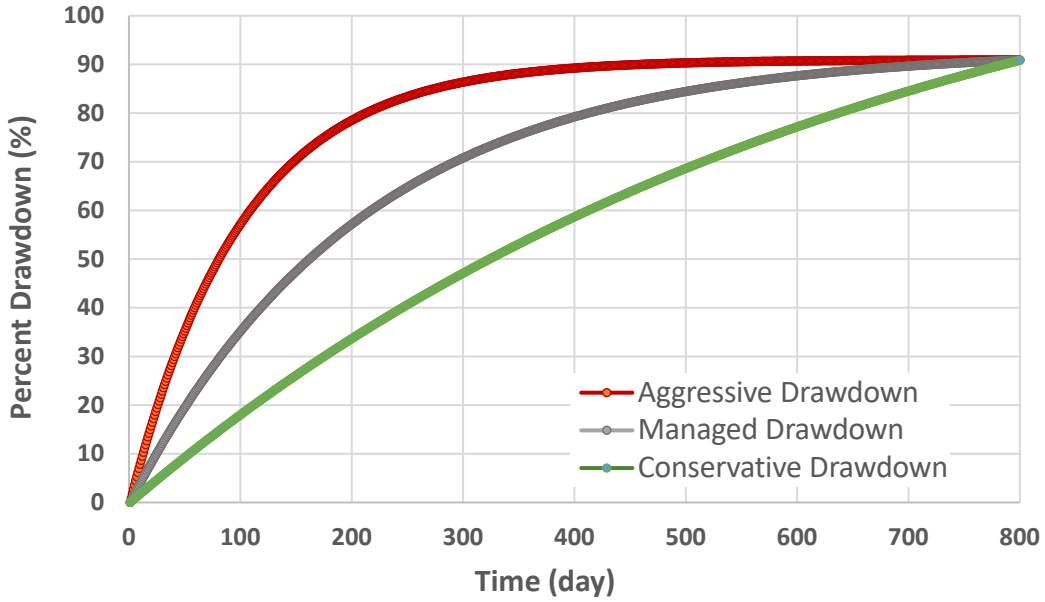

Figure 2-20- Percent drawdown for different BHP schedules.

Results show lower initial oil rates for conservative drawdown and similar oil EUR as illustrated in Figure 2-21 shown below. Thus, based on these results, both capital budgeting metrics, ROR and NPV, favor the aggressive drawdown strategy. This is mainly due the concept of the time value of money by which oil volumes (cash inflows) available at the present time worth more than the identical sum in the future due to their earning potential. According to (Quintero and Devegowda 2015), the most optimal drawdown strategy depends on the largest choke setting from initial flowback. Authors claim that high initial production rates will overshadow the subsequent rapid rate declines. In the next section, the validity of this claim will be examined from both geomechanics and economics viewpoints.

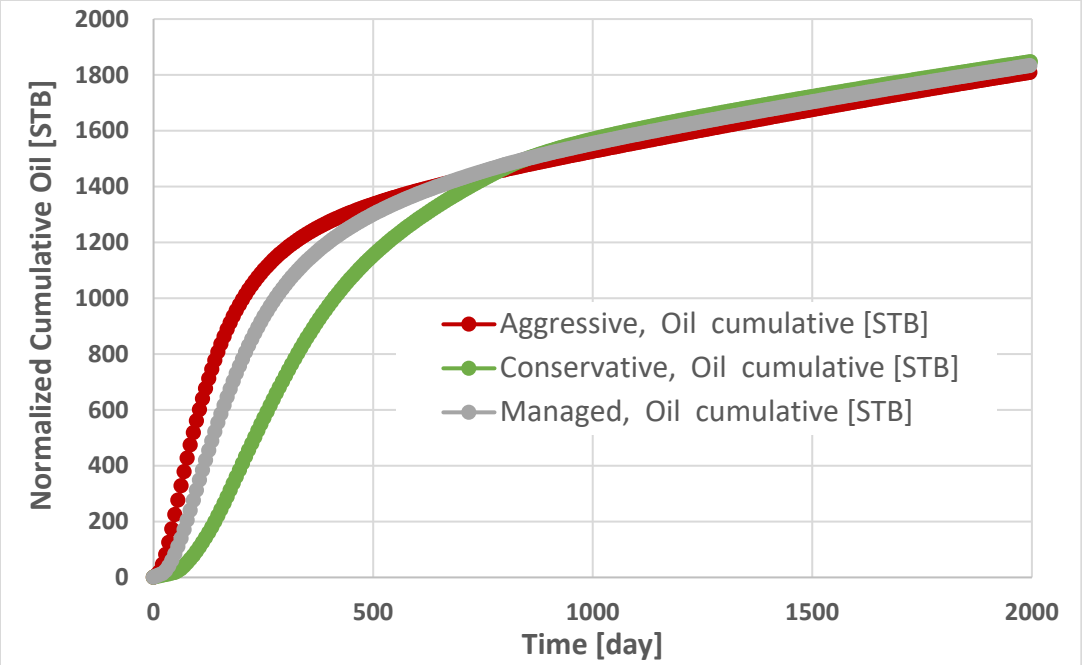

Figure 2-21- Normalized cumulative oil production for different drawdown schedules.

2.7 Practical Approach to Couple Loss of Hydraulic Fracture Conductivity with Choke Management

By examining the rate decline of hundred wells in Vaca Muerta shale, (Rojas and Lerza 2018) reported more that 20% EUR loss due to aggressive choke management. Authors provide compelling evidence of production dependence on drawdown management based on empirical data of horizonal wells in Loma Campana Oilfield. The primary objective of this section is to understand the interplay between the optimal cluster spacing, financial benefit due to production acceleration, and loss of reserves as result of hydraulic fracture conductivity degradation.

More than 40 multi-stage hydraulically fractured horizontal wells were used to identify wells with aggressive and conservative drawdown strategies based on percent drawdown. Subsequently, only pairs of comparable completions and reservoir characteristics were selected to be forecasted using decline curve analysis. Those characteristics include initial gas-oil ratio, landing zone, cluster spacing, proppant per foot, and total fluid per foot. The well pairs were then forecasted methodically via decline curve analysis by using similar b factor, terminal decline, and final rate. It is important to mention that the analysis has only included parent wells to eliminate the effect of well-spacing due to infill operations. Results show loss of oil EUR of more than 10% due to aggressive choke management in the Meramec formation. Also, based on the limited data, it appears that percent of EUR loss is more pronounced in wells with closely spaced fractures. In order to incorporate findings about oil EUR degradation from field observations explained earlier, two aspects need to be considered which are:

1. The Definition of aggressive versus conservative drawdown. In simple words, what dictates aggressive drawdown?
2. The construction of geomechanical model that couples drawdown strategy with loss of EUR.

To address the aspects outlined above, flowing bottom-hole pressure (FBHP) was calculated from surface tubing and casing wellhead pressures (WHP). Drawdown percent was then calculated for more than 15 horizontal wells from the same area of the history matched well. Percent drawdown was then plotted versus normalized time for each well

for the first four months. Time was needed to be normalized because the wells came online at different times. Figure 2-22 presents percent drawdown versus normalized time and it is a manifestation of the effect of various choke settings. The data presented in Figure 2-22 shows a wide range of pressure drawdown ranging from 30%-65% after 4 months of production. By capitalizing on this variability, upper and lower bounds of drawdown were constructed as shown in Figure 2-23. Those bounds were extrapolated to reach 500 psi of terminal pressure (90% drawdown) as shown in Figure 2-24 to be used to simulate production rates. Now that aggressive and conservative drawdown managements have been defined based on actual field data, hydraulic fracture conductivity need to be degraded in the aggressive scenario to mimic oil EUR degradation of 10%. Figure 2-25 presents hydraulic fracture multiplier based on the model shown in equation (5) to model the loss of hydraulic fracture conductivity due to pressure depletion.

$$k = k_i e^{-\gamma(P_i - P_{wf})} \qquad (5)$$

Where k is the hydraulic fracture permeability, k_i is the initial fracture permeability, γ value is obtained by trial and error via several simulations to match 10% loss of EUR based on observed field data, P_i is the initial reservoir pressure, and P_{wf} is the flowing bottom-hole pressure. The model may not explain the complex downhole physics, changes in effective stresses due to depletion and the subsequent fracture width reduction, or the fracture reduction due fine migration due to detachment from the fracture face. However, it is practical and easy to implement after being calibrated to field observations.

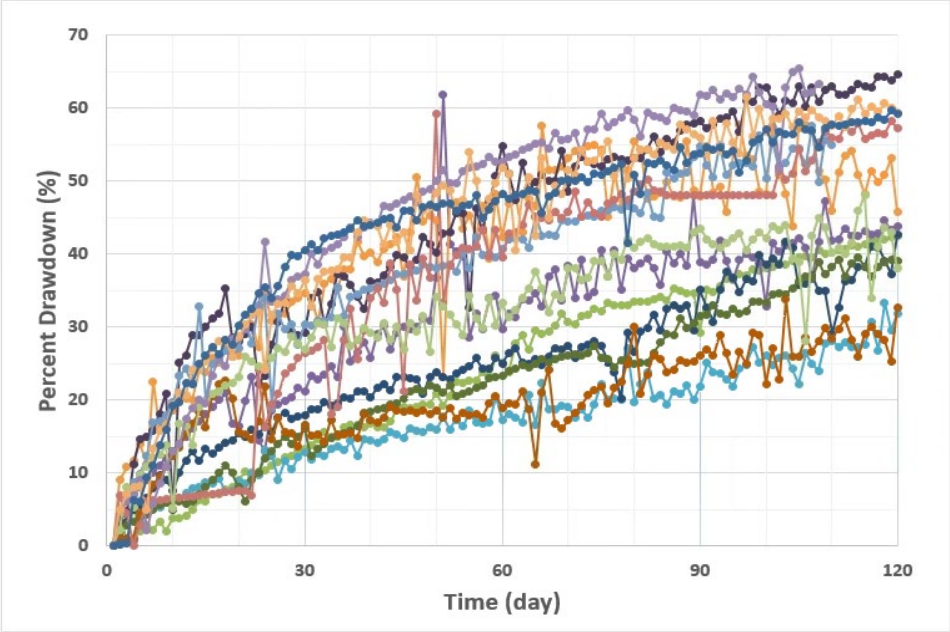

Figure 2-22- Normalized percent drawdown from various wells within the study area of the history matched well.

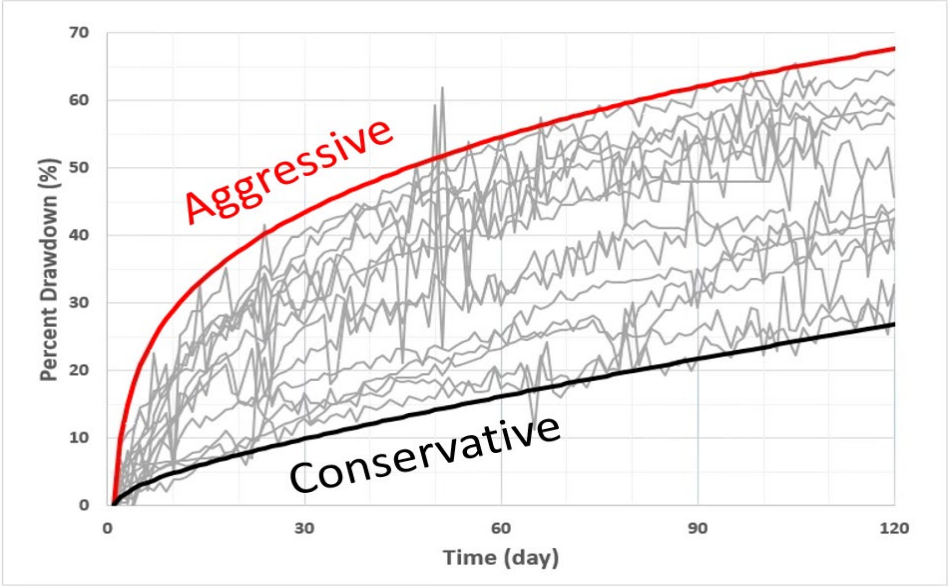

Figure 2-23- Upper and lower bounds of drawdown based on field observations. Red and black profiles represent aggressive and conservative drawdowns respectively.

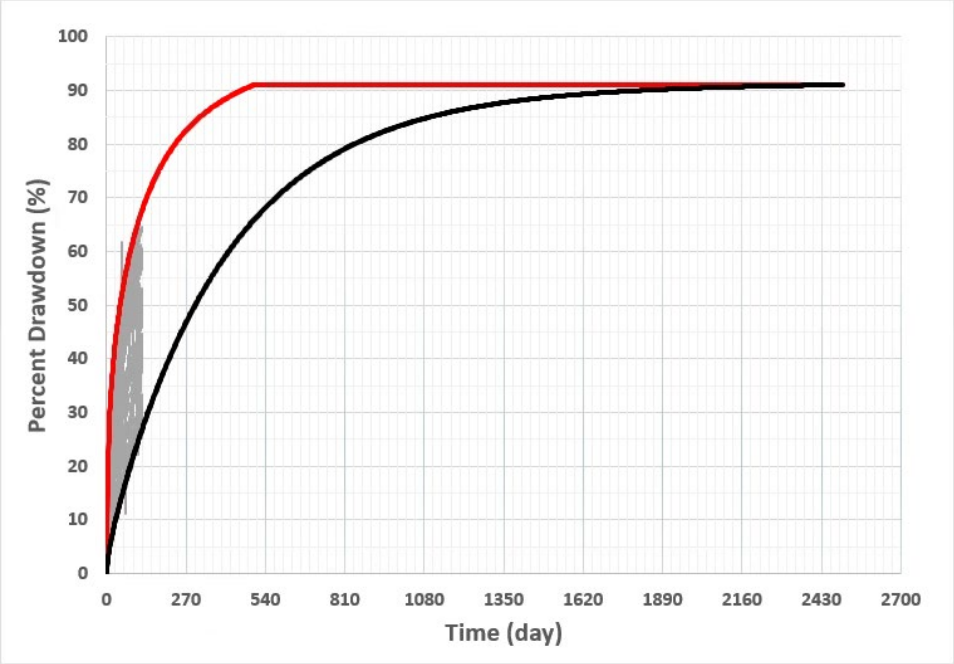

Figure 2-24- Upper and lower drawdown schedules.

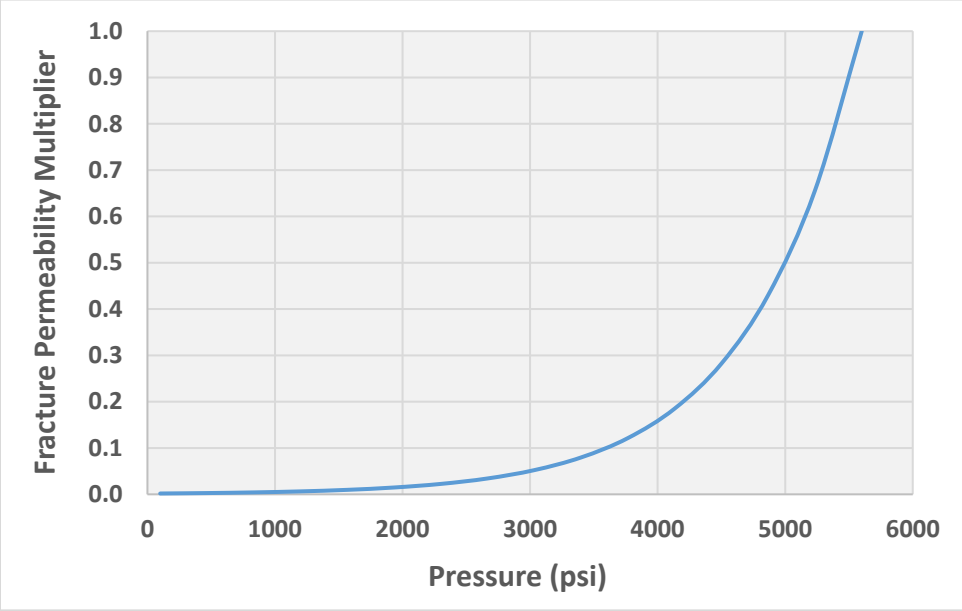

Figure 2-25- Loss of hydraulic fracture conductivity due to pressure depletion.

2.8 Modeling the Economics of Drawdown Management and Fracture Spacing

The results of the most aggressive and most conservative drawdowns are shown in Figure 2-26. Results clearly show higher initial rates associated with steeper decline due to loss of hydraulic fracture conductivity. Additionally, results show the 10% reduction in oil EUR as illustrated by the normalized cumulative oil production on the secondary vertical axis. Next, the interplay between higher initial rates and loss of long-term performance will be evaluated. It is important to mention that the 10% oil EUR loss is on the conservative side.

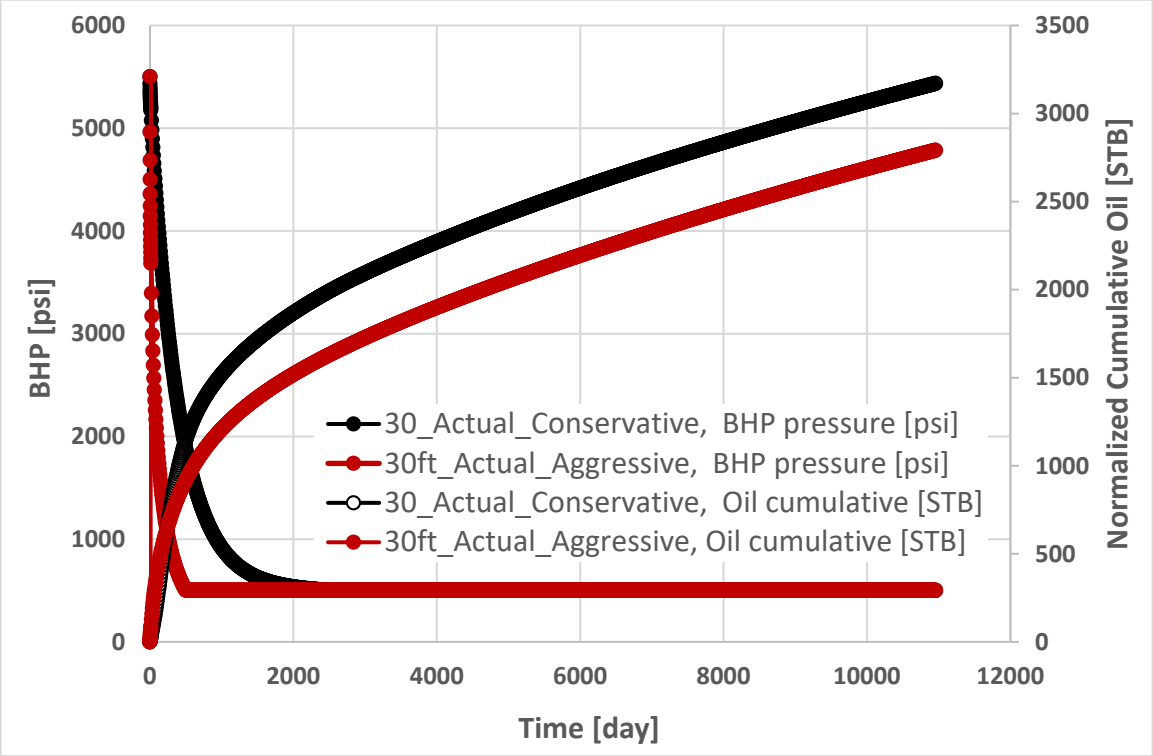

Figure 2-26- Oil production based on based on upper and lower drawdown bounds.

Economic assumptions can have large impact of the results and thus significant time was spent to ensure the accuracy of the economic model. Although the details are not stated, constant costs such as drilling, and completions were considered. Gas shrinkage and yield were modeled based on historical data. Rate of return and net present value discounted at predetermined hurdle rate will be the economic metrics used in this analysis.

Table 4 - Comparison of the economics of aggressive and conservative drawdown.

30 ft Fracture Spacing		
	Conservative	Aggressive with Compaction
NPV ($)	$ 1	$ 0.81
ROR (%)	1.00	1.06
Oil EUR (MSTB)	1	0.88
Gas EUR (BSCF)	1.0	0.89

Oil and gas monthly volume generated by aggressive and conservative drawdowns from 30 ft fracture spacing model were run under the same economics model. Gross gas volumes were converted to net volumes by considering the shrunk gas volumes. Monthly NGL volumes were calculated by incorporating the yield rate. Based on predetermined price deck for oil, gas, and NGL, the total revenue was computed and then converted into cash flows. Table 4 presents a comparison between the two cases. Results show the short-term gain in rate of return due to aggressive drawdown is immaterial in comparison to 19% loss in net present value. Results shed light on the interaction between the choice of choke operations and pricing environment. Figure 2-27 shows the rate of return gain and the corresponding net present value loss due to aggressive choke management under various oil pricing environments. At higher oil prices loss of net

present value is less important relative to gains in rate of return. Those analyses do not take into account potential drilling and completions costs escalation due to oil price increase.

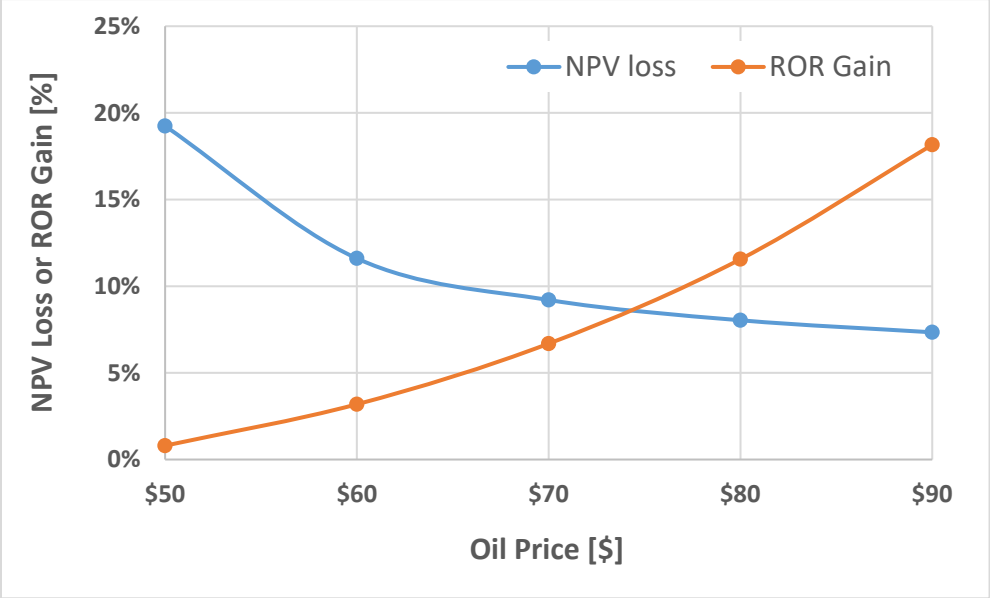

Figure 2-27- NPV loss and ROR gain from normalized to the conservative scenario as function of oil price.

Furthermore, four additional cases were created based on 50 ft and 90 ft fracture spacing that were ran under aggressive and conservative scenarios to evaluate the interplay between fracture spacing, and drawdown management. Results, presented in Table 5, suggest conservative drawdown strategy with 50 ft fracture spacing is the optimal design from net present value perspective. Also, results clearly show that 90 ft fracture spacing erodes the value of the investment, yielding the least NPV. The economics have considered the change in producing gas-oil ratio due to fracture spacing. Closely spaced

fractures show steeper rise in gas-oil ratio due to fracture-fracture interference which impacts the economics of the project. Figure 2-28 presents gas-oil ratio profiles for different fracture spacings from the aggressive drawdown scenario.

Table 5- Comparison of fracture spacing and drawdown

30 ft Cluster Spacing		
	Conservative	Aggressive
NPV ($)	$ 0.58	$ 0.46
ROR (%)	0.74	0.78
50 ft Cluster Spacing		
	Conservative	Aggressive
NPV ($)	$ 1.00	$ 0.77
ROR (%)	0.92	1.00
90 ft Cluster Spacing		
	Conservative	Aggressive
NPV ($)	$ 0.80	$ 0.60
ROR (%)	0.90	0.94

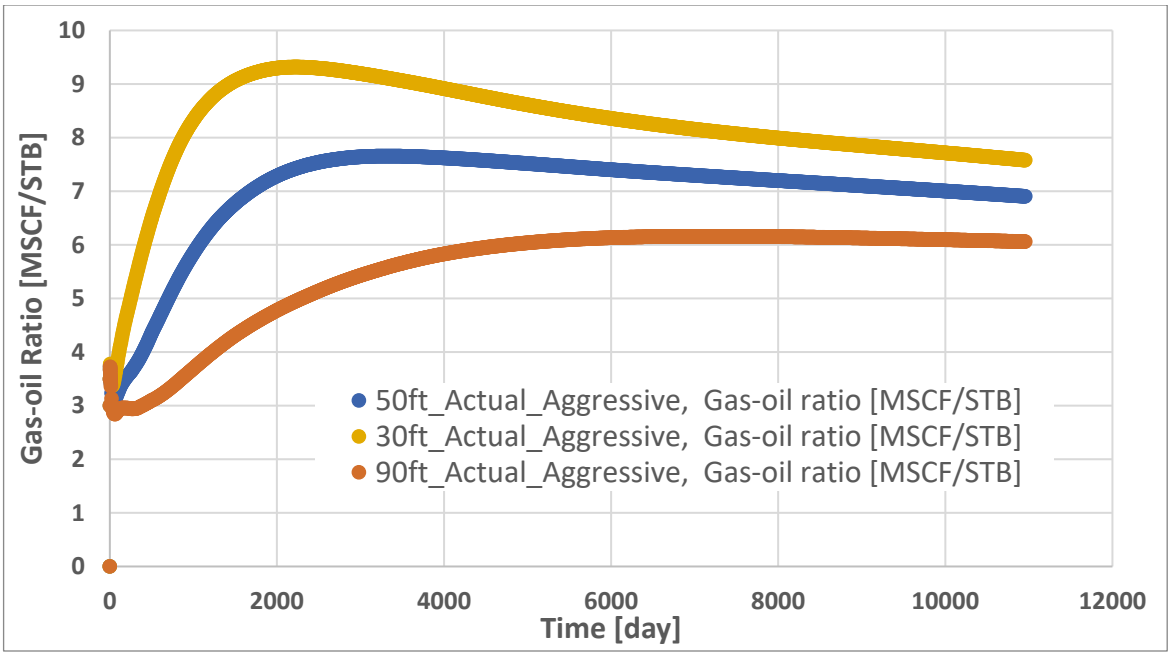

Figure 2-28- Producing gas-oil ratio trends as function fracture spacing based on the most aggressive drawdown schedule from field data.

2.9 Sensitivity Analysis to Investigative the Relative Importance of Fracture Spacing

2.9.1 Loss of Hydraulic Fracture Conductivity

Hydraulic fractures undergo a wide range of stress conditions during their lifetime. Once the completions fluid and proppant are pumped, hydraulic fractures experience relatively low effective stresses as the reservoir pore pressure is still at virgin conditions, or perhaps "supercharged" by fracturing fluids as illustrated by (Wilson and Alla 2017). However, once the producing well is online, effective stress starts to increase as the flowing bottom-hole pressure decreases. The increase in effective stresses lead to loss of hydraulic

fracture conductivity due to fines migration, formation spalling, gel damage, and many other effects. Figure 2-29 presents four scenarios of conductivity loss that were used in the sensitivity study.

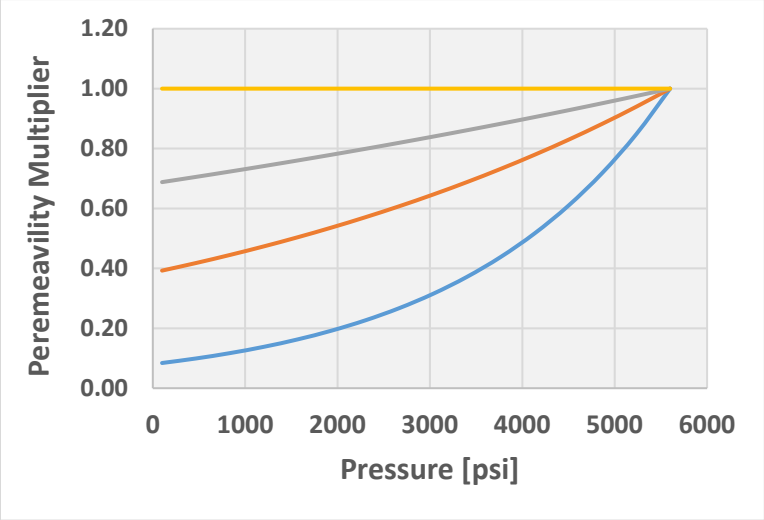

Figure 2-29- Scenarios to model reduction in hydraulic fracture conductivity.

2.9.2 Effective Fracture Half-Length

It has been demonstrated that hydraulically fractured wells produce form an effective fracture length that is much smaller than the designed length. Current modeling procedures rely on either numerical models developed by services providers, or analytical theories such as (Perkins and Kern 1961), (Geertsma and De Klerk 1969), (Nordgren 1972). One of the major shortcoming of analytical methods is the fracture height needs to be pre-defined which influences the computations of fracture half-length, width, and proppant transport as explained by (Van Eekelen 1982). Recently, field-based hydraulic fracturing experiment was conducted in West Texas in the Permian basin known as HFTS (Hydraulic Fracture Test Site). The experiment was financially supported by the DOE

and it encompasses 11 horizontal wells in upper and middle Wolfcamp formations. Slanted whole core was collected from the stimulated rock volume between two producing wells to understand proppant distribution and fracture geometry. Results suggest that proppant is distributed within highly complex fracture networks at higher concentrations near the wellbore. Observed proppant distribution was a small percentage of the recorded microseismic cloud as demonstrated by (Ciezobka, Courtier, and Wicker 2018). Hence, four scenarios of fracture half-length were modeled to cover a wide range of 95 ft to 500 ft as shown in Figure 2-30.

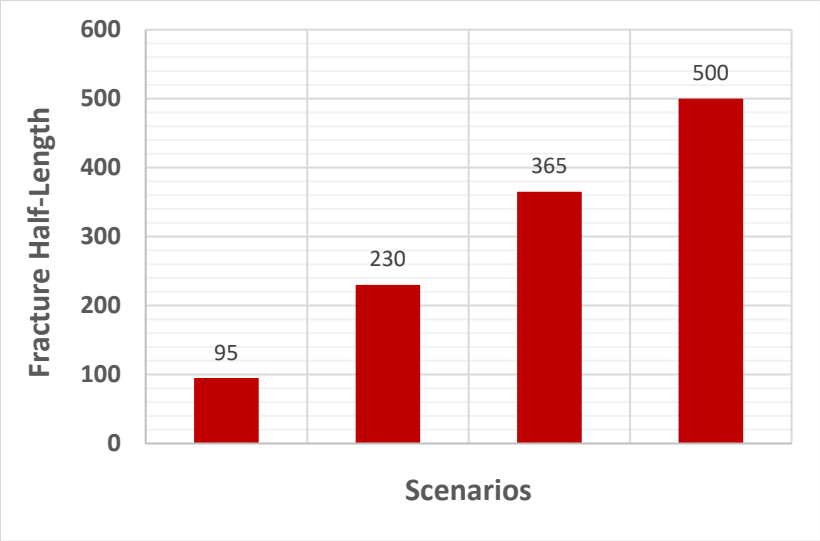

Figure 2-30- Conductive fracture half-length sensitivities.

2.9.3 Critical Gas Saturation

Depletion drive, or solution gas drive is a mechanism by which dissolved gas in the reservoir expand and becomes source of energy to produce reservoir fluid. When pressure drops below the saturation pressure, bubble point in this case, the oil phase

becomes saturated with gas and gas bubbles start to form. Gas bubbles are then connected to form the gas phase; this state is known as critical gas saturation. In other words, the critical gas saturation is the saturation at which gas becomes mobile. A wide range of critical gas saturations ranging from 1% to 20% was modeled as presented in Figure 2-31. The producing gas-oil ratio was then plotted for the first year as shown in Figure 2-32. Looking closely at the first 60 days, a drop followed by an increase in producing GOR was observed. The producing GOR decreases because the gas phase is immobile inside the reservoir, once the gas saturation above the critical gas saturation, the producing GOR starts to increase.

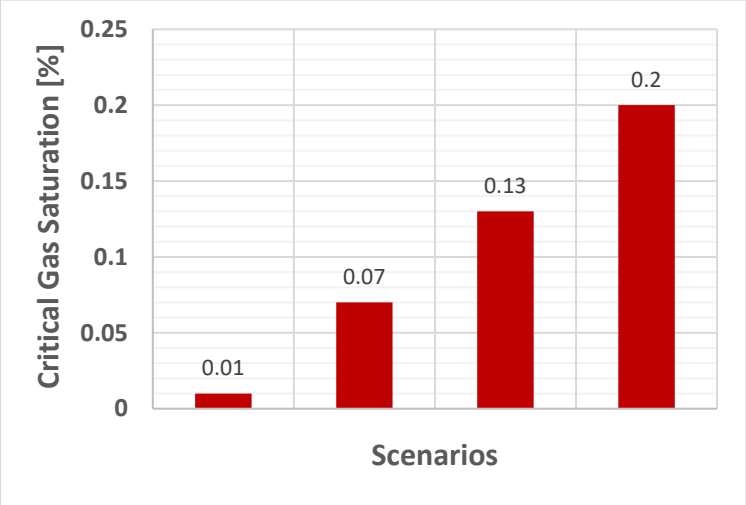

Figure 2-31- Critical gas saturation sensitivities.

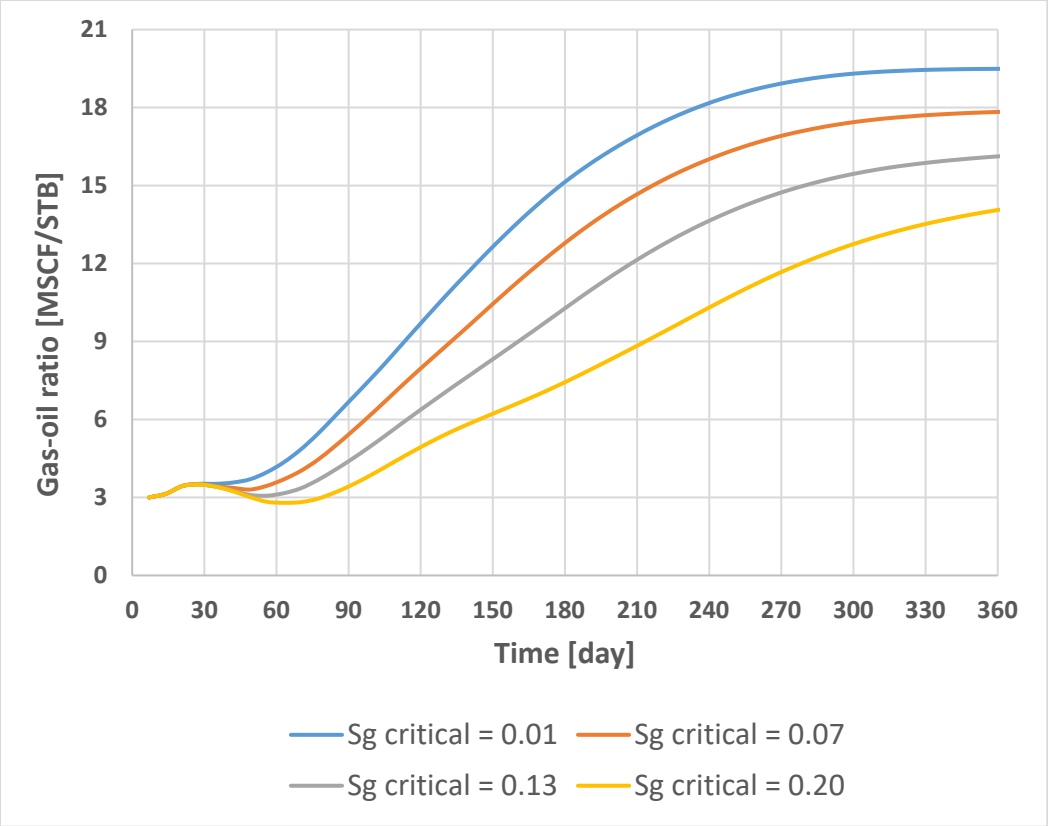

Figure 2-32- Producing gas-oil ratio dependence on critical gas saturation in the Meramec formation under aggressive drawdown schedule, and 30 ft fracture spacing.

2.9.4 Rock Properties

Petrophysical properties that characterize the storage and flow capacity of the reservoir were included in the sensitivity study such as pore volume, water saturation, and matrix permeability. Pore volume and water saturation were varied by ±20% from the baseline values obtained by history matching field production and pressure data. Matrix permeability which represents a major unknown, not only in the Meramec formation, but in tight oil reservoirs in general, was varied from 0.1 to 10 micro Darcy.

2.9.5 Sensitivity Results and Discussions

Results of the sensitivity analysis are presented in Figures 2-30 to 2-33. Variables under investigation are listed along the y-axis and sorted from highest to lowest, according to their impact on the output variable. The x-axis presents the spread in the output due to changes in the inputs. Each input variable was varied separately while maintaining other variable at their base value. The base value was obtained by history matching the production data as described in the history matching section. Fracture spacing, and drawdown strategy are highlighted in red and green respectively. 60, and 360 days cumulative oil production were defined as metrics for short-term and mid-term well performance whereas 30 years cumulative oil production was defined as long-term well performance. Figure 2-33 shows drawdown strategy is the second highest variable in terms of impact to 60 days cumulative oil production. During this time of the well life, drawdown strategy is more important to early productivity than fracture spacing. Furthermore, Figure 2-34 sheds light on factors that impact 1 year of cumulative oil production. The most impactful parameters on oil production are permeability, fracture half-length, and pore volume which altogether impact $A\sqrt{k}$ and pore compressibility. In contrast, the first year producing gas-oil ratio is primarily influenced by drawdown management and fracture spacing. Finally, long-term oil production, presented by Figure 2-35, indicates that drawdown strategy and fracture spacing are the least impactful to productivity if compared to fracture half-length and matrix permeability.

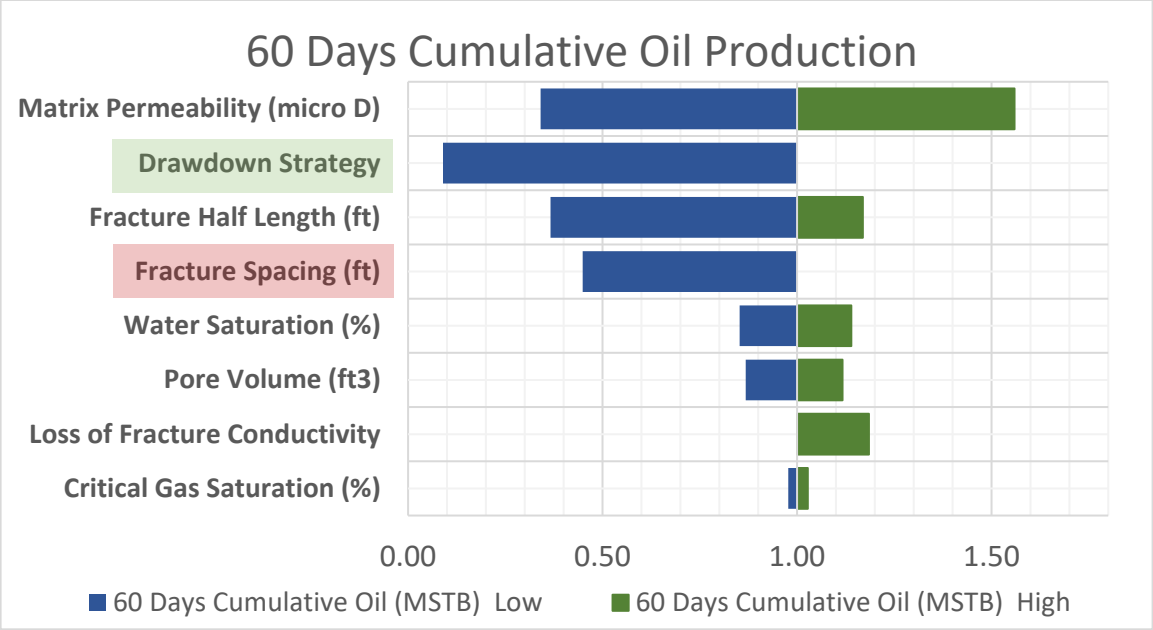

Figure 2-33- Sensitivity results of cumulative oil production for first 60 days.

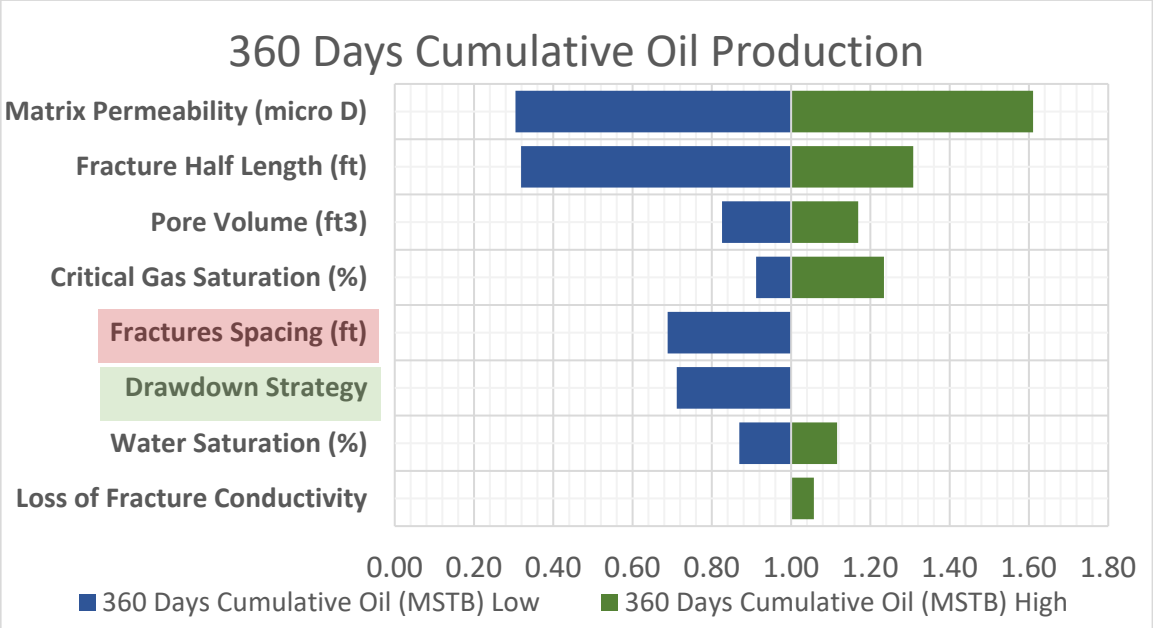

Figure 2-34- Sensitivity results of cumulative oil production for first 360 days.

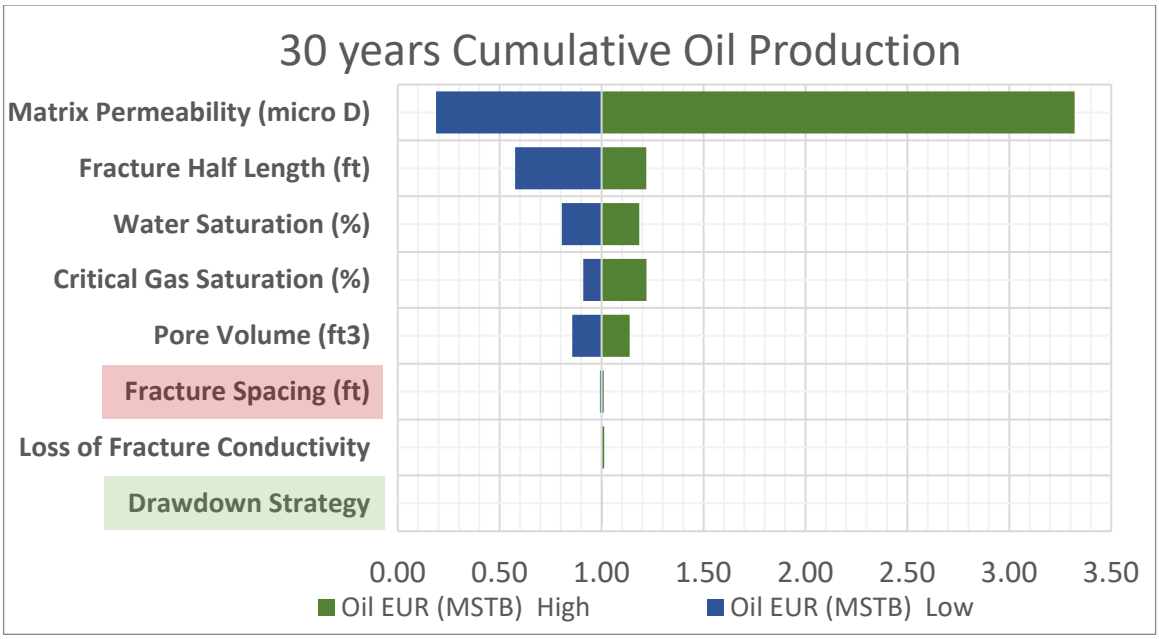

Figure 2-35- Sensitivity results of cumulative oil production for 30 years

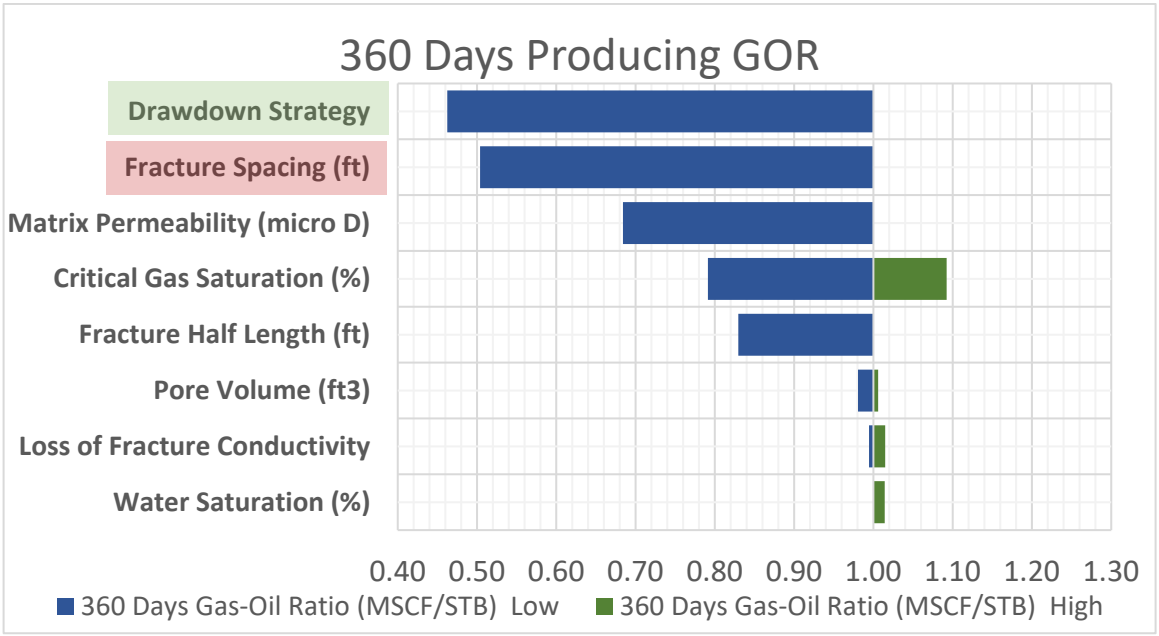

Figure 2-36- Sensitivity results of gas-oil ratio for the first year of production.

Chapter 3: Modeling of Inter-Well Interference

One of the critical decisions in developing any unconventional resource is to optimize the spacing between horizontal wells. Due to uncertainties in the distribution of rock properties, phase behavior, fracture geometry, operating conditions, and commercial criteria, it is very challenging to get a reliable solution for optimum well spacing. According to a report from Shell (Cao et al., 2017) "Although there are more than 4,000 wells had been drilled at Wolfcamp formation in the Midland basin and Delaware basin, it is still not clear to the industry what is the optimum well spacing of long-term field development". As discussed in Chapter 1, inter-well interference is the main driver for optimal well spacing. Hence, the following analyses will be devoted to multi-well simulation from Wolfcamp to understand inter-well interference and develop a diagnostics technique to investigate pressure depletion at the stage level.

3.1 Well Overview

Two stack-staggered wells (P1H and P2H) were drilled in the Wolfcamp formation in Texas as shown in Figure 3-1. The wells have a lateral length of 5,000. They were separated by 360 ft vertically, and 680 ft laterally. The subject wells have production history of more than two years, and they were completed with proppant intensity of 1500 lbs/ft. The lower well (P1H) brought online first, and then the upper well was brought

online after 6 months of (P1H) production. Thus, well (P1H) is considered as a parent well whereas well (P2H) is considered a child well. The objectives behind the subsequent analyses are listed below:

- Map the extent of pressure depletion caused by producing (P1H) and (P2H).
- Identify whether the rock column between the two landing zones has been drained efficiently, or not.
- Understand the impact of producing (P1H) six months prior to (P2H).

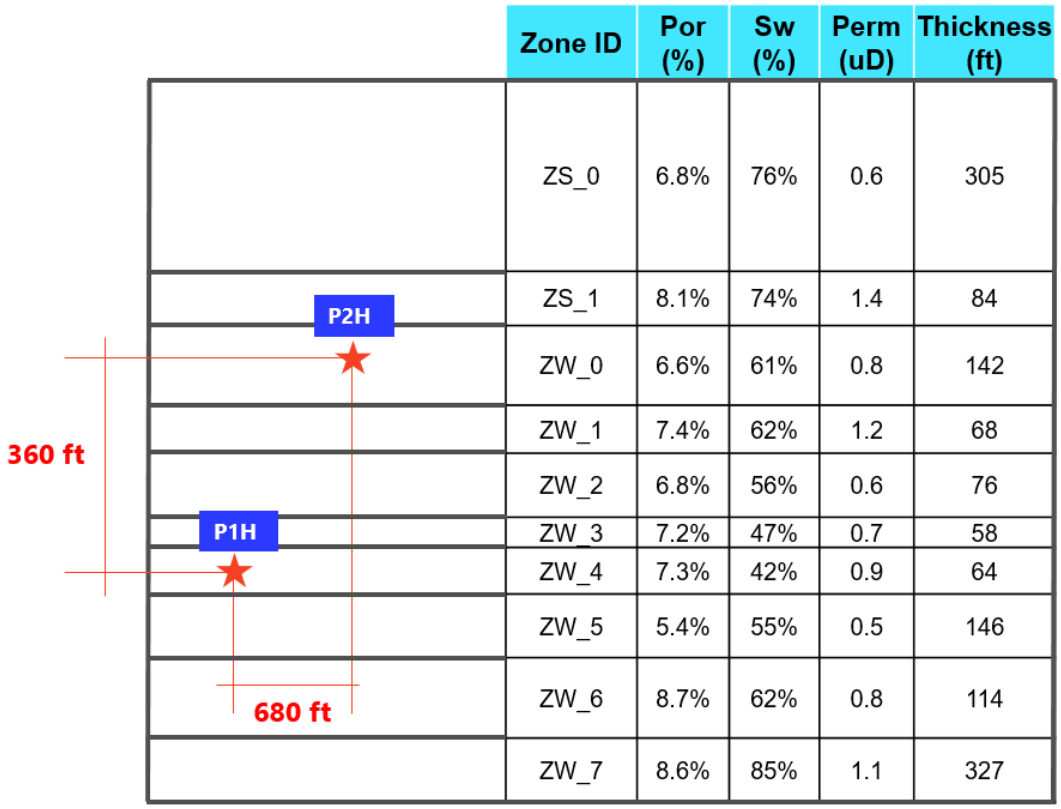

Zone ID	Por (%)	Sw (%)	Perm (uD)	Thickness (ft)
ZS_0	6.8%	76%	0.6	305
ZS_1	8.1%	74%	1.4	84
ZW_0	6.6%	61%	0.8	142
ZW_1	7.4%	62%	1.2	68
ZW_2	6.8%	56%	0.6	76
ZW_3	7.2%	47%	0.7	58
ZW_4	7.3%	42%	0.9	64
ZW_5	5.4%	55%	0.5	146
ZW_6	8.7%	62%	0.8	114
ZW_7	8.6%	85%	1.1	327

Figure 3-1- Gun barrel view of wellbore landing and average petrophysical properties.

Furthermore, Figure 3-1 shows average petrophysical properties per zone that were estimated from an offset vertical well. Those properties include zone thickness, porosity, water saturation, and permeability. Higher fracture intensity detected by core and image log in ZW_5 which has highest carbonate content and lowest average permeability and porosity.

3.2 Fluid Characterization

3.2.1 Peng-Robinson Equation of State

Peng-Robinson equation of state has been used to model the reservoir fluid and predict its thermodynamic state. The equation needs to be fine-tuned to match actual laboratory data. Hence, all the necessary laboratory experiments were conducted to describe the fluid phase-behavior and PVT properties. The details behind Peng-Robinson model are shown in Appendix 1. The following sections are devoted to the results of laboratory experiments performed on a fluid sample from the Wolfcamp formation. The data was successfully used to fine-tune Peng-Robinson equation and build a representative fluid model for reservoir simulation. The regression parameters are shown in Appendix 2.

3.2.2 Fluid Composition

Separator vapor and liquid were physically combined in a PVT cell. The separator samples were recombined to a gas-oil ratio of 3000 (standard cubic feet of separator gas to barrel of separator liquid). The recombined well-stream fluid shows a bubble point

pressure of 4648 psia at 187 °F and exists as an under saturated volatile oil at reservoir conditions. The laboratory report identified more than 30 components. However, the cost of numerical simulation increases substantially with number of components. Hence, the heptane plus fraction was lumped into pseudo components as shown in

Table 6. The reduced-component characterization was designed to reproduce the original complete characterization provided by the laboratory.

Table 6- Fluid Composition

Component	Mole Percentage
N2	0.56
CO2	0.09
CH4	61.39
C2H6	10.41
C3H8	5.56
IC4	0.94
NC4	2.42
IC5	0.87
NC5	1.21
FC6	1.51
C07-C10	7.26
C11-C13	3.03
C14-C16	1.85
C17-C20	1.40
C21+	1.50
Sum	**100%**

3.2.3 Constant Composition Expansion

The Constant Composition Expansion (CCE) experiment was used to obtain bubble point pressure, oil density and oil isothermal compressibility. After recombining the oil and gas to the right proportions, the mixture was charged to a cell. The temperature

was controlled via a thermostat and maintained constant at the reservoir temperature. The pressure was controlled and recorded by a positive displacement pump. The experiment started at the reservoir pressure, then the pressure is lowered which led to oil volume expansion. The volume increased more rapidly below the bubble point because the gas phase evolved from the oil phase resulting in higher system compressibility. The pressure was lowered in multiple steps and the volume was recorded at each step. Pressure-volume data was used to fine tune the equation of state. Figure 3-2 shows the match quality to the lab data as predicted by Peng Robinson equation of state. Robust equation of state is crucial to accurately model phase changes due to pressure depletion.

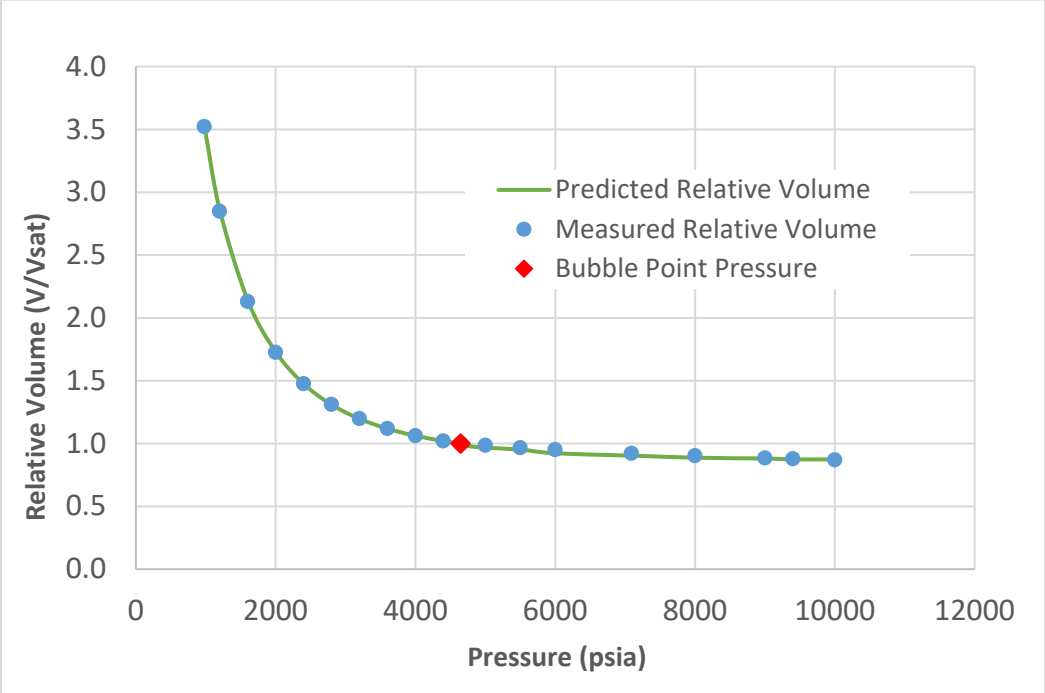

Figure 3-2- Actual versus prediction pressure-volume relationship.

Furthermore, isothermal oil compressibility was calculated for pressure intervals above the bubble point. As expected, oil compressibility varied continuously with pressure depletion as shown in Figure 3-3. Equation of state was used to predict the oil compressibility and it shows good agreement with actual lab data.

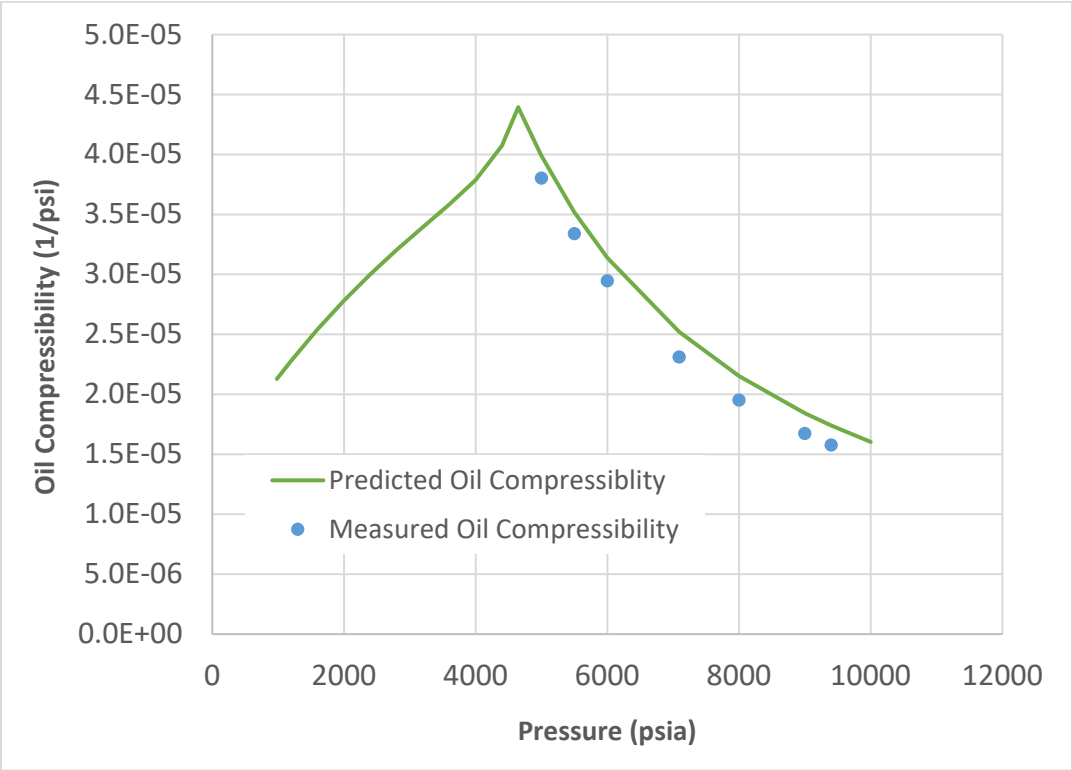

Figure 3-3- Actual versus prediction undersaturated oil compressibility.

3.2.4 Differential Liberation (Vaporization) Test

The objective of this test is to mimic the depletion process of an oil reservoir and to provide necessary data to estimate reservoir performance. Unlike Constant Composition Expansion, reservoir pressure is gradually depleted, and any liberated gas is removed from the oil phase. Hence, the average molecular weight progressively

increases because the remaining oil is richer in heavier components. All depletion stages were performed under the same reservoir temperature. Differential gas-oil ratio, differential formation volume factor, oil density, and gas Z factor were calculated based on the measured data. Information from multi-stage separator test were utilized to adjust gas-oil ratio, and formation volume factor to separator conditions. Figure 3-4 shows the unadjusted actual versus predicted gas-oil ratio and formation volume factor.

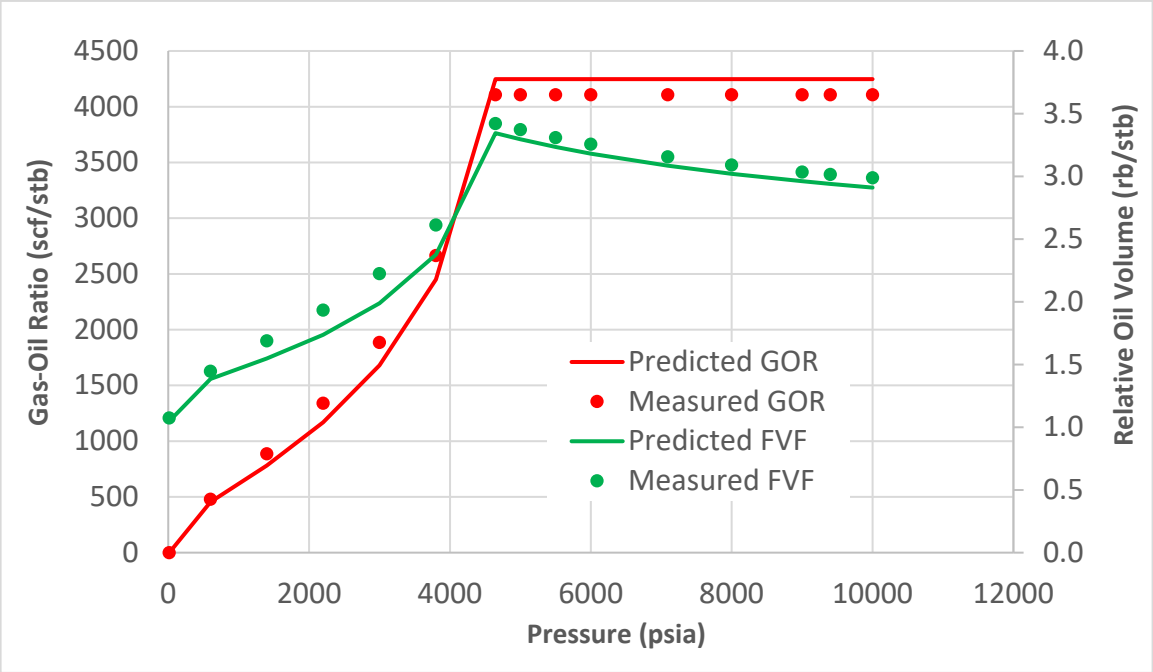

Figure 3-4- Actual versus predicted gas-oil ratio and formation volume factor from differential liberation test (not adjusted for separator conditions).

Furthermore, liberated gas properties were measured and then gas viscosity was calculated. Oil viscosity was measured as well at each pressure interval. The measured

data was used to modify Pedersen Corresponding States Model. Measured versus modified Pedersen viscosities are shown in Figure 3-5.

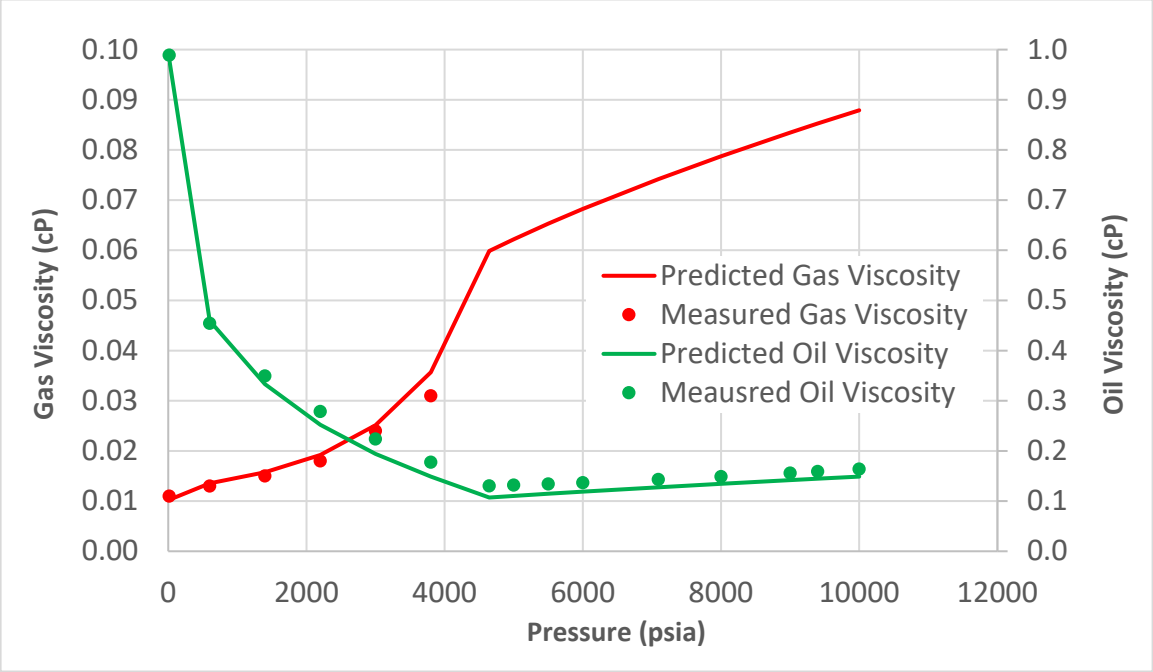

Figure 3-5- Actual versus modified Pedersen for oil and gas viscosities as function of pressure.

3.3 Model Setup

3.3.1 Mesh Preparation and Initialization

The concepts used to formulate the governing equations for fluid in porous media are well documented. The physical principals that were utilized in the analyses are conservation of mass, Darcy's law, and thermodynamic equilibrium of components between phases. In addition, the definitions of phase saturation and mole fraction are used

to complete the system. The governing equations are shown in detail in Appendix 3. CMG was used to solve those equations via finite-difference method.

The flow domain was discretized such that the grid size honors the actual spacing between hydraulic fractures. The vertical layering was obtained by minimizing the standard deviation in permeability which resulted in 31 layers. Figure 3-6. The grid size was set to 30 ft between two consecutive hydraulic fractures and 75 ft in direction perpendicular to the wellbore. Horizontal permeability was assumed to be isotropic, i.e. (K_x=K_y), whereas as vertical permeability was assumed to be 0.1 of horizontal permeability. Reservoir pressure was initialized with 0.8 psi/ft gradient based on data from a downhole pressure gauge. Porosity and initial water saturation were specified from well logs. Finally, the fluid model presented in section (3.2) was used to describe the phase behavior.

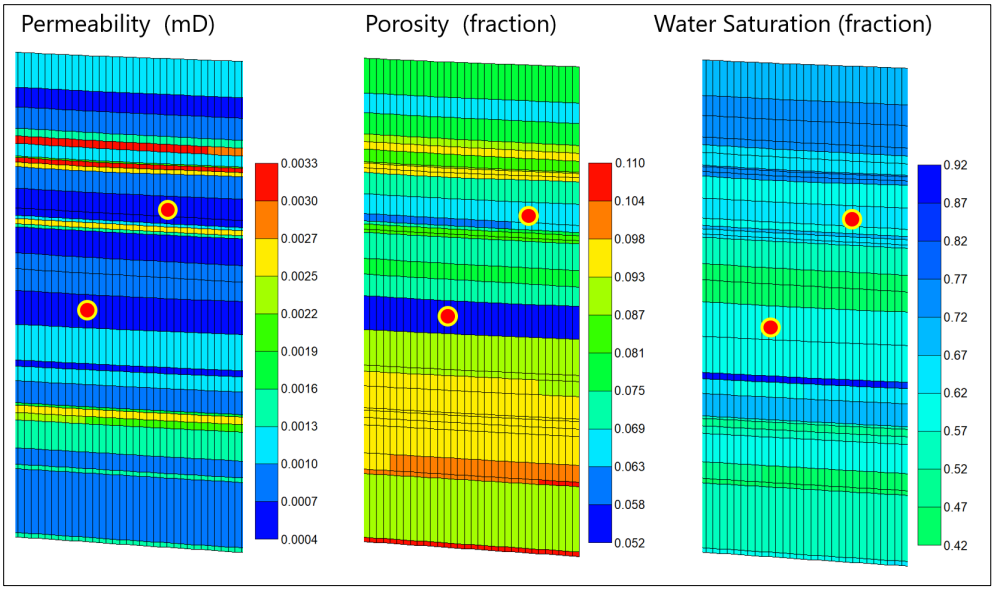

Figure 3-6- Cross sections along plane 163 that show petrophysical properties per layer, and model mesh relative to the locations of the two wells.

3.3.2 Hydraulic Fracture Geometry

A numerical simulator was used to predict fracture geometries during propagation of height and length. Actual field fluid and proppant volumes from the two wells were utilized to obtain fracture geometry for each stage. Fracture geometries were integrated into the flow simulator and discretized into two regions which are propped and unpropped fracture regions. Fracture conductivity of (0.2 mD. ft) was used as a cutoff to define the propped region. Results suggest asymmetric fracture geometries and upward growth of fracture height. This growth is dictated by contrast in minimum horizontal stress between rock layers and variability in their mechanical properties. Figure 3-7 Figure 1-1shows cross section of fracture geometry from plane 67 to illustrate fractures complexity and distribution.

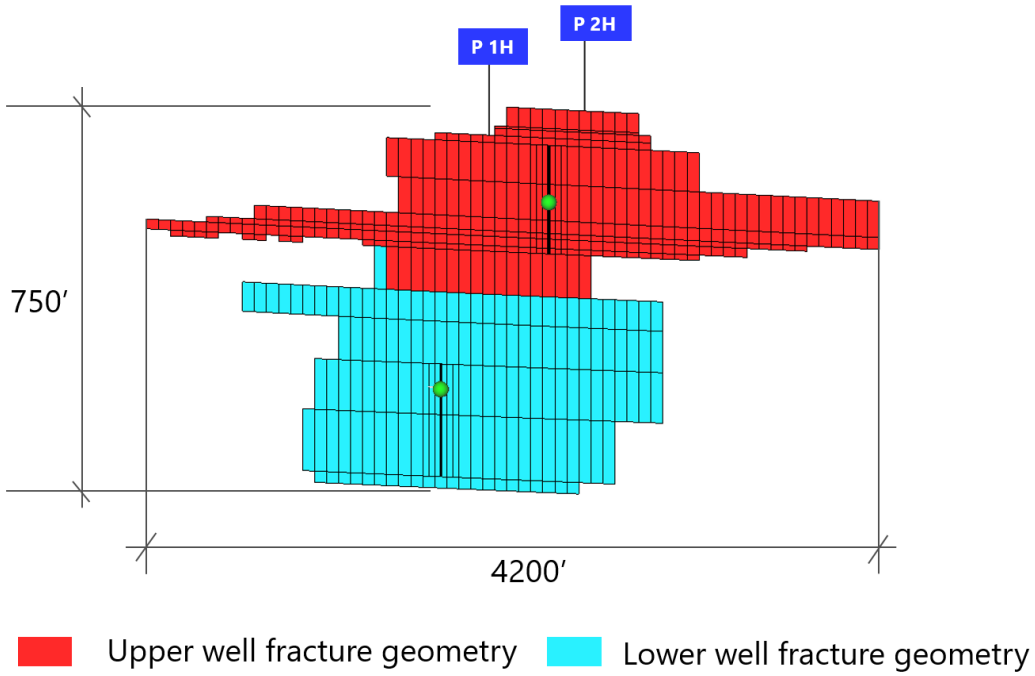

Figure 3-7- Cross section that shows hydraulic fractures from the upper and lower wells.

Furthermore, Figure 3-8 Figure 1-1shows aerial view of fracture geometry from layer 16 to illustrate hydraulic fracture complexity and distribution. It also shows a cross-section overlap between fractures from upper and lower wells.

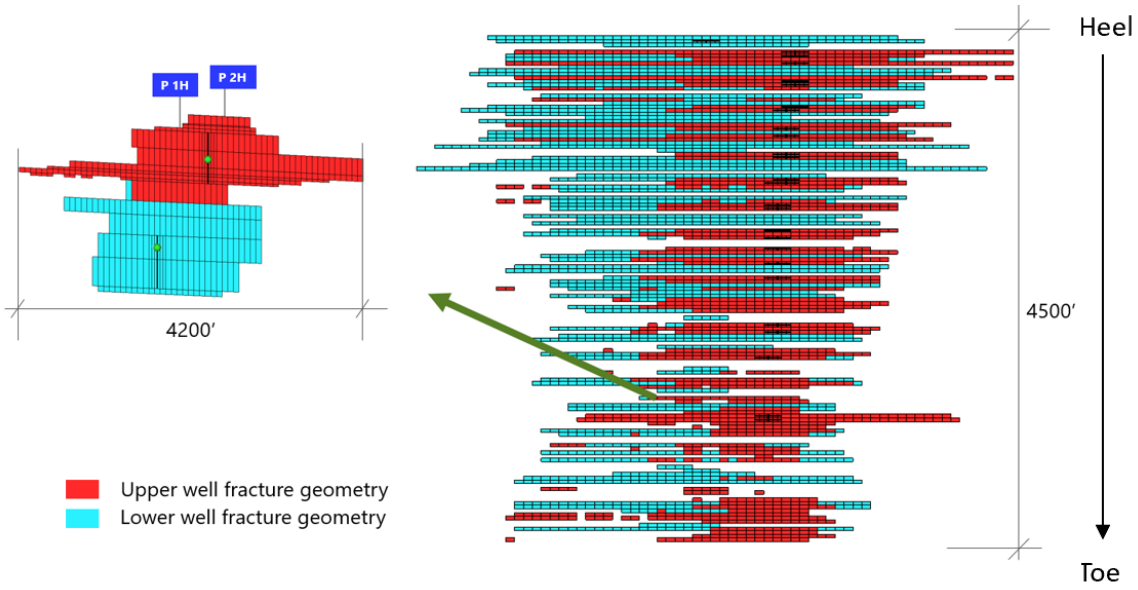

Figure 3-8- Aerial view from layer 16 to illustrate fracture overlaps and complexity from lower and upper wells, P1H and P2H respectively.

3.3.3 Relative Permeability

Relative permeability conveys the reduction in flow capability due to the presence of multiple mobile fluids. It is dependent on pore architecture, wettability, and fluid saturation history. Relative permeability measurements were not available for this analysis. Hence, they were obtained through the history-matching process to three-phase production data and bottom-hole pressure from two wells. Figure 3-9 presents oil-water and liquid-gas curves used to describe flow in the matrix. On the other hand, straight-line relative permeability was used to describe flow in hydraulic fractures.

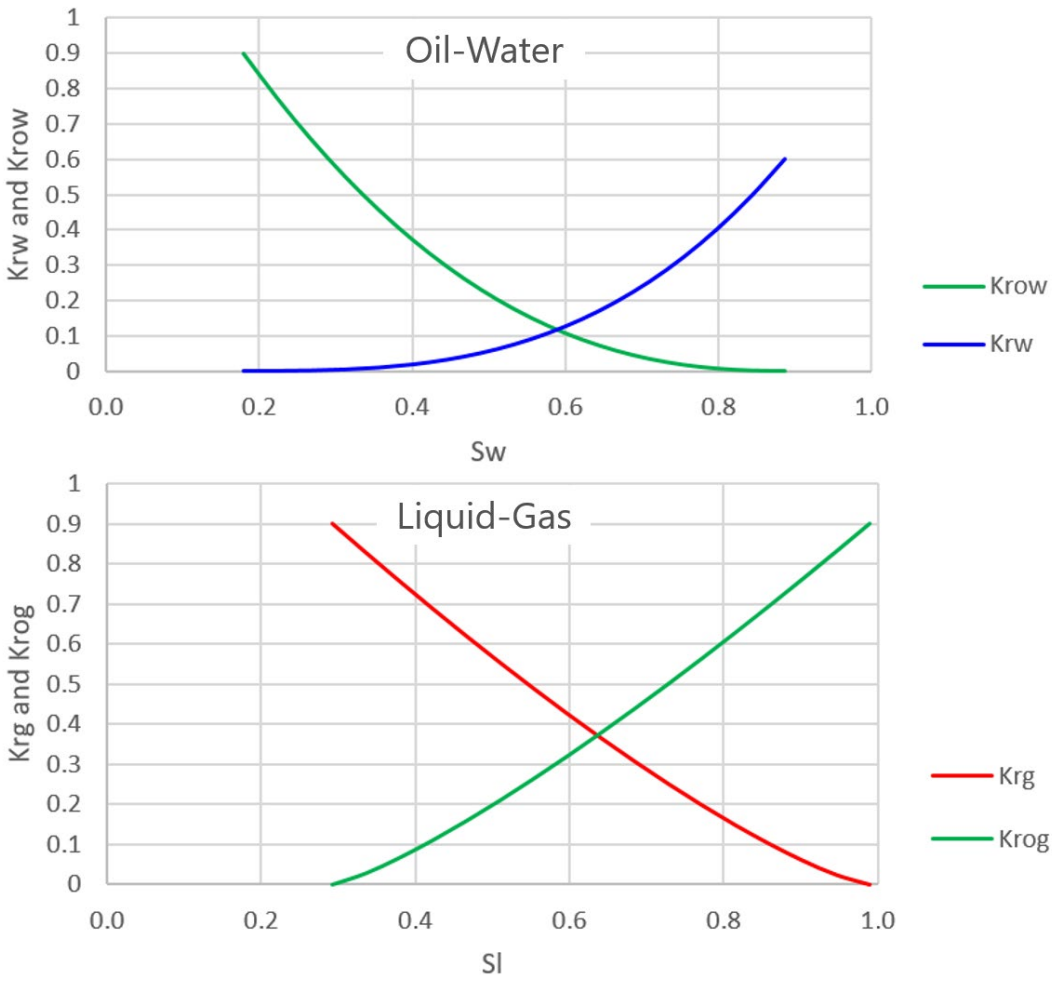

Figure 3-9- Matrix relative permeability curves for oil-water, and liquid-gas.

3.3.4 Rock Compaction

As explained in 2.8.1, hydraulic fractures undergo a wide range of stress conditions during their lifetime. Once the wells are online, effective stress starts to increase as the flowing bottom-hole pressure decreases. The increase in effective stresses lead to loss of hydraulic fracture conductivity. Data were not available to model loss of hydraulic fracture conductivity. However, as a common engineering practice, this

behavior is modeled as exponential decay in fracture permeability. The degree of conductivity loss was calibrated against actual production data during the history matching process. Figure 3-10 presents conductivity loss that were used in the sensitivity study.

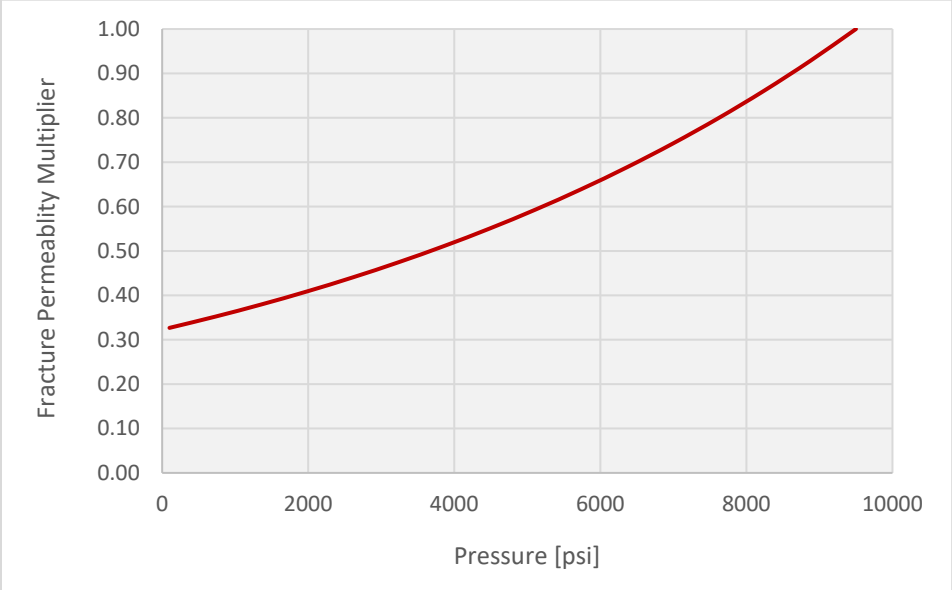

Figure 3-10- Reduction in hydraulic fracture conductivity for P1H and P2H.

3.4 History Matching Results

Once the reservoir simulation model is constructed, the validity of the model is examined by using it to simulate the performance P1H and P2H under past operating conditions. The differences between the simulated performance and the known

performance from field data are reduced by adjusting the model parameters. History match was obtained to three-phase production and flowing bottom-hole pressure for both P1H and P2H. The simulator was constrained to produce total reservoir fluid.

Manual history match resulted in 16% error between actual and simulated data. More than 500 scenarios were run to reduce the error from the manual match. Optimal solution was identified with an error of 9.5% as shown in Figure 3-11. History matching parameters are summarized in Table 7. Formation compressibility was estimated at 5e-6 1/psi. Results suggest that after three years of production, hydraulic fractures lost 67% of their initial permeability.

Furthermore, it was not necessary to adjust initial reservoir pressure, porosity, and water saturation from their initial values. However, matrix permeability was reduced by 20% to achieve the optimal history match. Simulation results suggest that unpropped fractures have 10 to 20 times higher permeability than matrix permeability. Finally, critical gas saturation was found to be about 1%. Field rates and pressure time-series are confidential and thus not shown in this section.

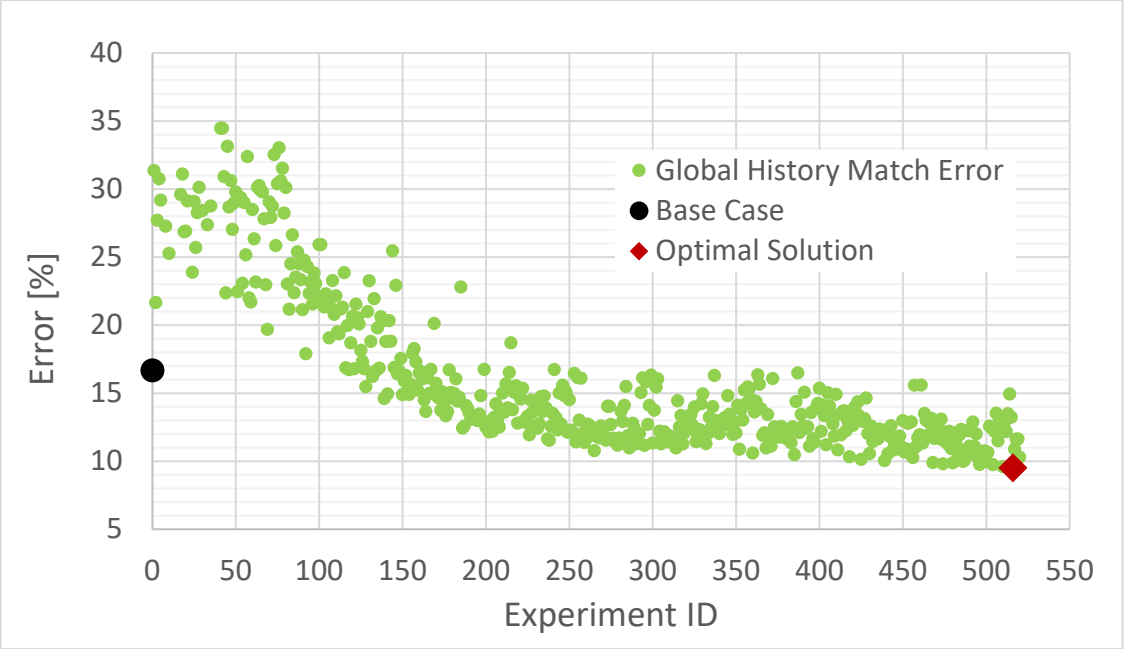

Figure 3-11- Percent error between actual field data and simulated response. Percent error is an average of water, oil, gas, and BHP errors. Top 10 matches are shown in Appendix 4.

Table 7- Simulation results to match field data for P1H and P2H

Unknowns	History Match Value
Fracture Compaction	Exponential decay as shown in Figure 3-10
Rock Compressibility	5E-6 1/psi
Unpropped Fracture Permeability P1H	10X matrix permeability
Unpropped Fracture Permeability P2H	20X matrix permeability
Propped Fracture Permeability P1H	Infinite conductivity
Propped Fracture Permeability P2H	Infinite conductivity
Initial Pressure	Unchanged from initial earth model values
Matrix Porosity	Unchanged from initial earth model values
Matrix Water Saturation	Unchanged from initial earth model values
Matrix Permeability	Reduced by 20% from initial values
Relative Permeability	Tables are shown in Figure 3-9
Hydraulic Fracture Geometry for P1H and P2H	Geometries from hydraulic fracture simulator
Phase Behavior (Volume, Pressure, Temperature)	Based on equation of state presented in Section 3.2

3.5 Diagnostics of Inter-Well Interference

Simulation results clearly show that several hydraulic fractures have overlapped between upper and lower wells. The overlap occurs at various degrees of intensity along the lateral length which impacts inter-well interference accordingly. Hence, 10 regions were defined as shown in Figure 3-12Figure 3-12- Top and cross-sectional views of inter-well regions. to diagnose inter-well pressure depletion. Each region spans the distance between the two wells vertically and laterally. Each sector covers about 500 ft of lateral length and 360 ft of vertical separation as shown in the top view in Figure 3-12.

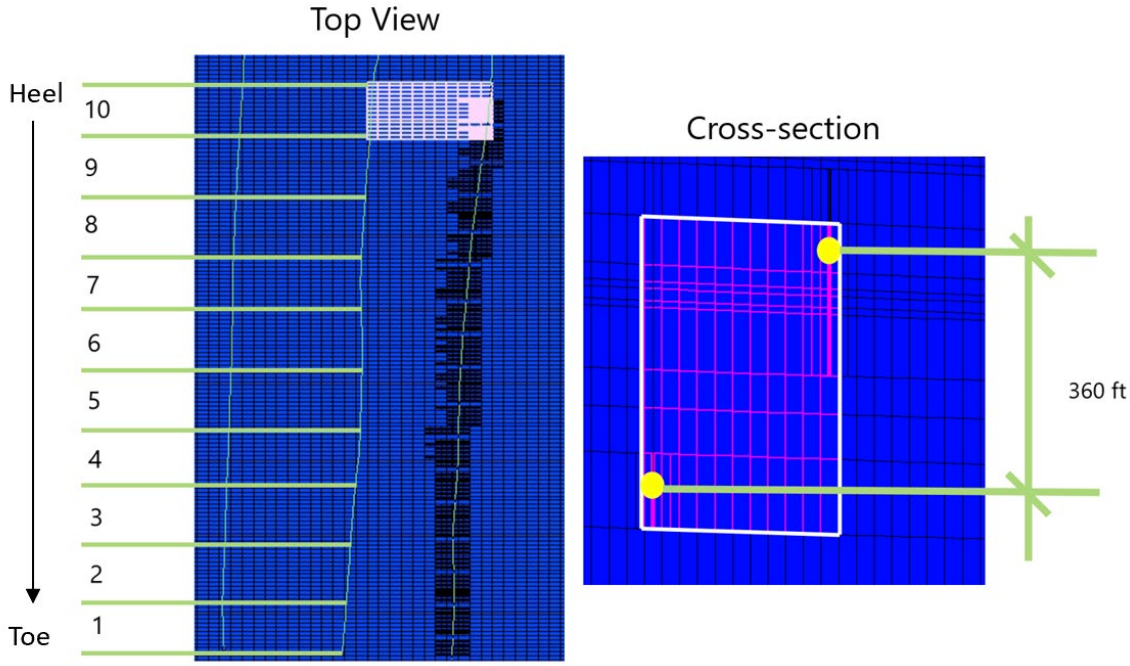

Figure 3-12- Top and cross-sectional views of inter-well regions.

The 10 regions were simulated and the average pressure per region was calculated. The average pressure represents the average pressure of the cells within each region per

time step. Pressure trends are shown in Figure 3-13. The vertical line represents the time at which the P2H brought online. Pressure trends within each sector clearly suggest that bringing P2H online has helped in further depleting the resource. Also, results show that sector-9 has experienced the most interference whereas sector-1 has seen the least interference.

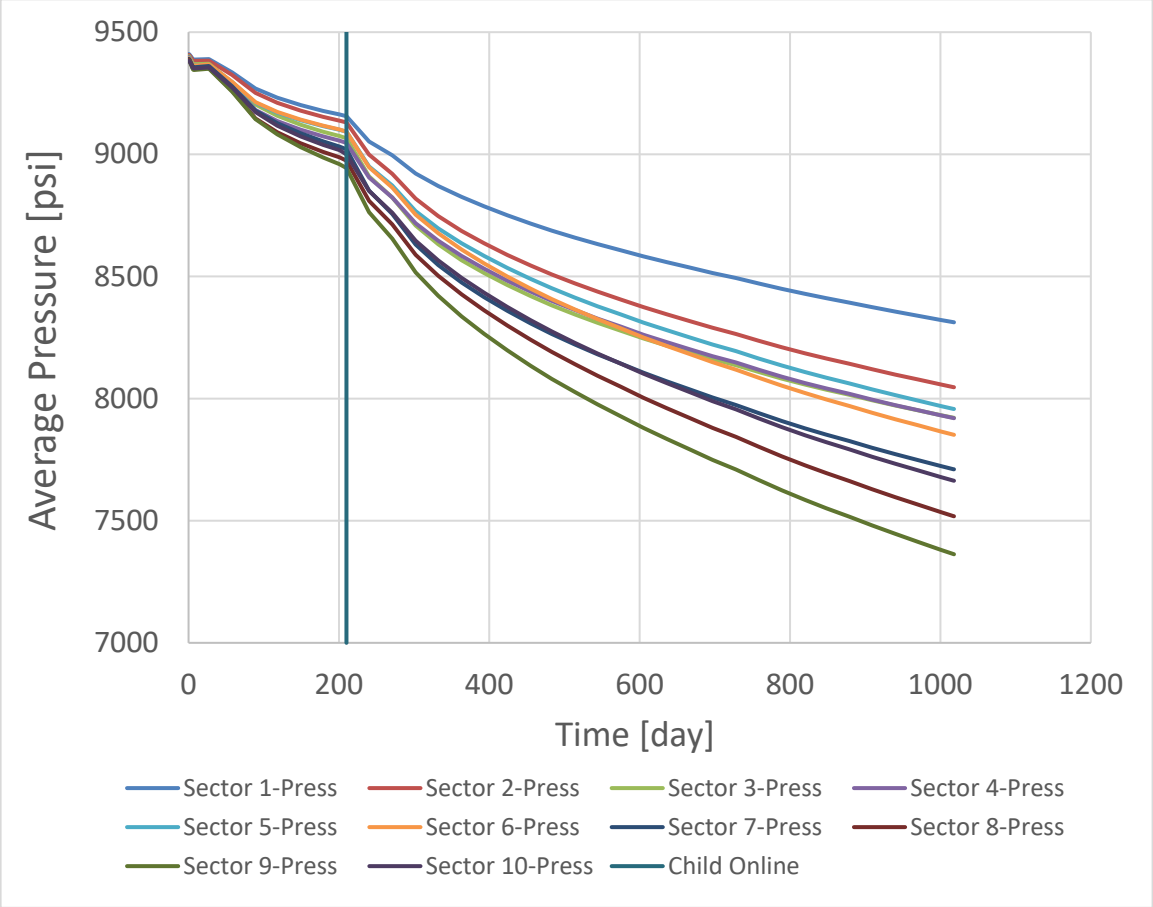

Figure 3-13- Inter-well average pressure per sector.

Figure 3-14 presents a 3D view of 5 sectors only which are 2, 4, 6, 8, and 10. It shows pressure interference in the inter-well region. Results suggest that despite inter-well interference, there is significant amount of pressure that has not been depleted by

upper and lower wells. If well cost and oil pricing are favorable, these results suggest potential for adding additional well.

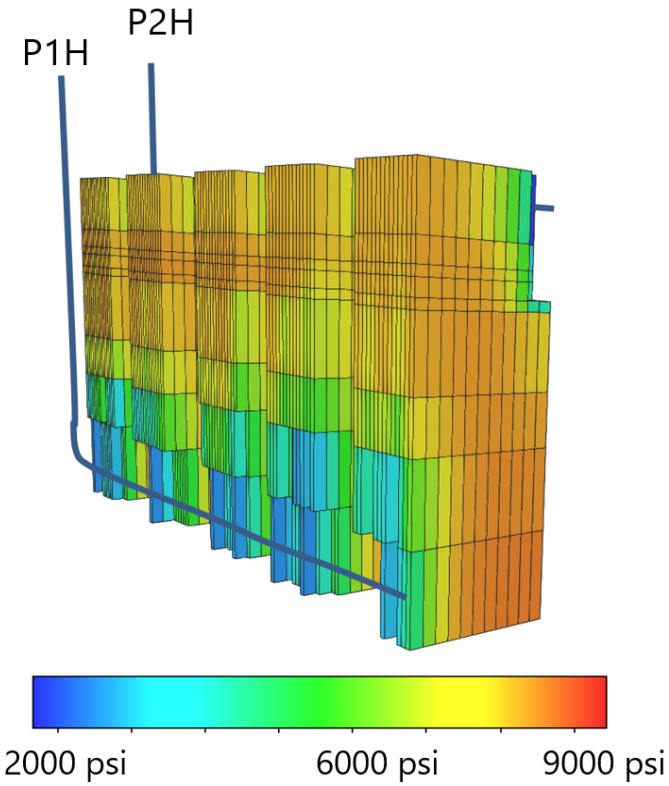

Figure 3-14- 3D view of inter-well pressure depletion after 1000 days of production.

Primary phase recovery factor was calculated for each sector as function of time as shown in Figure 3-15. Sector recovery factor was defined as the ratio of produced oil volume to original in-place oil volume and it is expressed in percentage. Results expose the variability in oil recovery between the inter-well regions and along the lateral of the two wells. Results also show that regions with high inter-well interference registered high oil recovery. This observation show that inter-well interference is beneficial as it

improves oil recovery. The amount of acceptable inter-well interference is dependent business commercial objectives, oil pricing, and well cost structure. This diagnostics technique provides the means to evaluate inter-well interference and impact development decisions.

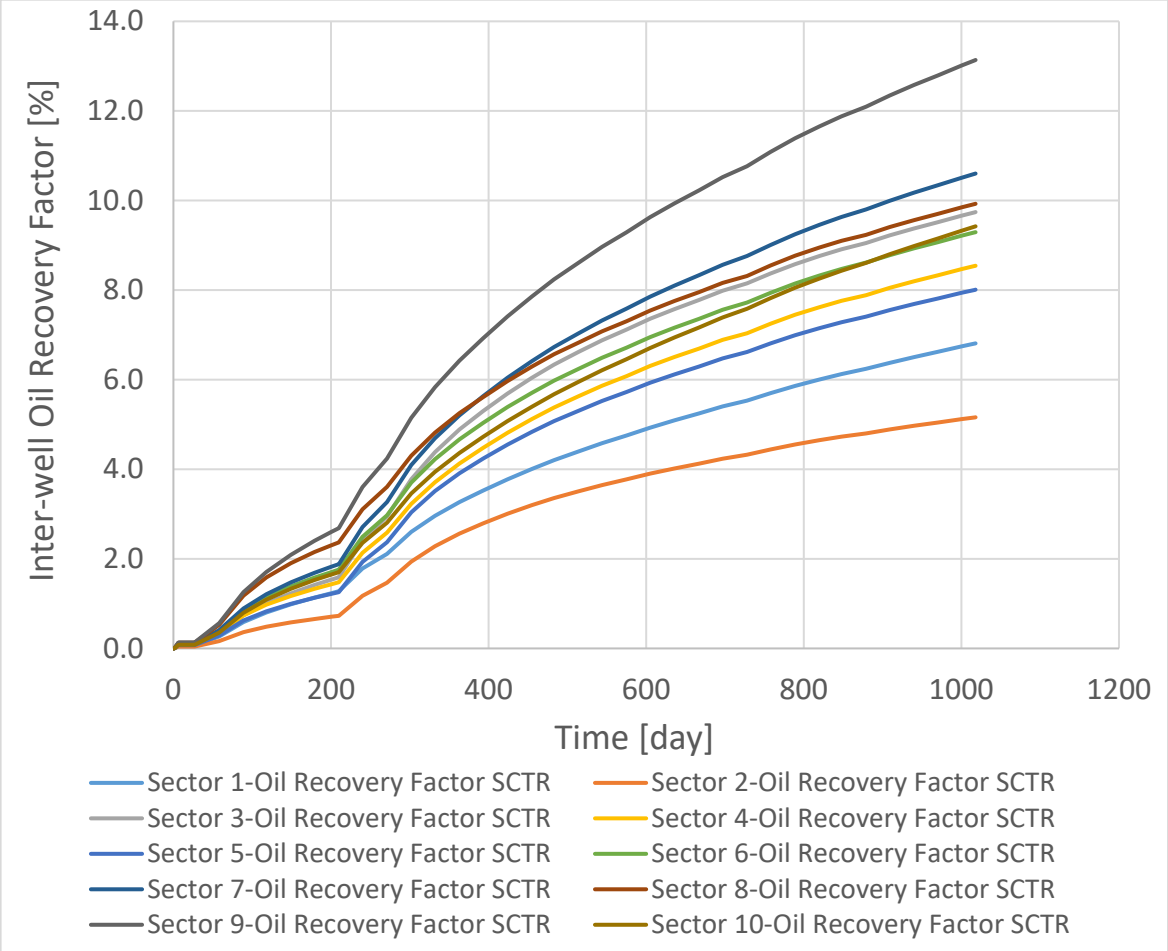

Figure 3-15- Inter-well oil recovery factor per sector illustrate the variability in oil recovery along the lateral of the well.

Chapter 4: Finite-Volume Modeling of Transport Properties from SEM Images

4.1 Sample Description and Preparation

Three-dimensional connected and isolated pore networks were extracted from a shale sample using FIB-SEM technology. Isolated pores were ignored since they are not connected to the flow domain. However, tight reservoirs are often stimulated by hydraulic fracturing which could connect isolated pores and increase permeability. The sample minimum pore throat was approximately 30 nanometers. Figure 4-1 presents the isometric projections of the 3D pore geometry that was used for the tortuosity and permeability simulations; it also shows the position of the inlet and outlet. The dimensions of the pore geometry are 2.36, 1.89, and 1.67 micron along x, y, and z axes respectively. The sample porosity was computed to be 4% by taking the ratio of the pore volume to the bulk volume of the rock sample. The sample was imaged and processed at the laboratories of the University of Oklahoma. The sample was cut and mounted to an aluminum stub using a conductive carbon paste. The sample was then coated with Au/Pd in a Denton Vacuum Desk V sputtering system to provide a conductive coating on the

sample surface. Next, the sample was prepared for 3D SEM imaging using a dual beam FIB-SEM system. Platinum pad was deposited on the edge of the sample to minimize curtaining effects. Data acquisition was performed via FEI Slice N View software.

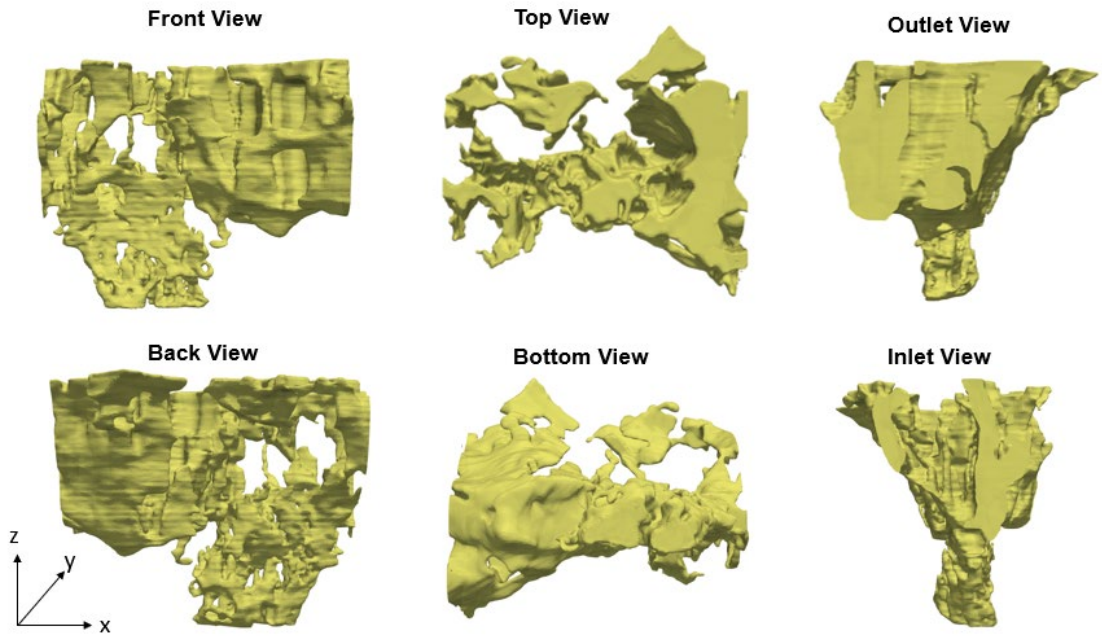

Figure 4-1- Connected pore geometry scanned by the FIB-SEM technology. The sample has dimensions of 2.36, 1.89, and 1.67 micron along $\boldsymbol{x}$, $\boldsymbol{y}$, and $\boldsymbol{z}$ axes respectively.

In order to utilize the 3-D pore system for flow simulation, a mesh needs to be created. Mesh generation is the most important and laborious step in the modeling process (Dennis et al., 2005; Paraschivoiu et al., 2014; Power et al., 2003). Good quality mesh must ensure accurate representation of the rock pore structure and allow the utilization of higher order numerical schemes. The meshing process started by creating a background mesh containing hexahedral cells. The 3-D pore network was embedded inside the

background mesh. Cells were refined near the surface of the pore geometry to accurately capture the sample morphology. Finally, cells outside the sample geometry were removed. Figure 4-2 shows the FIB-SEM model of the pore space in blue color prior to the meshing process, and the final mesh in gray color.

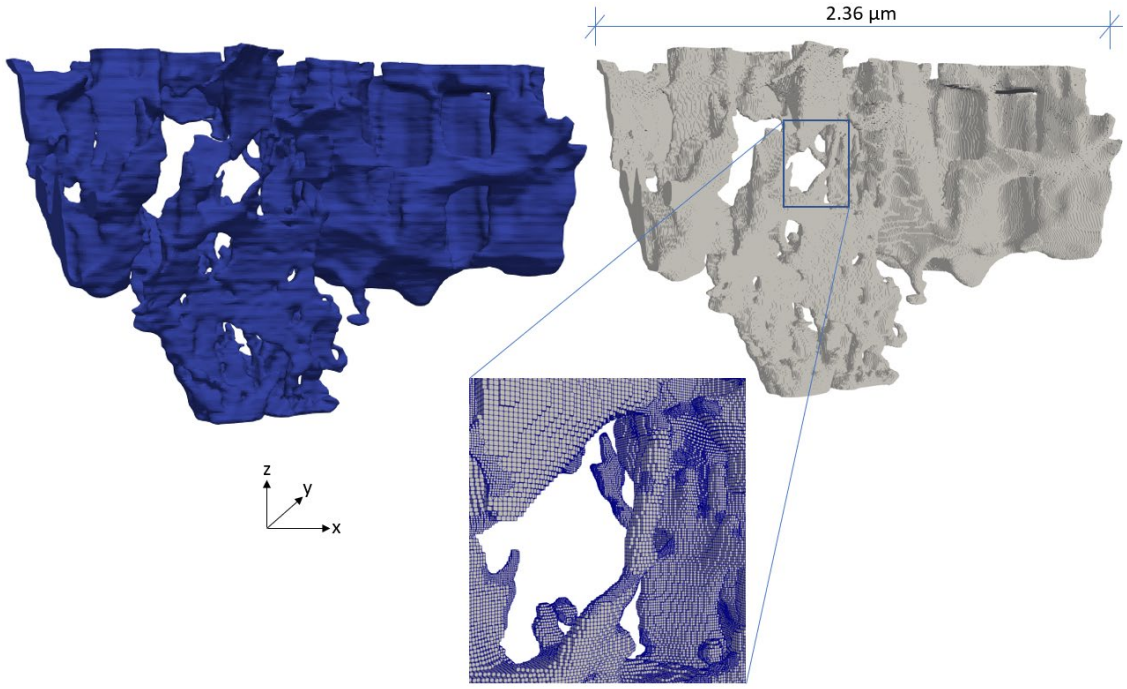

Figure 4-2- The imaged pore geometry is shown in blue color, whereas the mesh is shown in gray color with a zoom-in view to show the cell refinement along one of the pore throats.

4.2 Mathematical Model

Once the void fraction is identified and the mesh is prepared, the continuity equation for incompressible fluid can be written as follow:

$$\nabla \cdot \vec{V} = 0 \qquad (6)$$

By substituting the constitutive relationships that link the shear stress to the rate of deformation for a Newtonian fluid, the conservation of momentum can be written as follow:

$$\rho\left[\frac{\partial\vec{V}}{\partial t}+\ \vec{V}\cdot\nabla\vec{V}\right]=-\nabla P+\mu\nabla^2\vec{V} \qquad (7)$$

Where P is the pressure, μ is the dynamic viscosity, and $\vec{V}$ is the velocity vector. Equation (7) is a representation of Newton's second law and it is known as the Navier-Stokes equation. The right-hand side has two terms that represent the pressure gradient and diffusion terms. The left-hand side has two acceleration terms which are linear local acceleration and non-linear advective acceleration. The non-linearity due to the advective term will be addressed via an iterative numerical framework.

After solving the velocity and pressure fields numerically, streamlines within the pore system were computed by integrating the equation of motion for massless particle shown below:

$$\frac{d}{dt}\vec{x}(t)=\vec{V}(\vec{x}(t),t) \qquad (8)$$

The particle position components along x, y, and z axes were identified by applying 4th order Runge-Kutta method as integration technique. The particle position was then related to tortuosity as it will be discussed in detail in the results section.

One of the difficulties in solving Equation (7) is the weak coupling between pressure and velocity as there is no explicit differential equation for the pressure. For compressible flow, the velocity and pressure are coupled via an equation of state. However, for incompressible flow, the continuity equation is used along with the momentum divergence to formulate additional equation known as Poisson's equation.

4.3 Numerical Approach and Simulation Setup

Numerical implementation and simulation assumptions will be discussed in this section. Finite-volume method was used to solve the mathematical model discussed in the previous section. The goal of the finite-volume method is to represent and evaluate partial differential equations in the form of algebraic equations. Besides its computational efficiency, it is capable of handling unstructured grids which are needed to capture the details of the shale sample pore morphology. Essentially, the flow domain was divided into subdomains called control volumes, and then the conservation equations (mass and momentum) were integrated over each control volume. Therefore, the finite-volume technique inherently satisfies the conservation property and there is no need to impose conservativeness to the formulation. The volume integrals were then converted to surface integrals with the aid of the divergence theorem to arrive at the discretized form. PISO (Pressure-Implicit with Splitting of Operators) was used as a procedure to solve the pressure-velocity coupling; the PISO technique was originally proposed by (Issa, 1986). Finally, the results were presented in terms of algebraic quantities that were solved iteratively.

The finite-volume method was implemented via openFOAM® toolbox. Details regarding required hardware and software along with code are provided in the code availability section. The open source code offers a variety of schemes for discretizing the gradient, convection, and diffusion terms. Depending on the mesh quality, the choice of the scheme is determined. For instance, when the mesh has good quality cells, such as full hexahedrons, the gradient can be discretized by applying Gauss's linear scheme which is a central differencing scheme. Otherwise, the gradient limiter scheme needs to be applied to ensure that the extrapolated gradient falls within the minimum and maximum of neighboring points.

Regarding the pore fluid physical properties, water was selected as pore fluid during the simulation; it has density of 1000 $kg.m^{-3}$ and dynamic viscosity of 0.001 Pa.s. The slip boundary condition was adopted at the solid boundaries and the flow domain was initialized by applying a pressure gradient between inlet and outlet of 100 psi.

4.4 Novel Workflow to Compute Tortuosity from Streamlines

Streamlines are paths that imaginary particles would take if they were released into the flow stream. Streamlines carry significant information about the velocity field direction and magnitude at each point. Tortuosity is defined a as the ratio of streamline length to the straight-line distance between its two ends as shown in equation (9), where T_s is the streamline tortuosity, L_s is streamline tortuous length, and L is the streamline straight-line distance between its two ends.

$$T_s = \frac{L_s}{L} \qquad (9)$$

After solving for the velocity field that was derived in the mathematical model section, the equation of motion for massless particle was integrated to compute streamlines within the sample pore body. The cumulative distance between the particles of each streamline was computed to determine the tortuous length of the streamline. The straight-line distance was also calculated for each streamline by simply utilizing the distance equation between two points. Figure 4-3 presents flow streamlines colored by their corresponding tortuosity value. Results suggest that the sample has tortuosity range of 1.1 to 3.9, and a mean of 1.7. Figure 4-4 depicts a filtered version that shows tortuosity values greater, or equal to 2 to illustrate the highly tortuous paths within the tight shale sample.

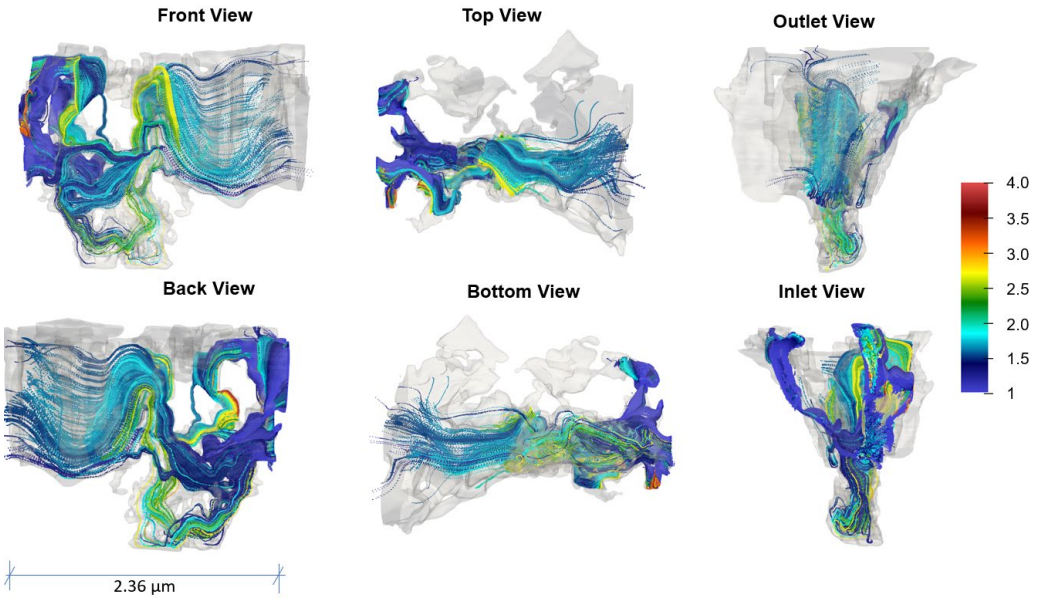

Figure 4-3- Transparent 3D pore geometry reveals streamlines colored by their corresponding tortuosity.

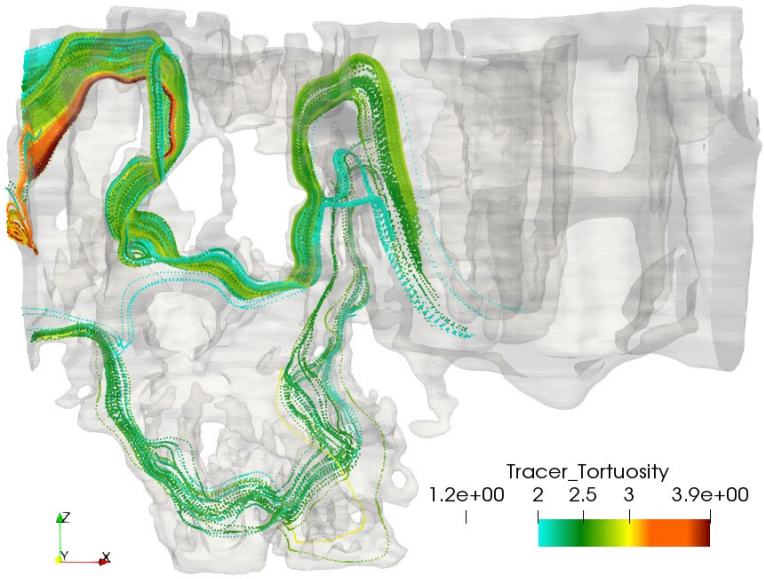

Figure 4-4- Streamlines registered tortuosity greater, or equal to 2.

Tortuosity is often estimated from empirical models, especially in the absence of laboratory experiments and simulation results. One of the most commonly used empirical models is the model proposed by (Comiti and Renaud, 1989). The model represents tortuosity as logarithmic function of porosity as show in equation (10).

$$T = 1 - P \ln \emptyset \qquad (10)$$

Where φ is porosity and P is an empirical parameter that is usually estimated by simulations, or experiments. The model satisfies $T = 1$ when $\emptyset = 100\%$, and satisfies $T = \infty$ when $\emptyset = 0\%$. Streamline based simulation can be used to fine-tune empirical models. For instance, since the shale sample has 4% porosity and average tortuosity of 1.8, the P value is estimated to be 0.25. Obviously, more samples need to be simulated to inform the appropriate P value for shale reservoirs. Additionally, the simulated tortuosity

results are well aligned with findings derived from (Pisani, 2011) model for spherical particles shown in equation (11). Based on Pisani's model, tortuosity is calculated to be 1.6.

$$T = 1 + 0.64(1 - \emptyset) \qquad (11)$$

Furthermore, to gain insights into the statistical distribution of tortuosity within the shale sample, three theoretical probability density functions (log-normal, Weibull, and gamma) were attempted to model the tortuosity distribution. Based on the maximum likelihood estimation, log-normal distribution was found to fit the data best as shown in Figure 4-5. The fitting parameters were 0.57, and 0.25 logarithmic mean and standard deviation respectively.

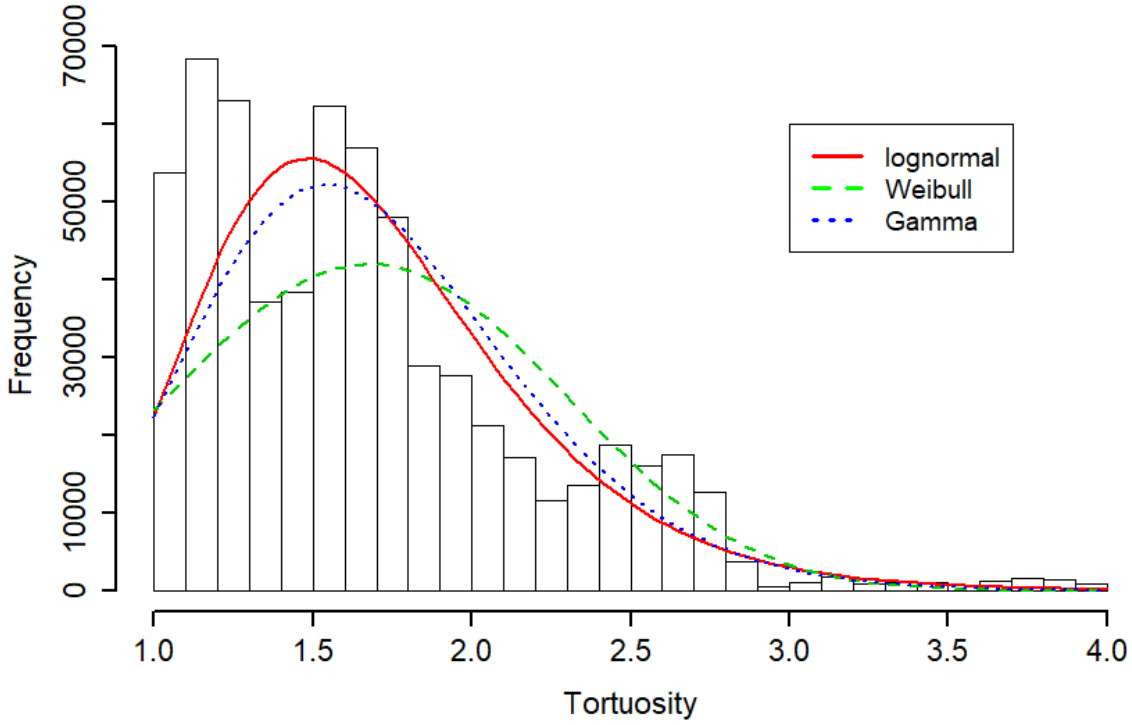

Figure 4-5- Simulated tortuosity histogram overlain by theoretical probability density functions.

4.5 Computation of Permeability with Varying Mesh Sizes

It is imperative to accurately estimate reservoir permeability to identify optimal number of horizontal wells and mitigate economical risks due to over capitalization. In this section, permeability will be computed numerically based on transient incompressible simulation, and mesh convergence study will be conducted to investigate the dependence of permeability on the mesh size.

Five transient simulations were run with varying mesh sizes as shown in Figure 4-6. The meshes were designed such that the minimum pore throat has at least 10 cells from wall to wall. Simulation cases were terminated once the velocity had stabilized. The

average inlet and outlet pressures were calculated by performing surface integration at the inlet and outlet faces for each time step. The average velocity was obtained by conducting volume integration over the control volumes that constituted the pore geometry. Consequently, permeability values were calculated via Darcy formulation at each time step. Similar discretization schemes were applied to all cases. Essentially, the time schemes were discretized using (Crank and Nicolson, 1996) method which is a second-order accurate and implicit scheme. The gradient calculation was performed using least squares approach.

Moreover, Courant number (convergence measure) was calculated independently for each cell because it depends on the cell size, time step, and velocity. Courant number was maintained below 1 by automatically adjusting the time step to avoid convergence problems. Finally, permeabilities were plotted against simulation time as shown in Figure 4-6. Results suggest lower permeability values for finer meshes during the transient period. Eventually, the 5 mesh sizes reached comparable steady-state permeability of 480 nano-Darcy after about 20 nanoseconds.

Table 8- Number of cells in each direction with final mesh size.

Mesh ID	Cells in (X, Y, Z)	Background cells	Final cells
1	236X189X167	7,474,087	54,094,873
2	95X76X67	478,342	8,349,364
3	59X47X42	116,783	3,208,171
4	43X34X30	43,860	1,666,819
5	34X27X24	22,032	1,180,087

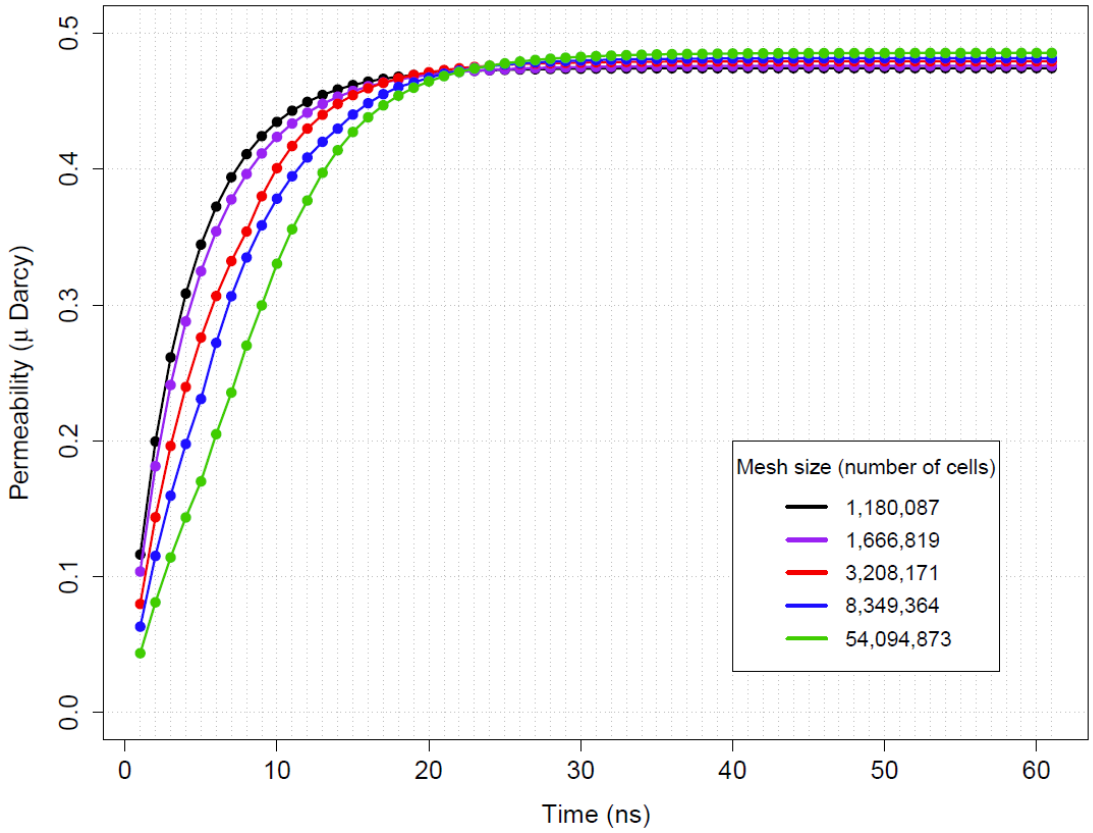

Figure 4-6- Permeability mesh sensitivities based on five mesh densities.

Numerical results need to be calibrated with experimental data once a consistent methodology for measuring shale permeability becomes available. Several studies have pointed out that standardized methods for measuring shale permeability do not exist such as (Sondergeld et al., 2010) and (Tinni et al., 2012). Likewise, (Passey et al. 2010) conducted a comparative study on permeability measured by different laboratories using crushed rock samples in which each laboratory received sample splits from the same depth interval. Authors found that permeability values reported by different laboratories varied by 2-3 orders of magnitude. However, more recently, there have been several

encouraging developments to measure shale permeability experimentally. For instance, (Krumm and Howard 2017) developed a workflow for measuring shale permeability in the presence of micro-cracks. Authors have integrated micro-CT scanning, and NMR technology with standard steady-state permeability rig for measurement of the hydrocarbon flow. Authors claim that a full permeability test requires 7-14 days to complete. It is worth mentioning that permeability results presented in this study need to be verified with similar experimental tests.

4.6 Analysis of Permeability Representative Elementary Volume (REV)

Several statistical techniques have been attempted to characterize the microstructure of porous media at various length scales such as the recent work of (Adeleye and Akanji, 2017). In this work, computational approach is implemented to assess the dependence of permeability on the pore volume size. The finest mesh size was used to compute permeability at different volume increments. The pore volume was reduced by 10% successively to create 10 sub-volumes. S-1 represents the smallest volume, whereas S-10 represents the full pore volume as shown in Figure 4-7.

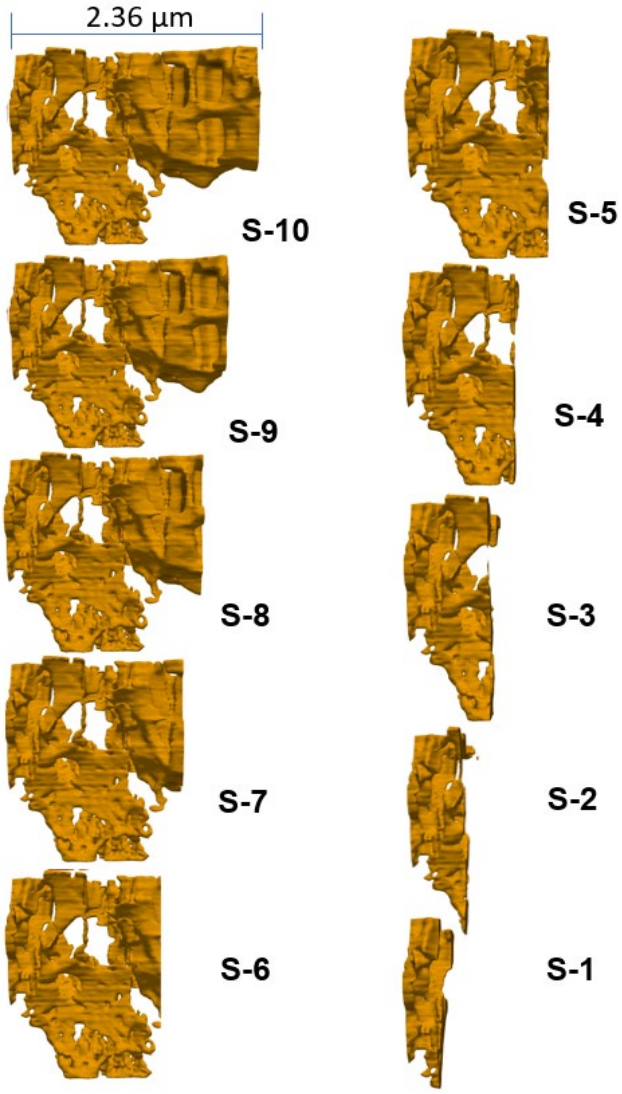

Figure 4-7- Volume increments of the original shale sample. (S-1) depicts the smallest volume whereas (S-10) depicts the full pore volume.

The sub-volume inlet and outlet pressures were calculated by performing surface integration. The corresponding flow velocity was obtained by performing volume integration over the volume of the sample. By knowing the sub-volume pressure drop and flow velocity, Darcy's law is used to compute permeability. Those steps were repeated for each sector to obtain permeability. Figure 4-8 presents a bar chart with the

permeability value for each volume increment. Furthermore, uniform volume reductions of 25%, 50%, and 75% of the original volume have been applied and then solved for permeability. Permeability values for reduction of 0%, 25%, 50%, and 75% were 0.480, 0.146, 4.808, and 4.744 micro Darcy respectively.

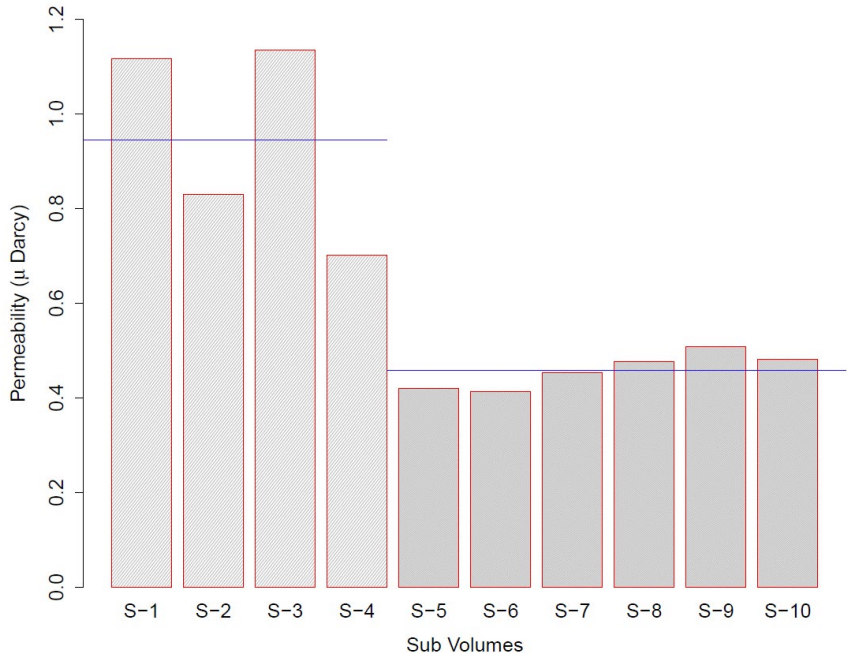

Figure 4-8- Permeability values for each volume increment. Blue horizontal lines represent the average permeability for intervals S-1 to S-4 and S-5 to S-10 respectively.

Looking closely at the results, two permeability groups can be distinguished (S1-S4) and (S5-S10). Blue horizontal lines indicating the average permeability for each group are shown on Figure 4-8. Results suggest that a shale sample of volume 7.44 cubic micron is not enough to identify the REV of permeability. Findings from recent studies such as (Al-Raoush and Papadopoulos, 2010), and (Mostaghimi et al., 2012) have

revealed that the REV is property specific, which makes the task of upscaling learnings from one scale to the next even more challenging.

4.7 Assumptions and Limitations

Transport properties of tight reservoirs such as shales are difficult to measure, and measurements can often be inaccurate and expensive. Computational means to obtain shale transport properties of pore-scale samples is viable; however, it is computationally intensive and requires proper diligence. Fluid flow within a 3D pore network was modeled as continuum because the minimum diameter of the pore throat was 30 nanometers which leads to a Knudson number in the order of 0.01. However, the concept of continuum flow breaks whenever the smallest characteristic length becomes in the same order as the mean free path of the fluid molecules such as the case of shale gas reservoirs. Hence, the assumption of fluid continuity is sample-specific and needs to be evaluated on case by case basis. Luckily, such reservoirs have significantly less economic value if compared to oil rich shale reservoirs. Otherwise, if the pore system is small in comparison to the distance between molecules, fluid flow needs to be simulated as discrete particles using Lattice-Boltzmann method.

It is imperative to develop knowledge about the morphology of the porous media to predict movement of hydrocarbons and evaluate the reservoir commercial viability. The average tortuosity within the shale sample was 1.7 with 29% of the streamlines registered tortuosity greater, or equal to 2. Findings from studies conducted on sandstone

rocks show tortuosity values of 1.4 and 1.2 based on (Gommes et al., 2009) and (Spearing and Matthews, 1991) respectively. Hence, the results suggest substantial resistance to fluid flow within tight reservoirs in comparison to sandstone reservoirs. Findings aim to assist the efforts of designing and implementing optimal field development strategies by providing better understanding of the flow capacity and visualizing the intricate pathways traced by reservoir fluids within tight reservoirs.

Furthermore, despite mesh convergence studies are done routinely in the CFD community, they are not performed regularly during pore-scale simulation which could be detrimental to the accuracy and reliability of the solution. Results suggest that denser meshes lead to slower flow development during the transient period (less than 20 nanoseconds). Because denser meshes can resolve more flow features, they lead to lower intrinsic permeability during the transient time.

FIB-SEM tomography provides detailed realizations of the complex pore-network. However, the imaged volumes are small and expensive. Therefore, it is crucial to identify the representative elementary volume prior to populating results to the reservoir scale. Despite the FIB-SEM technology has provided high resolution images of the pore structure, the size of the simulated pore volume was insufficient to identify the REV of permeability. Results suggest that a shale sample of volume (2.36 X 1.89 X 1.67) cubic micron is within the domain of microscopic heterogeneity. In other words, the observation scale is smaller than the representative elementary volume. Emerging plasma FIB-SEM technology offers the promise of larger volumes at shorter imaging time that

could reach up to 50 times faster compared to conventional FIB-SEM technology (Burnett et al., 2016).

Chapter 5: Recommendations and Conclusions

5.1 Recommendations to Mitigate Well Interference

Oil and gas operators commenced asset appraisal activities by drilling, completing, and producing one, or two horizontal wells to hold the lease. These wells are known as a "parent wells".

The process of holding the lease by parent wells is called Held-By-Production (HBP) which is a provision that perpetuates a company's right to fully operate the lease. HBP provides asset teams with the time needed to go through the learning curve to understand the physical properties of the rock as well as the expected well performance (well commerciality). Subsequent infill wells, known as "child wells", are then drilled at a later time to commence full field development. While the parent wells are continually depleting the reservoir, child wells could be drilled as late as three years after the initial parent well.

operators observed that when a new horizontal well (child) is drilled next to a depleted zone, the new well's fracture geometry tends to be asymmetric. Hydraulic fractures of the new well preferentially grow in the direction of the depleted zone because it is the path of least resistance, and thus both parent and child wells suffer from adverse consequences

such as loss of initial productivity, casing collapse, and loss of reserves. Field-based mitigation techniques that can be attempted to address parent-child interactions are summarized below:

- Parent wells can be re-pressurized by injecting fluid to reduce effective stresses within the stimulated rock volume and thus mitigate the issue of asymmetric fracture growth. (Gala, Manchanda, and Sharma 2018) has attempted to model fluid injection in a parent well to compare water and gas injections. Obviously, pressure build-up in the parent well can be achieved much faster when water is injected. This is mainly because of the difference between water and gas compressibility. Gala's numerical simulation can be expanded to investigate the following:
    - Optimal injection rate relative fracture gradient.
    - Quantity of the fluid need to be injected.
    - Feasibility of the injection in the presence of natural fractures.
    - Cost-benefit analysis associated with such operations (cash flow analysis).
- The effect of heel-bias (dominant fractures within a stage) can be mitigated by implementing extreme limited entry approach. Reducing number of perforations, achieving equal hole size, and increasing treatment rate amplify bottom-hole treating pressure which in turn lead to more even distribution of treatment fluid. The downhole injection pressure needs to be higher than the fracture extension pressure during stage treatment. Thus, any perforation erosion leads to a decreased

differential pressure. Shell Canada tested extreme limited entry designs to investigate if differential perforation pressure improves treatment distribution (Somanchi et al., 2017). Results were validated by fiber optics measurements. The authors claim 40% improvement in fluid and proppant distribution per cluster.

- The parent well can be re-fractured to re-establish connection with the reservoir, and perhaps create additional surface area. Unlike re-pressurization, re-fracturing involves the addition of proppant to the parent well either by perforating new clusters, or by using existing clusters. Recently, (Garza et al. 2019) presented promising results based on a re-fracturing treatment from the Eagle Ford Shale. Results show that the re-fracturing procedure has protected the parent well reserves. Also, authors have provided the details associated with well preparation, fracturing, and drill-outs procedures need to be followed to achieve successful re-fracturing operation.
- Depending on the remaining value in the parent well, increasing well-spacing by reducing the number of infill wells could help in alleviating the effect of depletion from the parent well. Alternatively, the location of first child offset can be skipped without altering the spacing of other child wells.

5.2 Conclusions

Moving into full field development via stack-staggering has amplified the amount of attention being paid to inter- and intra-well interference. Hence, this research aimed to

simulate well performance under various conditions to better understand well interference.

Based on a numerical approach, this thesis sedulously interrogated the relative contribution of rock matrix, fracture parameters, economics, and operational characteristics, vis-a-vis short and long term well performance in tight oil reservoirs.

The physical principals that were utilized in this work are conservation of mass, Darcy's law, thermodynamic equilibrium. Numerical models presented in this work are three-phase, transient, and consider compressible fluid flow. Fluid thermodynamics were addressed via equation of state. Key learnings are summarized below.

5.2.1 Modeling of Intra-Well Interference

- Depending on the desired economic metric (NPV, or IRR), the magnitude of intra-well interference can be optimized. For instance, if the objective is to maximize rate of return, then tighter fracture spacing may be accepted.
- History match was obtained to three-phase production and flowing bottom-hole pressure for a well from the Meramec Formation. Gas-oil ratio was history matched without the need to invoke bubble point suppression, or high critical gas saturation.
- Modeling reduction in hydraulic fracture conductivity due to depletion was needed to match field data. Based on wells from Meramec and Wolfcamp

formations, the loss of hydraulic fracture conductivity exceeds 60% after 3 years of production.

- Based on the assumptions presented in intra-well modeling, results show that gain in rate of return due to aggressive drawdown is much less if compared to the loss in net present value. However, at higher oil prices loss of net present value is less important relative to gains in rate of return. Results shed light on the interplay between choke management strategy and oil price environment.
- 50 ft cluster spacing with conservative drawdown was found to be the optimal design in the Meramec example well. Results show that 90 ft fracture spacing erodes the value of the investment, yielding the least NPV. The economics evaluation has taken into consideration the different profiles of gas-oil ratio due to fracture spacing.
- Closely spaced fractures accelerate the onset of Boundary Dominated Flow (BDF) which results in steeper rise in gas-oil ratio due to intra-well interference.
- Simulation results of inter-well interference suggest that the hydraulic fracture height tends to grow upward for both parent wells.

5.2.2 Modeling of Inter-Well Interference

- Simulation results also show that propped fracture half-length for P1H, and P2H are115 ft, and 300 ft respectively.

- P1H (lower well) has slightly underperformed P2H (upper well) on oil production. Upward growth of P1H hydraulic fractures into better porosity zones and landing in a higher natural fracture zone has helped P1H performance, but drainage pathways were less efficient if compared P2H.
- Multi-well simulation results show that the P2H unpropped fracture permeability is 20 uD whereas the P1H unpropped fracture permeability is 10 uD. Those unpropped fractures lead to preferential growth toward the depleted region of the parent well. Obviously, this will lead to asymmetric fractures in child well with reduced chance of effective stimulation.
- Inter-well interference diagnostics reveal that there is 7000 psi of un-depleted pressure after 3 years of production between P1H and P2H. If well cost and oil pricing are favorable, these results suggest potential for adding additional well to drain the resource efficiently.

5.2.3 Finite-Volume Modeling at the Pore Scale

- Matrix permeability represents a major unknown that impacts both inter- and intra-well interference as shown in section 2.9.5. By capitalizing on recent advancements in pore-scale imaging and modeling, fluid flow was successfully simulated in a sample based on a three-dimensional pore network.
- Given the remarkable diversity of tortuosity definitions in the literature, a consistent approach that benefits from the concept of flow streamlines was

implemented to develop a novel method to compute tortuosity. It was observed that shales can have significant tortuosity that can reach up to 3.9. Findings reveal the highly tortuous nature of shale reservoirs.

- Mesh convergence study was conducted for the first time on a shale sample to evaluate its permeability dependence on mesh density. Results suggest permeability dependence on the mesh size during the transient period, and less so, during the steady-state period.
- Based on Representative Elementary Volume (REV) analysis, the numerical investigation confirms that even at the nano-scale, depending on the heterogeneity, permeability can have significant variation. However, clusters of similar permeability can exist as well. Ultimately, results suggest that a shale sample of volume (2.36 X 1.89 X 1.67) cubic micron is within the domain of microscopic heterogeneity, and insufficient to derive permeability REV.

5.3 Statement of Research Contribution

The problem of well interference provides critical insights into a variety of interesting physical concepts ranging from phase-behavior to fluid and rock mechanics. One-third of the fractured horizontal well contributes to more than 50% of the overall well production. This is mainly due to poor well spacing and/or inefficient completions design. Hence, improving hydraulic fracture efficiency will increase well production

without the need to increase sand, water, chemicals, and pump horsepower. This translates into positive environmental impact, and significant cost savings. Findings from this research offer practical recommendations to mitigate and diagnose well interference and identify its implications on completions design, and well-spacing decisions in unconventional reservoirs.

References

Adeleye, J.O., Akanji, L.T., 2017. Pore-scale analyses of heterogeneity and representative elementary volume for unconventional shale rocks using statistical tools. J. Pet. Explor. Prod. Technol. 1–13. https://doi.org/10.1007/s13202-017-0377-4.

Al-Raoush, R., Papadopoulos, A., 2010. Representative elementary volume analysis of porous media using X-ray computed tomography. Powder Technol. 200, 69–77.

Andrä, H., Combaret, N., Dvorkin, J., Glatt, E., Han, J., Kabel, M., Keehm, Y., Krzikalla, F., Lee, M., Madonna, C., 2013. Digital rock physics benchmarks—Part I: Imaging and segmentation. Comput. Geosci. 50, 25–32.

Aslannejad, H., Hassanizadeh, S.M., 2017. Study of Hydraulic Properties of Uncoated Paper: Image Analysis and Pore-Scale Modeling. Transp. Porous Media 120, 67–81. https://doi.org/10.1007/s11242-017-0909-x

Agrawal, Shivam, and Mukul M. Sharma. 2018. "Impact of Pore Pressure Depletion on Stress Reorientation and Its Implications on the Growth of Child Well Fractures." In Unconventional Resources Technology Conference, Houston, Texas, 23-25 July 2018, 31–42. Society of Exploration Geophysicists, American Association of Petroleum Geologists.

Ajisafe, Foluke O., Irina Solovyeva, Adrian Morales, Efe Ejofodomi, and Matteo Marongiu Porcu. 2017. "Impact of Well Spacing and Interference on Production Performance in Unconventional Reservoirs, Permian Basin." In Unconventional Resources Technology Conference (URTEC).

Almasoodi, Mouin M., Younane N. Abousleiman, and Son K. Hoang. 2014. "Viscoelastic Creep of Eagle Ford Shale: Investigating Fluid-Shale Interaction." In SPE/CSUR Unconventional Resources Conference–Canada. Society of Petroleum Engineers.

"Annual Energy Outlook 2018 with Projections to 2050." 2018. US Energy Information Administration, February 2018.

Bazan, Lucas W., Samuel Dale Larkin, Michael G. Lattibeaudiere, and Terrence T. Palisch. 2010. “Improving Production in the Eagle Ford Shale with Fracture Modeling, Increased Fracture Conductivity, and Optimized Stage and Cluster Spacing along the Horizontal Wellbore.” In Tight Gas Completions Conference. Society of Petroleum Engineers.

Beggs, H. Dale, and JRs Robinson. "Estimating the viscosity of crude oil systems." Journal of Petroleum technology 27.09 (1975): 1-140.

Berg, S., Rücker, M., Ott, H., Georgiadis, A., Van der Linde, H., Enzmann, F., Kersten, M., Armstrong, R.T., Becker, J., Wiegmann, A., 2016. Connected pathway relative permeability from pore-scale imaging of imbibition. Adv. Water Resour. 90, 24–35.

Blasingame, Thomas Alwin. "The characteristic flow behavior of low-permeability reservoir systems." SPE Unconventional Reservoirs Conference. Society of Petroleum Engineers, 2008.

Blasingame, T. A., and W. J. Lee. "Pressure-buildup test analysis-Variable-rate case." SPE (Society of Petroleum Engineers) Format. Eval.;(United States) 4.2 (1989).

Blasingame, T. A., and W. J. Lee. "Pressure-buildup test analysis-variable-rate case: a new approach." SPE Formation Evaluation 4.02 (1989): 273-280.

Blunt, M.J., Bijeljic, B., Dong, H., Gharbi, O., Iglauer, S., Mostaghimi, P., Paluszny, A., Pentland, C., 2013. Pore-scale imaging and modelling. Adv. Water Resour., 35th Year Anniversary Issue 51, 197–216. https://doi.org/10.1016/j.advwatres.2012.03.003

Burnett, T.L., Kelley, R., Winiarski, B., Contreras, L., Daly, M., Gholinia, A., Burke, M.G., Withers, P.J., 2016. Large volume serial section tomography by Xe Plasma FIB dual beam microscopy. Ultramicroscopy 161, 119–129. https://doi.org/10.1016/j.ultramic.2015.11.001

Cao, R., Li, R., Girardi, A., Chowdhury, N. and Chen, C., 2017, September. Well interference and optimum well spacing for Wolfcamp development at Permian Basin. In Unconventional Resources Technology Conference, Austin, Texas, 24-26 July 2017 (pp. 2756-2766). Society of Exploration Geophysicists, American Association of Petroleum Geologists, Society of Petroleum Engineers.

Cheng, Yueming. 2012. "Impacts of the Number of Perforation Clusters and Cluster Spacing on Production Performance of Horizontal Shale-Gas Wells." SPE Reservoir Evaluation & Engineering 15 (01): 31–40.

Chu, L., P. Ye, I. Harmawan, and L. Du. 2015. "Characterizing and Simulating the Non-Stationarity and Non-Linearity in Unconventional Oil Reservoirs: Bakken Application." Journal of Unconventional Oil and Gas Resources 9: 40–53.

Ciezobka, Jordan, James Courtier, and Joe Wicker. 2018. "Hydraulic Fracturing Test Site (HFTS)–Project Overview and Summary of Results." In Unconventional Resources Technology Conference, Houston, Texas, 23-25 July 2018, 1331–1339. Society of Exploration Geophysicists.

Cipolla, Craig, Xiaowei Weng, Mark Mack, Utpal Ganguly, Hongren Gu, Olga Kresse, and C. Cohen. 2012. "Integrating Microseismic Mapping and Complex Fracture Modeling to Characterize Fracture Complexity." In SPE/EAGE European Unconventional Resources Conference & Exhibition-From Potential to Production.

Carman, P.C., 1937. Fluid flow through granular beds. Trans Inst Chem Eng 15, 150–166.

Comiti, J., Renaud, M., 1989. A new model for determining mean structure parameters of fixed beds from pressure drop measurements: application to beds packed with parallelepipedal particles. Chem. Eng. Sci. 44, 1539–1545.

Crank, J., Nicolson, P., 1996. A practical method for numerical evaluation of solutions of partial differential equations of the heat-conduction type. Adv. Comput. Math. 6, 207–226.

Delattre, B., Amin, R., Sander, J., Coninck, J.D., Tomsia, A.P., Chiang, Y.-M., 2018. Impact of Pore Tortuosity on Electrode Kinetics in Lithium Battery Electrodes: Study in Directionally Freeze-Cast LiNi0.8Co0.15Al0.05O2 (NCA). J. Electrochem. Soc. 165, A388–A395.

Dennis, J., Fournier, A., Spotz, W.F., St-Cyr, A., Taylor, M.A., Thomas, S.J., Tufo, H., 2005. High-resolution mesh convergence properties and parallel efficiency of a spectral element atmospheric dynamical core. Int. J. High Perform. Comput. Appl. 19, 225–235.

Ebner, Martin, Ding-Wen Chung, R. Edwin García, and Vanessa Wood. 2014. "Tortuosity Anisotropy in Lithium-Ion Battery Electrodes." Advanced Energy Materials 4 (5): 1301278. https://doi.org/10.1002/aenm.201301278.

Fu, Yingkun, Hassan Dehghanpour, Obinna Ezulike, Claudio Virues, and Doug Bearinger. 2017. "Investigating Well Interference in a Multi-Well Pad by Combined Flowback and Tracer Analysis." In Unconventional Resources Technology Conference, Austin, Texas, 24-26 July 2017, 3490–3502. Society of Exploration Geophysicists, American Association of Petroleum Geologists.

Gala, Deepen P., Ripudaman Manchanda, and Mukul M. Sharma. 2018. "Modeling of Fluid Injection in Depleted Parent Wells to Minimize Damage Due to Frac-Hits." In Unconventional Resources Technology Conference, Houston, Texas, 23-25 July 2018, 4118–4131. Society of Exploration Geophysicists.

Garza, Mary, Joshua Baumbach, James Prosser, Spencer Pettigrew, and Kirsten Elvig. 2019. "An Eagle Ford Case Study: Improving an Infill Well Completion Through Optimized Refracturing Treatment of the Offset Parent Wells." In SPE Hydraulic Fracturing Technology Conference and Exhibition. Society of Petroleum Engineers.

Geertsma, J., and F. De Klerk. 1969. "A Rapid Method of Predicting Width and Extent of Hydraulically Induced Fractures." Journal of Petroleum Technology 21 (12): 1–571.

Gommes, C.J., Bons, A.-J., Blacher, S., Dunsmuir, J.H., Tsou, A.H., 2009. Practical methods for measuring the tortuosity of porous materials from binary or gray-tone tomographic reconstructions. AIChE J. 55, 2000–2012.

Haustveit, Kyle, K. Dahlgren, H. Greenwood, T. Peryam, B. Kennedy, and M. Dawson. 2017. “New Age Fracture Mapping Diagnostic Tools-A STACK Case Study.” In SPE Hydraulic Fracturing Technology Conference and Exhibition. Society of Petroleum Engineers.

Huckabee, Paul Thomas. 2009. “Optic Fiber Distributed Temperature for Fracture Stimulation Diagnostics and Well Performance Evaluation.” In SPE Hydraulic Fracturing Technology Conference. Society of Petroleum Engineers.

Hwang, Jongsoo, Matthew J. Szabian, and Mukul M. Sharma. 2017. “Hydraulic Fracture Diagnostics and Stress Interference Analysis by Water Hammer Signatures in Multi-Stage Pumping Data.” In Unconventional Resources Technology Conference, Austin, Texas, 24-26 July 2017, 2172–2183. Society of Exploration Geophysicists, American Association of Petroleum Geologists.

Iino, Atsushi, Tsubasa Onishi, Feyi Olalotiti-Lawal, and Akhil Datta-Gupta. 2018. “Rapid Field-Scale Well Spacing Optimization in Tight and Shale Oil Reservoirs Using Fast Marching Method.” In Unconventional Resources Technology Conference, Houston, Texas, 23-25 July 2018, 1864–1880. Society of Exploration Geophysicists.

Jones Jr, R. Steven. 2017. “Producing-Gas/Oil-Ratio Behavior of Multifractured Horizontal Wells in Tight Oil Reservoirs.” SPE Reservoir Evaluation & Engineering 20 (03): 589–601.

Khoshghadam, Mohammad, A. Khanal, and W. J. Lee. 2015. “Numerical Study of Impact of Nano-Pores on Gas-Oil Ratio and Production Mechanisms in Liquid-Rich Shale Oil Reservoirs.” In Unconventional Resources Technology Conference, San Antonio, Texas, 20-22 July 2015, 1799–1817. Society of Exploration Geophysicists, American Association of Petroleum Geologists.

Khoshghadam, Mohammad, Aaditya Khanal, C. Yu, Neda Rabinejadganji, and W. John Lee. 2017. “Producing Gas-Oil Ratio Behavior of Unconventional Volatile-Oil Reservoirs, and Its Application in Production Diagnostics and Decline Curve Analysis.” In Unconventional Resources Technology Conference, Austin, Texas,

24-26 July 2017, 1532–1548. Society of Exploration Geophysicists, American Association of Petroleum Geologists.

Kozeny, Josef. 1927. “Uber Kapillare Leitung Der Wasser in Boden.” Royal Academy of Science, Vienna, Proc. Class I 136: 271–306.

Krumm, Robert L., and James J. Howard. 2017. “WORKFLOW FOR MEASUREMENT OF STEADY-STATE TO LIQUID PERMEABILITY IN NANO-DARCY RESERVOIR ROCK.”

Kumar, Ashish, Puneet Seth, Kaustubh Shrivastava, Ripudaman Manchanda, and Mukul M. Sharma. 2018. “Well Interference Diagnosis through Integrated Analysis of Tracer and Pressure Interference Tests.” In Unconventional Resources Technology Conference, Houston, Texas, 23-25 July 2018, 1404–1415. Society of Exploration Geophysicists.

Lalehrokh, Farshad, and Jared Bouma. 2014. “Well Spacing Optimization in Eagle Ford.” In SPE/CSUR Unconventional Resources Conference–Canada. Society of Petroleum Engineers.

Liang, Baosheng, Meilin Du, and Pablo Paez Yanez. 2019. “Subsurface Well Spacing Optimization in the Permian Basin.” Journal of Petroleum Science and Engineering 174: 235–243.

Liang, Baosheng, Shahzad Khan, and Yula Tang. 2017. “Section Development Optimization and Frac Hit Mitigation in the Wolfcamp Stacked Pay in the Midland Basin Through Data Monitoring and Integrated Modeling.” In Unconventional Resources Technology Conference, Austin, Texas, 24-26 July 2017, 1763–1778. Society of Exploration Geophysicists.

Lee, Y., Barthel, S.D., Dłotko, P., Moosavi, S.M., Hess, K., Smit, B., 2017. Quantifying similarity of pore-geometry in nanoporous materials. Nat. Commun. 8, 15396. https://doi.org/10.1038/ncomms15396

Madonna, Claudio, Beatriz Quintal, Marcel Frehner, Bjarne SG Almqvist, Nicola Tisato, Mattia Pistone, Federica Marone, and Erik H. Saenger. 2013. “Synchrotron-Based X-Ray Tomographic Microscopy for Rock Physics InvestigationsSynchrotron-Based Rock Images.” Geophysics 78 (1): D53–D64.

Manchanda, Ripudaman, Prateek Bhardwaj, Jongsoo Hwang, and Mukul M. Sharma. 2018. “Parent-Child Fracture Interference: Explanation and Mitigation of Child Well Underperformance.” In SPE Hydraulic Fracturing Technology Conference and Exhibition. Society of Petroleum Engineers.

Manchanda, Ripudaman, Mukul M. Sharma, Mehdi Rafiee, and Lionel H. Ribeiro. 2017. “Overcoming the Impact of Reservoir Depletion to Achieve Effective Parent Well Refracturing.” In Unconventional Resources Technology Conference, Austin, Texas, 24-26 July 2017, 2888–2901. Society of Exploration Geophysicists, American Association of Petroleum Geologists.

Miller, Grant, Garrett Lindsay, Jason Baihly, and Tao Xu. 2016. “Parent Well Refracturing: Economic Safety Nets in an Uneconomic Market.” In SPE Low Perm Symposium. Society of Petroleum Engineers.

Min, Kyoung Suk, Vikram Sen, Lujun Ji, and Richard B. Sullivan. 2018. “Optimization of Completion and Well Spacing for Development of Multi-Stacked Reservoirs Using Integration of Data Analytics, Geomechanics and Reservoir Flow Modeling.” In Unconventional Resources Technology Conference, Houston, Texas, 23-25 July 2018, 615–625. Society of Exploration Geophysicists, American Association of Petroleum Geologists.

Mohammadmoradi, Peyman, and Apostolos Kantzas. 2016. “Pore-Scale Permeability Calculation Using CFD and DSMC Techniques.” Journal of Petroleum Science and Engineering 146: 515–525.

Mostaghimi, P., Bijeljic, B., Blunt, M., 2012. Simulation of flow and dispersion on pore-space images. SPE J. 17, 1–131.

Nieto, John, Graham Janega, Bogdan Batlai, and Hugo Martinez. 2018. “An Integrated Approach to Optimizing Completions and Protecting Parent Wells in the Montney Formation, NEBC.” In Unconventional Resources Technology Conference, Houston, Texas, 23-25 July 2018, 2346–2360. Society of Exploration Geophysicists, American Association of Petroleum Geologists.

Nordgren, R. P. 1972. “Propagation of a Vertical Hydraulic Fracture.” Society of Petroleum Engineers Journal 12 (04): 306–314.

Pankaj, Piyush. 2018. “Decoding Positives or Negatives of Fracture-Hits: A Geomechanical Investigation of Fracture-Hits and Its Implications for Well Productivity and Integrity.” In Unconventional Resources Technology Conference, Houston, Texas, 23-25 July 2018, 3717–3742. Society of Exploration Geophysicists, American Association of Petroleum Geologists.

Passey, Quinn R., Kevin Bohacs, William Lee Esch, Robert Klimentidis, and Somnath Sinha. 2010. “From Oil-Prone Source Rock to Gas-Producing Shale Reservoir-Geologic and Petrophysical Characterization of Unconventional Shale Gas Reservoirs.” In International Oil and Gas Conference and Exhibition in China. Society of Petroleum Engineers.

Pathak, Manas, Hyukmin Kweon, Palash Panja, Raul Velasco, and Milind D. Deo. 2017. “Suppression in the Bubble Points of Oils in Shales Combined Effect of Presence of Organic Matter and Confinement.” In SPE Unconventional Resources Conference. Society of Petroleum Engineers.

Paraschivoiu, M., Komeili, M., Zadeh, S.N., 2014. Mesh convergence study for 2-d straight-blade vertical axis wind turbine simulations and estimation for 3-d simulations. Trans. Can. Soc. Mech. Eng. 38.

Perkins, T. K., and L. R. Kern. 1961. “Widths of Hydraulic Fractures.” Journal of Petroleum Technology 13 (09): 937–949.

Piri, Mohammad, and Martin J. Blunt. 2005. “Three-Dimensional Mixed-Wet Random Pore-Scale Network Modeling of Two- and Three-Phase Flow in Porous Media. II. Results.” Physical Review E 71 (2): 026302. https://doi.org/10.1103/PhysRevE.71.026302.

Pisani, L., 2011. Simple Expression for the Tortuosity of Porous Media. Transp. Porous Media 88, 193–203. https://doi.org/10.1007/s11242-011-9734-9.

Power, C., Navarro, J.F., Jenkins, A., Frenk, C.S., White, S.D., Springel, V., Stadel, J., Quinn, T., 2003. The inner structure of ΛCDM haloes—I. A numerical convergence study. Mon. Not. R. Astron. Soc. 338, 14–34.

Quintero*, J., and D. Devegowda. 2015. “Modelling Based Recommendation for Choke Management in Shale Wells.” In Unconventional Resources Technology Conference, San Antonio, Texas, 20-22 July 2015, 1201–14. SEG Global Meeting Abstracts. Society of Exploration Geophysicists, American Association of Petroleum Geologists, Society of Petroleum Engineers. https://doi.org/10.15530/urtec-2015-2154991.

Raeini, Ali Q., Martin J. Blunt, and Branko Bijeljic. 2014. “Direct Simulations of Two-Phase Flow on Micro-CT Images of Porous Media and Upscaling of Pore-Scale Forces.” Advances in Water Resources 74: 116–126.

Rojas, Daniela, and Alejandro Lerza. 2018. “Horizontal Well Productivity Enhancement through Drawdown Management Approach in Vaca Muerta Shale.” In SPE Canada Unconventional Resources Conference. Society of Petroleum Engineers.

Ruspini, L. C., R. Farokhpoor, and P. E. Øren. 2017. “Pore-Scale Modeling of Capillary Trapping in Water-Wet Porous Media: A New Cooperative Pore-Body Filling Model.” Advances in Water Resources 108: 1–14.

Saomoto, H., and J. Katagiri. 2015. “Direct Comparison of Hydraulic Tortuosity and Electric Tortuosity Based on Finite Element Analysis.” Theoretical and Applied Mechanics Letters 5 (5): 177–80. https://doi.org/10.1016/j.taml.2015.07.001.

Scott*, Kyle D., Wei-Chun Chu, and Raymond W. Flumerfelt. 2015. “Application of Real-Time Bottom-Hole Pressure to Improve Field Development Strategies in the Midland Basin Wolfcamp Shale.” In Unconventional Resources Technology Conference, San Antonio, Texas, 20-22 July 2015, 1790–1798. Society of Exploration Geophysicists, American Association of Petroleum ….

Sen, Vikram, Kyoung Suk Min, Lujun Ji, and Richard Sullivan. 2018. “Completions and Well Spacing Optimization by Dynamic SRV Modeling for Multi-Stage Hydraulic Fracturing.” In SPE Annual Technical Conference and Exhibition. Society of Petroleum Engineers.

Shin, Do, and Drew Popovich. 2017. “Optimizing Vertical and Lateral Spacing of Horizontal Wells in Permian Basin Stacked Bench Developments.” In

Unconventional Resources Technology Conference. https://doi.org/10.15530/URTEC-2017-2669025.

Siddiqui, Shameem, and Amit Kumar. 2016. “Well Interference Effects for Multiwell Configurations in Unconventional Reservoirs.” In Abu Dhabi International Petroleum Exhibition & Conference. Society of Petroleum Engineers.

Siddiqui, Shameem, Doug Walser, and Ron Dusterhoft. 2016. “Effects of Well Placement Timing and Conductivity Loss on Hydrocarbon Production in Multiple Hydraulically Fractured Horizontal Wells in a Liquids-Rich Shale Play.” In SPE Western Regional Meeting. Society of Petroleum Engineers.

Silin, Dmitriy, Liviu Tomutsa, Sally M. Benson, and Tad W. Patzek. 2011. “Microtomography and Pore-Scale Modeling of Two-Phase Fluid Distribution.” Transport in Porous Media 86 (2): 495–515.

Somanchi, Kiran, James Brewer, and Alan Reynolds. "Extreme limited entry design improves distribution efficiency in plug-n-perf completions: Insights from fiber-optic diagnostics." SPE Hydraulic Fracturing Technology Conference and Exhibition. Society of Petroleum Engineers, 2017.

Sondergeld, Carl H., Kent Edward Newsham, Joseph Thomas Comisky, Morgan Craig Rice, and Chandra Shekhar Rai. 2010. “Petrophysical Considerations in Evaluating and Producing Shale Gas Resources.” In SPE Unconventional Gas Conference. Society of Petroleum Engineers.

Sun, Hao, Dengen Zhou, Adwait Chawathé, and Baosheng Liang. 2017. “Understanding the Mechanism of Fracture Hits on Midland Basin Tight-Oil Production.” In Unconventional Resources Technology Conference, Austin, Texas, 24-26 July 2017, 108–118. Society of Exploration Geophysicists, American Association of Petroleum ….

Swanson, Cory, W. A. Hill, Gary Nilson, Christian Griman, Randal Hill, Phil Sullivan, Carl Aften, Jose C. Jimenez, Gianna Pietrangeli, and Daniel C. Shedd. 2018. “Post-Frac-Hit Mitigation and Well Remediation of Woodford Horizontal Wells With Solvent/Surfactant Chemistry Blend.” In Unconventional Resources

Technology Conference, Houston, Texas, 23-25 July 2018, 1479–1494. Society of Exploration Geophysicists, American Association of Petroleum ….

Spearing, M., Matthews, G.P., 1991. Modelling characteristic properties of sandstones. Transp. Porous Media 6, 71–90.

Tinni, Ali, Ebrahim Fathi, Rajiv Agarwal, Carl H. Sondergeld, I. Yucel Akkutlu, and Chandra Shekhar Rai. 2012. “Shale Permeability Measurements on Plugs and Crushed Samples.” In SPE Canadian Unconventional Resources Conference. Society of Petroleum Engineers.

Van Eekelen, H. A. M. 1982. “Hydraulic Fracture Geometry: Fracture Containment in Layered Formations.” Society of Petroleum Engineers Journal 22 (03): 341–349.

Velarde, J., T. A. Blasingame, and W. D. McCain Jr. "Correlation of black oil properties at pressures below bubble point pressure-A new approach." Annual Technical Meeting. Petroleum Society of Canada, 1997.

Wilson, Kurt, and R. R. Hanna Alla. 2017. “Efficient Stress Characterization for Real-Time Drawdown Management.” In Unconventional Resources Technology Conference, Austin, Texas, 24-26 July 2017, 3723–3737. Society of Exploration Geophysicists, American Association of Petroleum ….

Wu, Ruiting, Olga Kresse, Xiaowei Weng, Charles-Edouard Cohen, and Hongren Gu. 2012. “Modeling of Interaction of Hydraulic Fractures in Complex Fracture Networks.” In SPE Hydraulic Fracturing Technology Conference. Society of Petroleum Engineers.

Yu*, Wei, and Kamy Sepehrnoori. 2014. “Optimization of Well Spacing for Bakken Tight Oil Reservoirs.” In Unconventional Resources Technology Conference, Denver, Colorado, 25-27 August 2014, 1981–1996. Society of Exploration Geophysicists, American Association of Petroleum ….

Yu*, Wei, Kan Wu, Lihua Zuo, Xiaosi Tan, and Ruud Weijermars. 2016. “Physical Models for Inter-Well Interference in Shale Reservoirs: Relative Impacts of Fracture Hits and Matrix Permeability.” In Unconventional Resources

Technology Conference, San Antonio, Texas, 1-3 August 2016, 1535–1558. Society of Exploration Geophysicists, American Association of Petroleum ….

Zapata, Yuliana, and A. Sakhaee-Pour. 2016. "Modeling Adsorption–Desorption Hysteresis in Shales: Acyclic Pore Model." Fuel 181: 557–565.

Zhang, Mingzhong. 2017. "Pore-Scale Modelling of Relative Permeability of Cementitious Materials Using X-Ray Computed Microtomography Images." Cement and Concrete Research 95: 18–29.

Zuo, Lin, Jonathan B. Ajo-Franklin, Marco Voltolini, Jil T. Geller, and Sally M. Benson. 2017. "Pore-Scale Multiphase Flow Modeling and Imaging of CO2 Exsolution in Sandstone." Journal of Petroleum Science and Engineering 155: 63–77.

Appendix 1

Peng-Robinson equation is presented below for a pure component. However, it can be easily modified for mixtures.

$$P = \frac{RT}{V_m - b} - \frac{a\beta}{V_m^2 + 2bV_m - b^2}$$

$$a = \frac{0.45724R^2T_c^2}{P_c}$$

$$b = \frac{0.07780RT_c}{P_c}$$

$$\beta = (1 + (0.37464 + 1.54226\omega - 0.26992\omega^2)(1 - T_r^{0.5}))^2$$

$$T_r = \frac{T}{T_c}$$

Where ω is the acentric factor for the species, P_c is critical pressure, Vm is the molar volume, and T_c is critical temperature. The ideal gas constant R = 8.314413 J/mol-K. For 100% methane, $\omega = 0.011, P_c = 4.65\ MPa,$ and $T_c = 190.4\ K$.

Appendix 2

	Comp.	HC	Pc (atm)	Tc (K)	Acentric Factor	Mole. Weight	Vc (viscosity)	Omega A	Omega B	SG
1	N2	0	33.50	126.20	0.0400	28.01	0.0895	0.45724	0.07780	0.809
2	CO2	3	72.80	304.20	0.2250	44.01	0.0940	0.45724	0.07780	0.818
3	CH4	1	45.40	190.60	0.0080	16.04	0.0990	0.45724	0.07780	0.300
4	C2H6	1	48.20	305.40	0.0980	30.07	0.1480	0.45724	0.07780	0.356
5	C3H8	1	41.90	369.80	0.1520	44.10	0.2030	0.45724	0.07780	0.507
6	IC4	1	36.00	408.10	0.1760	58.12	0.2630	0.45724	0.07780	0.563
7	NC4	1	37.50	425.20	0.1930	58.12	0.2550	0.45724	0.07780	0.584
8	IC5	1	33.40	460.40	0.2270	72.15	0.3060	0.45724	0.07780	0.625
9	NC5	1	33.30	469.60	0.2510	72.15	0.3040	0.45724	0.07780	0.631
10	FC6	1	32.46	507.50	0.2750	86.00	0.3440	0.45724	0.07780	0.690
11	C07-C10	1	27.61	580.41	0.3261	114.67	0.4485	0.45724	0.07780	0.750
12	C11-C13	1	21.50	624.84	0.5146	165.09	0.6325	0.46709	0.08100	0.798
13	C14-C16	1	17.03	700.56	0.6193	207.17	0.7735	0.54868	0.08652	0.827
14	C17-C20	1	14.30	745.18	0.7594	254.93	0.9219	0.36578	0.06834	0.854
15	C21+	1	12.47	786.47	1.0903	371.14	1.2273	0.54868	0.08468	0.904

Appendix 3

The concepts used to formulate the governing equations for fluid in porous media are well documented. The physical principals behind the governing equations are conservation of mass, Darcy's law, and thermodynamic equilibrium of components between phases. In addition, the definitions of phase saturation and mole fraction are used to complete the system. CMG was used to solve the governing equations via finite-difference method.

Component Balance

Conservation of mass is enforced for each cell and each component. For instance, the component balance for cell *j* is shown below:

$$\frac{\partial M_i^j}{\partial t} + \sum_k F_i^{jk} + \sum_w Q_i^{jw} = 0 \quad \forall\, i, j$$

Where:

$\frac{\partial M_i^j}{\partial t}$ represents the rate of change of number of moles for component *i* in cell *j*.

$\sum_k F_i^{jk}$ represents the sum of inter-cell flows of component *i* into cell *j* from connected cell k. This term basically represents the difference of mass flow rate in and out of cell *j*.

$\sum_w Q_i^{jw}$ represents the sum of flows of component *i* into cell *j* from an external source or, sink *w*.

Phase Equilibrium

Thermodynamic equilibrium is enforced when a fluid component partitions in more than one phase. For instance, if component i partitions in phases α and β, the component fugacity in both phases must be equal.

$$f_{\alpha,i} = f_{\beta,i} \qquad \text{if } (i \in \alpha)\ \&\ (i \in \beta)\ \forall\ i, \alpha, \beta$$

Where:

$f_{\alpha,i}$, $f_{\beta,i}$ is the fugacity of component i in α and β phases.

Saturation and Mole Fraction Constraints

Lastly, phase saturations and mole fractions need to satisfy their own fractional constraints as shown below.

$$\sum_{a} S_a = 1$$

$$\sum_{i} X_{a,i} = 1 \qquad \forall \ \ a$$

Appendix 4

ID	Fracture Compaction [%]	MatrixPermMultiplier	UnproppedFracPERM_1H [uD]
516	78.5%	78.8%	0.0050
510	75.6%	77.6%	0.0050
504	78.5%	77.0%	0.0050
496	78.9%	77.6%	0.0078
474	71.1%	76.4%	0.0055
480	72.6%	75.8%	0.0050
468	74.1%	77.6%	0.0050
498	72.6%	76.4%	0.0050
486	74.1%	77.6%	0.0050
439	73.7%	78.2%	0.0066
487	74.8%	78.7%	0.0060

ID	UnproppedFracPERM_2H [uD]	Swcrit	Sorw	Sgcrit	Sorg	Krocw	Krogcg	Error [%]
516	0.0500	19.3%	14.0%	1.7%	11.2%	0.6	0.6	9.5%
510	0.0484	20.5%	15.6%	2.0%	10.0%	0.7	0.7	9.6%
504	0.0500	21.3%	14.8%	1.7%	12.0%	0.6	0.6	9.7%
496	0.0432	17.3%	14.5%	2.3%	10.9%	0.7	0.7	9.8%
474	0.0496	23.8%	16.4%	1.7%	10.8%	0.6	0.6	9.8%
480	0.0480	23.8%	16.4%	1.7%	10.4%	0.6	0.6	9.9%
468	0.0496	23.8%	16.4%	1.7%	11.2%	0.6	0.6	9.9%
498	0.0500	22.5%	14.8%	1.9%	12.0%	0.6	0.6	9.9%
486	0.0500	25.0%	18.8%	1.7%	11.2%	0.6	0.6	10.0%
439	0.0500	25.0%	16.7%	1.4%	10.5%	0.6	0.6	10.0%
487	0.0438	19.8%	16.0%	1.9%	11.2%	0.7	0.7	10.1%